FACULTY OF TEXTILE ENGINEERING TUL

Dissertation Thesis

Knitted Conductive Fabrics With Enhanced Electromagnetic Interference Shielding

Study programme:	P3106 Textile Engineering
Study branch:	Textile Technics and Materials Engineering
Author:	**Sundaramoorthy Palanisamy, M.Tech.**
Thesis Supervisor:	Ing. Veronika Tunáková, Ph.D. Department of material engineering

Liberec 2023

Declaration

I hereby certify, I, myself, have written my dissertation as an original and primary work using the literature listed below and consulting it with my thesis supervisor and my thesis counsellor.

I acknowledge that my dissertation is fully governed by Act No. 121/2000 Coll., the Copyright Act, in particular Article 60 – School Work.

I acknowledge that the Technical University of Liberec does not infringe my copyrights by using my dissertation for internal purposes of the Technical University of Liberec.

I am aware of my obligation to inform the Technical University of Liberec on having used or granted license to use the results of my dissertation; in such a case the Technical University of Liberec may require reimbursement of the costs incurred for creating the result up to their actual amount.

At the same time, I honestly declare that the text of the printed version of my dissertation is identical with the text of the electronic version uploaded into the IS/STAG.

I acknowledge that the Technical University of Liberec will make my dissertation public in accordance with paragraph 47b of Act No. 111/1998 Coll., on Higher Education Institutions and on Amendment to Other Acts (the Higher Education Act), as amended.

I am aware of the consequences which may under the Higher Education Act result from a breach of this declaration.

February 24, 2023 Sundaramoorthy Palanisamy, M.Tech.

ACKNOWLEDGEMENT

"Arise! Awake! and stop not until the goal is reached"

-*Swami Vivekananda*

I would like to acknowledge both The Government of the Czech Republic and Municipality of the Liberec for giving this great opportunity to be in Czechia for PhD. It has been an honor to be the inaugural recipient of the Scholarship and I am indebted to the donors in providing me complete academic freedom in this research.

First and foremost I am extremely grateful to my supervisors, Dr. Veronika Tunakova for his invaluable advice, continuous support, and patience during my PhD study. Her immense knowledge and plentiful experience have encouraged me in all the time of my academic research and daily life. I would also like to thank Prof. Jiri Militky, and Prof. Jakub Wiener for their technical support on my study. Special thanks to Dr. Blanka Tomkova, Dr. Brigita Kolkavova Sirkova and Dr. Iva Mertova in particular for their extended support throughout my PhD work. Thank you to all the academics who helped me gets to this stage. Additionally, I would like to express gratitude to Dr. Maros Tunak, for his treasured support which was really influential in shaping my experiment methods and critiquing my results. Special thanks to Dr. Lieva Van Langenhove from Ghent University, Belgium and Dr. Youjiang Wang from Georgia Institute of Technology, USA for providing the internship course at their Universities' was a huge influence and without which I would have never followed this path. My "pre-doc" supervisors Dr. V. R. Giridev of Anna University, Chennai and in particular the remarkable Dr. N. Gobi of Anna University, Chennai from whom I learned so much. Thanks to Dr. Veerakumar Arumugam and Mr. Vignesh Balaji, M.Tech., for being so supportive when I was considering applying for PhDs.

It has been an amazing experience working with research groups across different departments, thanks to everyone from the Department of Material Engineering and Department of Technologies and Structures, Faculty of Textile Engineering, Technical University of Liberec, Liberec, Czech Republic, I've worked with and from whom I've learned so much.

Finally, I would like to express my gratitude to my parents, my brothers and sisters, my friends and my relatives. Without their tremendous understanding and encouragement in the past few years, it would be impossible for me to complete my study.

ABSTRACT

The work deals with the development of electrically conductive knitted fabrics and their deformation characteristics. The effect of deformation on changes in electrical characteristics is measured by the high-frequency electromagnetic radiation (EM) shielding method. EM radiation of these frequencies penetrates electrically non-conductive materials and is reflected or absorbed by electrically conductive materials. This makes it possible to monitor the change in electrical resistance of textiles, which characterizes the deformation of the sample in tension.

This work is divided into two basic parts: a part of the analysis of electrically conductive yarn and a part of the production and analysis of electrically conductive knitted fabrics. In the yarn analysis part, a conductive commercially available silver-plated polyamide yarn (Statex Inc., Bremen) with a fineness of 60 tex containing 36 filaments with a specific electrical resistance of 68±14 Ω/m and a tensile strength of 47 cN/tex was used. To simulate the electrical resistance of the yarn related with its length and to simulate the effect of contact resistance, three different yarn configurations (single yarn (SY), single loop yarn (SLY) and multiloop yarn (MLY)) were used. Electrical resistance was tested for all yarn arrangements. The tensile strength of the yarn arrangements was analyzed by tensile stress at a strain rate of 50 mm/min. Multiloop yarn has been found to have higher strength than other forms of yarn. Changes in electrical resistance during tensile stress were evaluated using Arduino resistance circuit probes that were connected to the jaws of the tensile strength tester and real-time values were recorded using a MATLAB programming language program. It was confirmed that the electrical resistance decreases as the number of loops increases.

In the subsequent part of the work, two patterns of knitwear were produced on a flat knitting machine, a plain "single jersey" and a 1x1 ribbed "double jersey". Three different densities were produced in each design: low, medium and high. The effectiveness of the electromagnetic shielding (SE) of knitted fabrics was tested using a frequency range of 30 MHz to 1.5 GHz according to the ASTM D4935-18 standard. It was found that the higher the sample density, the higher the SE. The double jersey had a higher SE than the single jersey and the difference was around 15 dB at 1.5 GHz frequency. The thickness of the knitted fabric and the porosity have decreased due to the increase in stitch density.

A special device with four independent jaws was used for tensile deformation of knitted samples in one direction (transverse and longitudinal) and in two directions (biaxial). The knitted fabrics were stretched up to 25% strain and electromagnetic shielding, electrical resistance and porosity were measured.

"Single Jersey" shielding efficiency has an increasing trend in all stretching directions. The effectiveness of the double Jersey shield has an increasing trend in vertical stretching, but horizontal and biaxial deformation initially reduces the shielding effectiveness. The porosity and electrical resistance results against stretching of the knitted fabric in all directions were also analyzed. The reason for changes in fabric behavior was analyzed using data from the electromechanical survey of simple yarn formations. A stochastic model based on multiple regression analysis and using partial regression graphs was proposed to predict the effectiveness of electromagnetic shielding of knitted fabrics based on knowledge of their electrical conductance/resistance and porosity.

Keywords: Wireless strain sensor, silver coated polyamide yarn, tensile strength, single loop yarn, multiloop yarn, single jersey, double jersey, flat knitting, electromagnetic shielding effectiveness, fabric porosity, electrical resistance, and biaxial elongation.

ABSTRAKT

Práce se zabývá vývojem elektricky vodivých pletenin a jejich deformační charakteristikou. Vliv deformace na změny elektrických charakteristik se měří metodou stínění vysokofrekvenčního elektromagnetického záření (EM). EM záření těchto frekvencí proniká elektricky nevodivými materiály a je odráženo nebo pohlcováno elektricky vodivými materiály. To umožňuje monitorovat změnu elektrického odporu textilií, což charakterizuje deformaci vzorku v tahu.

Tato práce je rozdělena na dvě základní části: část analýzy vodivé příze a část výroby a analýzy vodivých pletenin. V části analýzy příze byla použita vodivá komerčně dostupná postříbřená polyamidová příze (Statex Inc., Bremen) jemnosti 60 tex obsahujících 36 filamentů s měrným elektrickým odporem 68±14 Ω/m a pevností v tahu je 47 cN/tex. Pro simulaci elektrického odporu příze souvisejícího s její délkou a vlivu kontaktního odporu byla použita tři různá uspořádání příze (jednoduchá příze (SY), příze s jednou smyčkou (SLY) a příze s více smyčkami (MLY)). Pro všechna uspořádání přízí byl testován elektrický odpor. Pevnost v tahu přízových uspořádání byla analyzována tahovým namáháním při rychlosti deformace 50 mm/min. Bylo zjištěno, že příze s více smyčkami má vyšší pevnost než jiné formy příze. Změny elektrického odporu během tahového namáhání byly hodnoceny s využitím sond odporového obvodu Arduino, které byly spojeny s čelistmi trhacího přístroje a hodnoty v reálném čase byly zaznamenávány pomocí programovacího jazyka MATLAB. Bylo potvrzeno, že elektrický odpor klesá s růstem počtu smyček.

V navazující části práce byly na plochém pletacím stroji vyrobeny dva vzory pletenin, hladký „single Jersey“ a 1x1 žebrový „double Jersey“. V každém provedení byly vyrobeny tři různé hustoty: nízká, střední a vysoká. Byla testována účinnost elektromagnetického stínění (SE) pletenin od frekvence 30 MHz do 1.5 GHz podle normy ASTM D4935-18. Bylo zjištěno, že čím vyšší je hustota vzorku, tím vyšší je SE. Pletenina „double Jersey“ měla vyšší SE než pletenina „single Jersey“ a rozdíl byl kolem 15 dB při frekvenci 1,5 GHz. Tloušťka pleteniny a porozita se snížily díky zvýšení hustoty oček.

Pro tahovou deformaci pletenin v jednom směru (příčném i podélném) a ve dvou směrech (dvouosé) bylo použito speciální zařízení se čtyřmi nezávislými čelistmi. Pleteniny byly protaženy až do 25 % deformace a bylo měřeno elektromagnetické stínění, elektrický odpor a porozita.

Účinnost stínění „single Jersey“ má rostoucí trend ve všech směrech protažení. Účinnost stínění „double Jersey“ má rostoucí trend ve vertikálním i podélném protahování, ale biaxiální deformace zpočátku účinnost stínění snižuje. Rovněž byly analyzovány výsledky poréznosti a elektrického odporu proti napínání pleteniny ve všech směrech. Důvod změn v chování tkaniny byl analyzován pomocí dat z elektromechanického průzkumu jednoduchých přízových útvarů. Pro predikci účinnosti elektromagnetického stínění pletenin na základě znalosti jejich elektrické vodivosti/odporu a porozity byl navržen stochastický model na bázi vícenásobné regresní analýzy a s použitím parciálních regresních grafů.

Klíčová slova: Bezdrátový snímač deformace, stříbrem povrstvená polyamidová příze, pevnost v tahu, příze s jednou smyčkou, příze s více smyčkami, hladká pletenina, 1x1 žebrová pletenina, ploché pletací stroje, elektromagnetická stínící účinnost, porozita pleteniny, elektrický odpor, and dvouosé tahové namáhání.

LIST OF ABBREVIATIONS

Acronyms	Descriptions
ARDUINO	open-source electronics platform
DJ	Double jersey
DJH	Double jersey high density fabric
DJL	Double jersey low density fabric
DJM	Double jersey medium density fabric
ER	Electrical resistance
MLY	Multi-loop yarn
SJ	Single jersey
SJH	Single jersey high density fabric
SJL	Single jersey low density fabric
SJM	Single jersey medium density fabric
SLY	Single-loop yarn
SY	Single yarn
TLE	Two-line element set

LIST OF SYMBOLS

GL	Gauge length	cm
R_L	Length resistance	Ω/cm
T	Tensile load	cN/tex or N/10 cm

SUMMARY

LIST OF FIGURES

LIST OF TABLES

1 INTRODUCTION

Textile based materials and composites are generally suitable for EMI shielding applications. Traditional textile materials are electrically nonconductive, but the coating, deposition, and blending with conductive materials make them electrically conductive, which is suitable for EMI shielding applications. It is also possible to observe a change in electrical conductivity as well as a change in electromagnetic radiation during their mechanical stress, which is an interesting property for other purposes of use.

In the preliminary investigations, the nonconductive and conductive textile materials with different electrically conductive additives were analyzed for electromagnetic shielding effectiveness [1]. The effect of moisture content in the textile on its ability to shield electromagnetic fields was also investigated [2]. Further, the copper-coated nonwoven strips are modeled to study porosity and contact resistance on EMI shielding [3]. Since most of the findings are published in high-impact journals, the results of these studies are discussed in more detail in the literature review section of this thesis.

The main theme of the thesis is to study the deformation sensitivity of the weft-knitted fabrics made of silver-coated yarns. First, the electrical and mechanical properties of yarns were investigated, then the electromechanical properties of simple structural elements were explored, and then the change in electrical conductivity, electromagnetic shielding and other interesting characteristics during tensile stressing of two knitted fabrics were studied. A stochastic model is presented, which can be used to predict the level of the electromagnetic shielding ability of the knitted fabrics based on the knowledge of their electrical conductivity and the porosity.

2 PURPOSE AND AIM OF THE RESEARCH

Textile materials are used for many applications, from human clothing to advanced technology; electrically conductive textile is one part of the emerging field. In particular, electric and electronic devices' electromagnetic interference shielding is much needed; protecting human beings from this radiation is also important. The electrically conductive textile material has the property of shielding the EM radiation and it can be newly used also for deformation sensing applications. In this case the deformation sensing is measured with wireless technology with the help of EM radiation of conductive textile material. The applied strain on textile fabric changes the electrical conductivity and also changes the EM

shielding; in this way, the sensor works as a strain sensor. The main objectives of the work are:

To study the contact force resistance of different arrangements of silver coated yarn simulating their interaction in knitted fabrics

From the previous investigation, it was noticed that the contact points at the electrically conductive yarn-yarn interface affect the electrical resistance and also affect the EM SE of the knitted fabrics made of electrically conductive yarns. That is why the effect of the yarn contact points was analyzed using the silver-coated yarn. In the knitted textile fabric, the yarn was interlaced with each other to form the fabric. The silver coated PA yarn is taken to prepare three basic structural elements simulating structural elements of knitted fabrics and they are: single strand, single loop, and multiple chain loops.

To design the special device measuring electrical resistance of linear structures during stretching

The tensile instrument with an Arduino resistance circuit, and the MATLAB software program were used for construction of system measuring the electrical resistance response during stretching. Electromechanical behavior of single yarn, single loop and multiple loop were beneficial in predicting the yarn behavior in knitted fabric during the stretching process and justified the fabric stretching results.

To prepare silver coated knitted fabrics suitable for deformation sensors design

The silver coated PA yarn was used to prepare single jersey and double jersey fabric samples at three different stitch densities. The prepared samples were introduced in a biaxial device (in-house model) for deformation at uni- and bi-directional stretching using controlled lengths.

To investigate the strain sensing ability of the weft-knitted samples against the EM waves and electrical conductivity

The aims are to investigate the change in electrical resistance with respect to the stretch direction of weft-knitted conductive samples made of silver coated yarns. The produced knitted structures are used to analyze its EM SE with respect to the direction of stretch applied to it.

3 LITERATURE REVIEW

This chapter summarizes current status in the field of development of electromagnetic shielding of textile structures including the basics of EMI shielding, testing methods of electromagnetic shielding ability, applications of various conductive textiles materials, strain sensing ability of deformed conductive textile materials, and research gaps.

3.1. Mechanism of EM shielding by textile material

EM shielding's three main mechanisms are reflection (*R*), absorption (*A*), and multiple reflections or scattering (*B*) of EM waves (see Figure 1) [4][5]. Shield by reflection, the material must have mobile charge carriers (electrons or holes) to interact with the incoming EM waves; the higher electrically conductive materials like silver, gold, copper, steel, and carbon have excellent reflecting properties of EM waves [6]. Absorption is the second important mechanism and depends on the material's thickness. The highly magnetic permeable materials absorb EM waves; examples are mu-metal, ferrite, zinc, and carbon, which have very good absorption of EM waves. In electrically conductive materials, absorption can also arise from resistive losses, which transform the electromagnetic energy into heat by the Joule effect. Conductive textile materials are the best examples of the multiple reflections of EM waves because of their structure. The plane wave shielding theory developed by Schelkunoff [7] and Schultz et al. [8] defines the shielding effectiveness, SE, as shown in Equation 1:

$$\boldsymbol{SE = A + R + B,} \qquad \text{Eq. 1}$$

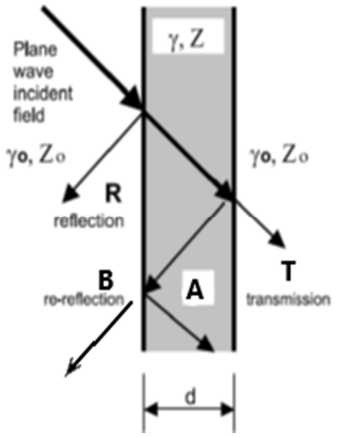

Figure 1. Electromagnetic radiation shielding principle [9].

where B is a term that considers the loss caused by multiple reflections inside the shield, R is the reflection loss, and A is the absorption loss. The shielding effectiveness of SE is represented in unit decibels [dB]. Based on the optical properties of the object and wavelength, incident radiation (heat intensity I_i [W m^{-2}]) separate into three components, i.e., reflected radiation (I_R), absorbed radiation (I_A), and transmitted radiation (I_T). It is simply to define relative dimensionless characteristics as transmittance T, absorbance A, and reflectance R as portions given in Equation 2.

$$\boldsymbol{T = \frac{I_t}{I_i}} \qquad \boldsymbol{A = \frac{I_A}{I_i}} \qquad \boldsymbol{R = \frac{I_R}{I_i}} \qquad \text{Eq. 2}$$

Operation of the electromagnetic shield is possible to be characterized by the so-called shielding attenuation coefficient, ES (dimensionless), defined as a ratio between electromagnetic field density in a specific place of shielded space P_t and incident electromagnetic field density P_i in below Equation 3:

$$\boldsymbol{ES = \frac{P_t}{P_i}\ [-]} \qquad \text{Eq. 3}$$

The logarithmic size of this coefficient, called electromagnetic shielding effectiveness (SE), is used more frequently, as shown in Equation 4.

$$\boldsymbol{SE = -10log\frac{P_t}{P_i} = -20log\frac{E_t}{E_i} = -20log\frac{H_t}{H_i}\ [dB]}, \qquad \text{Eq. 4}$$

Where H_t, E_t, *and* P_t are the electric field strength, magnetic field strength, and electromagnetic field density values measured in the presence of the textile material, H_i, E_i, *and* P_i is the same values measured without the textile material.

The scattering parameters are calculated for the vector network analyzer (VNA) with its power reflection P_r and transmission P_t at the two ports, and power absorption is P_a [10][11]. The power reflection P_i, written (Equation 5) as

$$\boldsymbol{P_i = P_r + P_a + P_t} \qquad \text{Eq. 5}$$

The scattering parameters S_{22} (or S_{11}) and S_{12} (or S_{21}) represent the R, T, and A as (Equation 6-8)

$$\boldsymbol{R = |S_{11}|^2 = \frac{P_r}{P_i}} \qquad \text{Eq. 6}$$

$$\boldsymbol{T = |S_{21}|^2 = \frac{P_t}{P_i}} \qquad \text{Eq. 7}$$

$$\boldsymbol{A = \frac{P_a}{P_i} = 1 - R - T} \qquad \text{Eq. 8}$$

Table 1. Classification of EM SE values based on professional use.

Grade	Excellent	Very good	Good	Moderate	Fair
Range	SE > 60 dB	60 dB ≥ SE > 50 dB	50 dB ≥ SE > 40 dB	40 dB ≥ SE > 30 dB	30 dB ≥ SE > 20 dB

Table 2. Classification of EM SE values based on general use.

Grade	Excellent	Very good	Good	Moderate	Fair
SE Range	SE > 30 dB	30 dB ≥ SE > 20 dB	20 dB ≥ SE > 10 dB	10 dB ≥ SE > 7 dB	7 dB ≥ SE > 5 dB

Deriving the *R*, *T*, and *A* scattering parameters with Equation 4 then, SE expressed as

$$\boldsymbol{SE = -10log\left|\frac{1}{|S_{21}|^2}\right|} \quad \text{Eq. 9}$$

The overall SE is calculated with the transmission coefficient S_{21} (forward voltage gain), according to Equation 9 [6][12]. According to the requirements of electromagnetic shielding textiles [13], depending on professional or general use, textiles can be classified into five grades, from a fair grade to an excellent grade, see Table 1 and Table 2. Professional use comprises professional protective uniforms for electronic manufacturers, shielding of medical equipment, etc., whereas casual wear, maternity clothes, aprons, shielding of consumptive electronic products, and communication-related products, etc., represent general use.

3.2. Methods of EM SE testing

The materials' electromagnetic shielding effectiveness is measured with four different methods: open field or free space method, shielded box method, shielded room method, and coaxial transmission line method.

Open field or free space method

Figure 2 shows the vector network analyzer (VNA) connected with antennas that are transmitting and receiving the EM waves. The sample is placed in between the antennas to measure the EM radiations. The scattering (*S*-) parameters like S_{11}, S_{12}, S_{21}, and S_{22} are measured for calculating the SE value. This testing method is used for solids, liquids, gases, radar domes in aerospace, composite materials, and Meta materials. The finished electronic

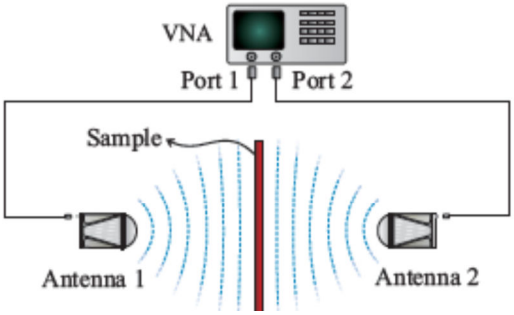

Figure 2. Transmission and reflection of electromagnetic waves on a sample with the free space method [14].

-device, which emits EM radiation, is tested with this method. Building materials, telecommunication devices, and wires are also tested with free space methods [14].

Shield box method

The shield box method of test setup has a metal box containing a specimen holder for the sample and a transmitter outside and receiver inside the metal box, as shown in Figure 3. This method has a limitation of a 500 MHz frequency range for testing and difficulties in holding the samples with a metal box [15].

Coaxial transmission line method

The coaxial transmission line method of SE measurement has been widely used for all materials. A wider frequency range was used to test the samples, and was easy to use with smaller sample sizes.

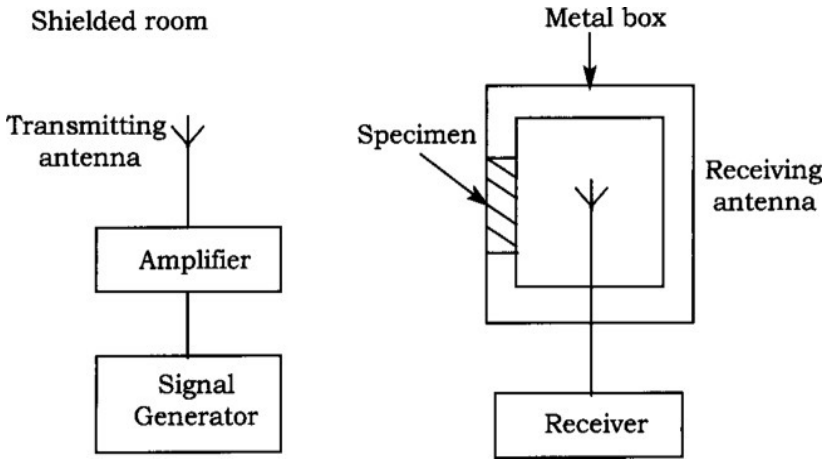

Figure 3. Shield box method [15].

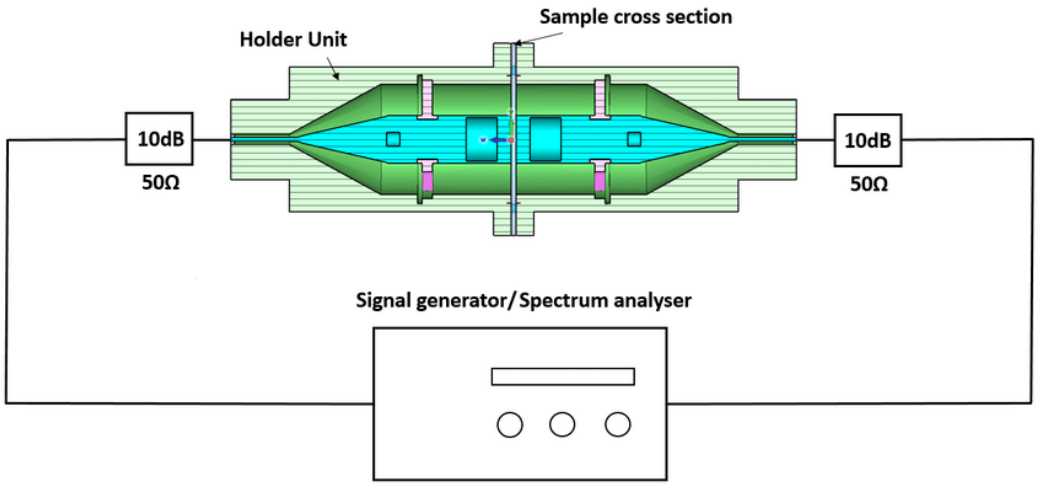

Figure 4. Coaxial transmission line method [12].

In Figure 4, the coaxial transmission line setup is shown; the test sample is placed in between the two holders in which one is transmitting the EM waves, and another is receiving them. The EM waves are generated in the signal generator and also received by the spectrum analyzer. The S_{11}, S_{12}, S_{21}, and S_{22} values are able measured with this measuring technique. The EM shielding test was carried out as per the ASTM D 4935 standard.

Shield room method

The shield room method is the method that has a separate shield room for the signal generator, receiver, and sample with transmitter and receiver, as shown in Figure 5. This method is also called an anechoic chamber and is used widely for SE testing of various materials. The shielded room of the transmitter and receiver is separated by the sample holder, which has space for the sample. A frequency of a broader range is used to measure the samples and test as per the EN50147 standard. Among the four methods of EM SE testing, the coaxial method and shielding room method are the most accurate and used for measuring textile and composite materials. The free space method has the disadvantage of perturbations from the surrounding environment.

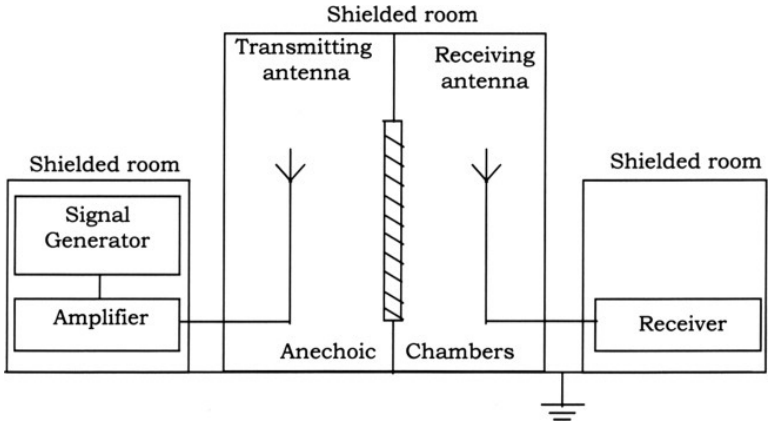

Figure 5. Shield room or anechoic chamber method [15].

3.3. Fibre-based materials for EM shielding

Commercial textile materials are mainly manufactured from cotton, polyester, viscose, linen, and wool. These materials are non-conductive materials but contain a certain percentage of moisture content. The EM shielding is mainly produced with highly conductive materials and semi-conductors, and insulators are not shielding the EM radiations. Palanisamy et al. [1] studied the nonconductive textile materials for shielding against EM radiation, and their results are in Figure 6. It is visible that samples made of traditional textile materials, including cotton, wool, linen, polyester, viscose, or glass fibres, have almost no SE, especially at high frequencies (frequencies higher than 150 MHz). This result was expected because a major part of textile fibres belongs to electric insulators, which is associated with the fact that each of the electrons is fixed to the atomic nucleus or shared in atomic bonds. However electric conductance of traditional fibres is not fully neutral, and it depends on the content of various additives or moisture content.

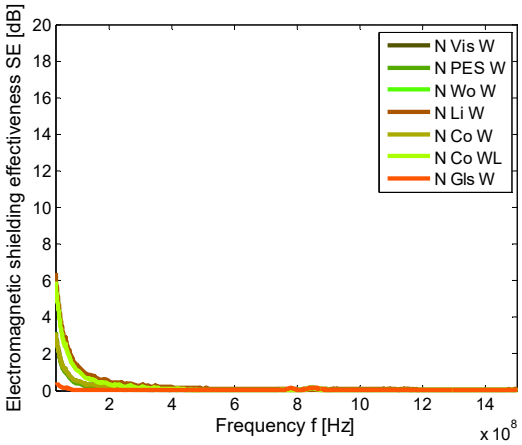

Figure 6. EM SE versus frequency of nonconductive fabrics [1].

Currently, many EM shielding studies are using electro-conductive textile materials. Incorporating conductive fillers and fabric surface coatings are the two primary methods to develop electromagnetic interference (EMI) shielding fabrics [16]. Several methods for developing electromagnetic radiation shields are available such as ionic plating, electroless plating, cathode sputtering, conductive paints, vacuum metallization, zinc paints, zinc flame spraying, zinc arc spraying, and conductive fillers such as copper, stainless steel, and aluminum in different forms (fibres, particles, wires). The methods mentioned above can be categorized under two headings the surface treatments and the fillers. The surface treatments are often time-consuming, laborious, and costly. Conductive fillers in particulates, fibres, and filaments are increasingly being used to shield electromagnetic radiation [17]. The application of electromagnetic shielding with textile materials is used more widely and commonly instead of metal screens and other traditional shielding materials because metal screening materials have many disadvantages, particularly weight, corrosion, difficulty in adjusting the shielding effectiveness (SE), and limited mechanical flexibility. In contrast, textile materials are generally lighter (having lower density), more flexible, and cheaper [18].

EM shielding, based on polymers with conductive fillers, has been gaining more significant roles in various technological domains, and they are getting into the research focus of numerous studies as a part of a growing research trend. Conductive filler particles like silver, copper, gold, zinc, nickel, titanium, and carbon particles (carbon nanotubes, graphite, and graphene) were used for EM shielding applications in many studies giving excellent results [19][20]. Conductive polymers, on the other hand, allow perfect control of the electrical stimulus, possess outstanding electrical and optical properties, have a high conductivity/weight ratio, and can be made biocompatible, biodegradable, and porous. Conductive polymers such as polypyrrole, polyaniline, and polyacetylene were described for their EM shielding applications in many scientific studies [21][22][23][24].

Electrically conductive fibres are very often used for EM shielding applications because natural or synthetic fibres, for example, cotton, polyester, polyamide, polyacrylic, and cellulose acetate fibres, exhibit low electric conductivity. Currently, many metal-coated textiles, metal, carbon-based, etc., are available in the market. A carbon-matrix composite with different forms of carbon (fibre, nanotube) was found to be an excellent electromagnetic interference shielding of 124 dB, most of the radiations are reflected on the

surface and absorbed inside the material in the frequency range from 0.3 MHz to 1.5 GHz in this studies [25][26][27].

Conductive fabrics are made of 100 % metal fibre yarns like stainless steel, copper, silver, gold, brass, and aluminum; however, they are challenging to process. These types of yarns tend to have low flexibility due to the high stiffness of metal fibres, which produces heavier and uncomfortable fabrics. Metallic yarns are replaced by blending with traditional fibres to diminish the fabric's overall stiffness and improve the fabric's touch properties [28]. Usage of various types of textile structures like woven [29][30], nonwoven [31][32], weft-knitted [33], warp-knitted [34], braided [27], and composite [33][35] containing metal fibre or wire has been reported for EMI shielding applications.

Some conductive fabric samples show interesting results on EM SE against elongation and layering. In the study [36], the warp-knitted fabric is used for measuring EM SE. Increased elongation of fabric shows no significance on EM shielding behavior (elongation range of 0 – 40 %). The EM SE of fabric displayed no significant difference when the fabrics were elongated in the wale direction. The EMSE of two-layer fabrics with 0°/90° lamination angles showed more SE when compared to those with 0°/0° lamination angles. The test results indicate that the elastic warp-knitted fabrics produced could be used as EM shielding protective clothing to protect humans from EM radiation from household electronic devices. The electrical conductivity of the samples is also important for the EM SE; in general, it is directly proportional to the EM SE. Higher conductivity ensures higher in shielding effectiveness (SE). In the study [37], the flat knitted fabric is modeled for length-related resistance and contact resistance, and the relationship of the resistance, tensile force, fabric length, and width was established. Under the unidirectional extension, regression modeling measured the resistance and showed a high coefficient of determination and low standard error. The proposed model could compute the resistance of the conductive knitting fabrics under unidirectional extension. The contact resistance acts as a decreasing factor to total electrical resistance of fabric during the initial stretching process, whereas the length-related resistance dominates the total equivalent resistance for the further increasing tensile force in the stretching process. The different woven structures with conductive yarn or coating are used for the EM SE applications. The plain weave fabric with polyester blended with silver-coated polyimide yarn was used in the study [38], and an analytical model for EM SE of material with aperture was developed. It was proven, that the thickness of the fabric affects the SE values, and the numbers of apertures in the fabric also influence the SE value. The

twill and sateen weave of stainless steel (SS) blended yarn fabric was prepared at different conductive yarn densities, and the fabric structural parameters, which are float length, interlace coefficient, and yarn float, significantly changed the EM SE of the fabrics [39]. In the study [17], the copper filament was used to weave twill fabric, and increased copper filament diameter decreased the SE.

3.3.1. Metal staple fibres and wires

The metallic fibres and wires are formed from metal, metal-coated plastics, plastic-coated metals, core wire-wrapped plastics, and core plastic-wrapped metal. Metallic fibres like gold and silver are used to manufacture textile fabric from an ancient period as decorative cloths and ornament cloths. The ancient people used metal ornaments and cloths to protect themselves from radiation and even absorb suitable radiation as needed for their bodies. In recent times, aluminized plastic yarns are replaced precious metals, but the main disadvantage is poor corrosion-resistant and inferior bonding strength. This topic discusses metal fibre, filament, and wires for EM shielding applications.

Palanisamy et al. [1] studied the EM SE of staple metal blended yarn woven fabrics with different percentages of stainless steel (SS) staple fiber, and the fabric results are shown in Figure 7. EM SE increases with increasing SS fibre content for woven samples totally made of hybrid yarns containing 1 %, 10 %, 20 %, 40 %, and 75 %. The sample with the highest content of metal fibre reaches the highest EM SE of 51 dB for a frequency of 1.5 GHz, and a sample containing the lowest proportion of conductive components displays the lowest EM SE of 12 dB for a frequency of 1.5 GHz. The overall SE is increasing according to power function with metal fibre content (P). At a very low percent of conductive fibre loading, the SE is more or less equal to zero, like a pure matrix (polypropylene yarn). At 3 to 7 % of metal fibre content, the SE value increases drastically over a very narrow range of conductive fibre concentrations, called the percolation threshold. The solid line in this graph corresponds to the linear regression model with parameters obtained by the minimizing sum of squared differences. A high R^2 value (0.99) confirms the prediction ability of the developed regression models.

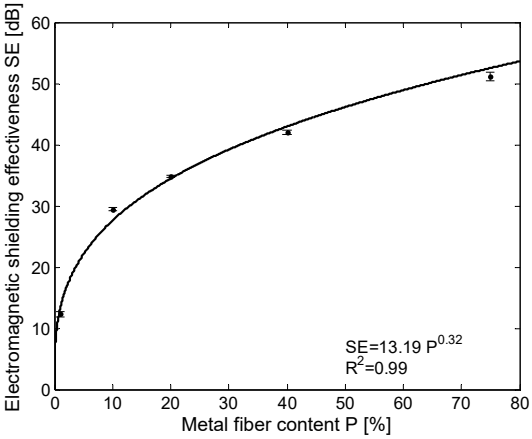

Figure 7. The dependence of EM SE on the metal fibre content of woven samples [1].

The EM SE results of incorporating staple stainless-steel fibres (diameter 8 or 12 μm), the textile structure has shielding effectiveness of 20 dB - 45 dB (which means that more than 99.9 % of EM fields were attenuated), and other favourable properties (mechanical flexibility, drape, and strength) as reported in [40][41][42]. Further, the incorporation of metal wires (stainless steel, copper, silver, gold) used as a core or shell of yarns offers an exciting solution for a limited number of applications due to their poor mechanical properties [43][44]. The siro core-spun yarn made with stainless steel and cotton was used for weft knitting, and EM SE was tested with an anechoic chamber method in the work [18]. The SE of the plain, double, and pique jersey knitted fabrics is between 20 and 50 dB at 30MHz to 1 GHz frequency, as shown in Figure 8. There is a significant change in SE values with a change in metal fibre content percentage, and the orientation with respect to the electric field was noticed. In the study [45], the plain and twill woven fabric was weaved with copper wire core cotton sheath friction spun yarn. The copper wire with 0.09 and 0.1mm diameters was used and tested for EM SE. The fabrics' SE values are between 20 and 66 dB at the 200 – 4000 MHz frequency range. The author described that the finer copper wire is better to perform against EM radiation compared with coarser diameter wire; it's quite the opposite of the EM theory. The courser wire is stiffer than finer, and during weaving, it acts rigidly, causing more openings in fabric and leading to leakage of radiation. The Zari yarn is gold or silver slit wrapped on silk or polyester yarn to prepare traditional South Asian dresses, and it is practicing from historic period onwards. In the work [46], the gold and silver Zari yarns were used to prepare twill, satin, and honey comb weave fabrics for EM SE. The honeycomb fabric made with gold Zari yarn has SE of 33 dB and silver Zari has SE of 30 dB at 300 MHz frequency.

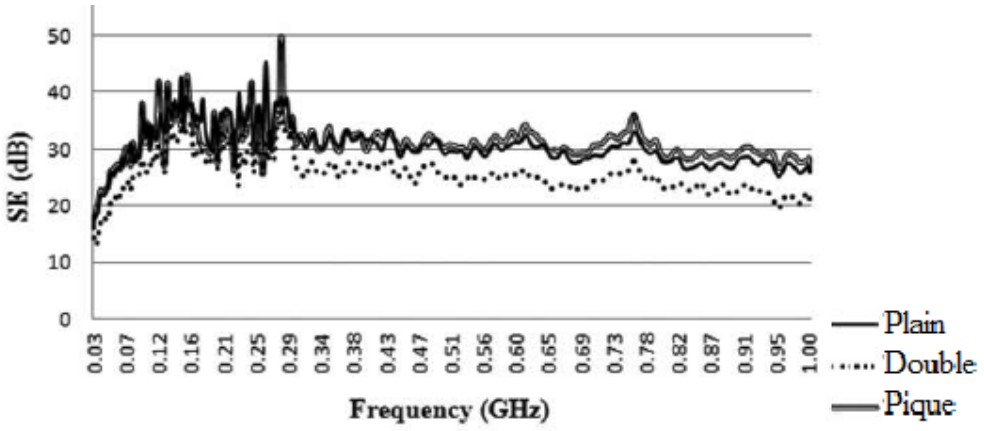

Figure 8. Shielding effectiveness results from the weft-knitted fabrics (SS/cotton siro spun yarn) [18].

3.3.2. Metal-coated textile materials

The coating of metals on textiles has been attractive for electrical conductivity applications. During coating, a thin layer of metal is applied on the textile substrate, which preserves the mechanical properties while increasing the surface's electrical conductivity. The techniques used for coating are electroplating, electroless plating, spray coating, and chemical reduction; among those techniques, electroplating and electroless plating is the commercial success with even coating with minimal material. In this part, a literature review on different coating methods for textile fabric and yarn with metals was discussed.

A 12 µm PET filament was vacuum coated with silver, copper, aluminium, and titanium at six different thicknesses and prepared plain-woven fabric. In the study [47], the fabric is tested for EM SE as per the ASTM D 4935 method. The author noticed that the thickness of the coating increases with increasing EM SE values, as shown in Figure 9(a); a 31µm thick silver-coated PET filament has an SE of 80 dB between 2.25 - 2.70 GHz frequency (Figure 9(b)). The orientation of the metal filament parallel to the oscillating direction of the magnetic field in a wave guide tube also increases the SE value. In general, EM waves travel in multiple orientations, and the orientation study is not so important for textile materials.

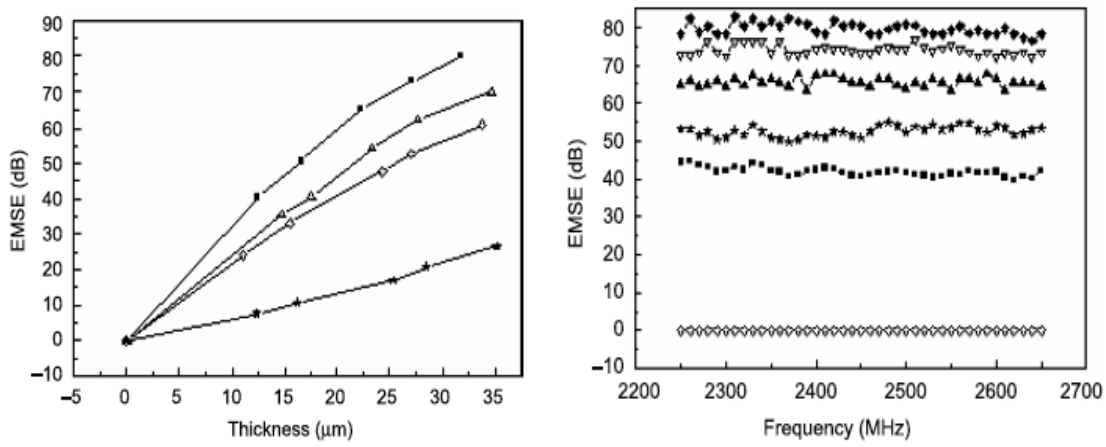

(a) (b)

Figure 9. (a) Thickness in μm versus EM SE in dB at 2.45 GHz frequency of ■ silver, Δ copper, ◊ aluminum, and * titanium-coated PET filament fabric and (b) Frequency (2.45 – 2.70 GHz) versus EM SE of silver-coated PET filament fabric at different thicknesses [47].

The copper-coated electroless plating on the chemical grafting method on modal plain-woven fabric was done in the study [48]. Grafting is a method for activating the nonconductive fabric surface with silver, gold, and palladium for metal deposition. The silver activation has the highest EM SE (40.3 dB at 1 GHz frequency) and electrical conductivity, among other activators. An autocatalytic copper coating is a technique used for electroless metal plating on fabrics. The plain weave polyester fabric is coated with copper at different concentrations to study this work's electrical and SE characterization [49]. At 11 g/l of copper sulphate concentration, the 128 MΩ/sq. of electrical resistivity and 40 – 50 dB of SE at 6 – 18 GHz frequency were obtained. Several processing parameters are also affecting the copper coating on fabric surfaces. In the study [50], the multi-step coating of copper on plain polyester fabric was done with scouring, rinsing, etching, catalyzation, acceleration, electroless Cu plating, and post-treatment for fixation. EM SE of the fabric was improved up to 50 dB at 100 MHz to 1.8 GHz frequency; also higher SE value was obtained at 1% surfactant concentration, 25 ºC surface etching, and 30 minutes of acid etching, 1:8 ration of $PdCl_2$:KCl activator, and 40 ºC acid activator. An increase in etching time, etching temperature, and activation temperature has decreased the fabric tensile strength and fabric drape stiffness results. This work noticed that the combined coating technique of electroplating and electroless plating of the textile fabric has the highest electrical conductivity and EM SE (52 dB at 1 GHz frequency) values [51]. From the above reviews, the copper-coated textile fabrics are achieving the SE of 50 dB approximately at a frequency range of 200 MHz to 18 GHz. Palanisamy et al. [3] studied the copper-nickel coated

Milife® nonwoven (Cu/Ni NW) fabric for EM SE. Figure 10 shows the frequency-dependent EM SE of single-layer fabric (SLF) and two-layer fabric (TLF) samples of Cu/Ni NW. TLF has the highest SE value of 74 dB at 1.5 GHz frequency, and the SE increases logarithmically with increasing frequency. For the SLF sample, the SE is about 52 dB at 30 MHz as well as at 1.5 GHz frequency; this result shows a 'very good' SE (see Table 1) for all measured frequencies.

Silver is an excellent electrical conductive metal with the antibacterial, antimicrobial, thermal conductor, and biocompatible properties. The silver is formed as nano-wire (NW) and coated on the fabric's surface in the study[52]. The AgNW/ polyvinyl butyral ethanol solution is used for the facile immersion method for coating a cotton-woven fabric. The coated fabric has a thickness of 1.4 mm, a density of 56 mg/cm^3, an SE of 55dB at the 5-12 GHz frequency range, and a specific SE (SSE) of 1053 dB.m^3/g was achieved. AgNW has very good features like less weight, higher conductivity, lesser surface area, and low density. Another study [53] in dip coating of AgNW on the cotton plain woven fabric was followed with Fe_3O_4 spray coating and dip coating of polydimethylsiloxane to control oxidation. The EMI SE of a coated fabric at 150 µm thickness coat has 60 dB, and 450 µm thickness coats have 101 dB at 8-12.5 GHz frequency. It was proved that this fabric has a passive heating ability with solar energy and is used as EMI shielding and thermal heater for humans. The chemical reduction of silver nitrate on cotton woven fabric on EMI SE was studied in this work [54].

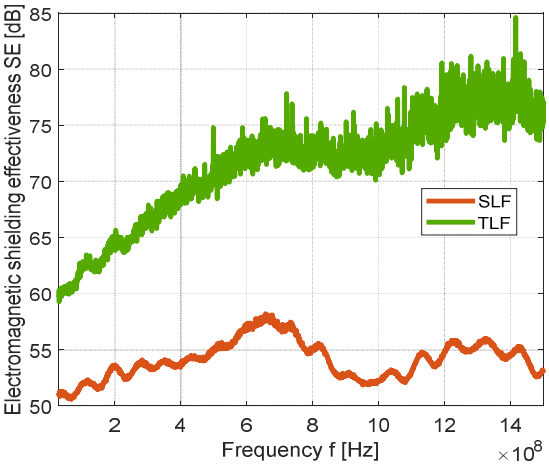

Figure 10. EM SE versus frequency of the Cu/Ni NW single layer (SLF) & two-layer (TLF) [3].

The coated fabric was gone under the sintering process at various temperatures, and the sintered fabric has improved in SE. At 225 ºC sintering temperature, the fabric has a higher SE of 19.2 dB at 1 GHz frequency and sheet resistance of 5.2 Ω/sq. The silver core weft yarn (Ag-coated PA filament core/ cotton sheath) and silver staple blended weft yarn (Ag-coated PA staple fibre/ cotton fibre) was 3/1 twill weaved with cotton warp yarn in this work [30]. The core yarn has a higher SE of 48 dB at 200 MHz frequency, and the blended yarn has 35.4 dB at the same frequency. The change in weft density has no significant effect on SE values for both kinds of fabrics. Silver has a higher conductivity compared with copper, and the above reviews have proved that silver-coated fabrics exhibit higher SE and electrical conductivity than copper-coated fabrics.

Other than copper and silver, many metals, alloys, and polymers are used as electrically conductive and EMI shielding materials. In recent research, MXenes material is attractive because of its higher electrical conductivity and heating capability. The two-dimensional metal carbides and nitrides have metallic conductivity and hydrophilic surfaces. The MXene-coated aramid nonwoven fabric has excellent flame retardant, EMI shielding, electrical conductivity, and electro-thermal properties reported in the study [55]. The single-layer coated fabric has an SE of 35 dB at 8-12 GHz frequency, and the double layer has 60 dB at the same frequency. The lowest sheet resistance of 4.36 Ω/sq. at 18.87 wt. % MXene and heating up to 263 ºC at a 5 V power supply was reported. The SE of 35 dB at 1.2 mg/sq.cm at 8 -12 GHz frequency and 900 S/m electrical conductivity of MXene-coated ramie fabric were achieved in this work [56]. The MXene polymer film with a thickness of 45 µm has an SE of 92 dB at 8-12 GHz frequency, and this study discovered the electrical conductivity of 4600 S/cm [57].

3.3.3. Carbon and polymer composites

Carbon is a non-metallic element and has higher tensile strength with moderate electrical conductivity. In the study [25], the carbon fibres roving fabric is used to form a carbon matrix composite, and its SE is 124 dB at 0.3-1.5 GHz frequency. The carbon fibre fabric with elastomer composite material has an SE of 73 dB (383 dB cm^2 g^{-1}), and tensile strength of 168 MPa was reported in this work [58]. In the study [6], the carbon nanotube/polypropylene composite was prepared and tested for EMI shielding. The SE of 36.6 dB at 8 GHz frequency and the absorption of EM radiation is around 75%, and the reflection is 25% on total shielding. The carbon material can absorb EM radiation, but

conductive metals reflect most of the radiation with lesser absorption. Graphene is a single-layer honeycomb carbon structure, and the multiple layers are called graphite. The graphene (GE) is coated on spun lace polyester nonwoven with the doctor knife method in the study [59]. The single-layer, double-layer, and triple-layer coating of GE on the fabric increase the EMI SE (25 to 32 dB at 1.4 GHz frequency) and electrical conductivity (0.2 to 0.7 S/cm), but the air permeability is decreased by two times. The graphene is also combined with other conductive materials to improve the electrical conductivity and SE of the final product. The graphene oxide with silver nanoparticle coated cotton fabric has SE of 27 dB at X-band frequency [60], GE/polyaniline nanocomposite SE is 51 dB at X-band [61], GE/ MWCNT plated on cotton knitted fabric exhibit an SE of 36 dB at 5.6-18 GHz frequency [62], and MXene/GE polymer composite has SE of 53 dB at X-band frequency [63]. The combination of two different conductive materials is improved in SE and electrical properties as well as mechanical properties.

Palanisamy et al. [64] tested the different forms of carbon preforms for EM SE. Carbon roving is laid at unidirectional (straight), bidirectional (cross and perpendicular), and quadri-directional and tested for EM SE and electrical resistance. Figure 11 shows the EM SE versus frequency graph of carbon preform fabrics. The perpendicular-laid sample has a higher SE from 200 MHz to 1 GHz frequency compared with a cross-laid sample. The quadri-axial laid sample has a higher SE of 59 dB at 1.5 GHz frequency and decreases as frequency increases.

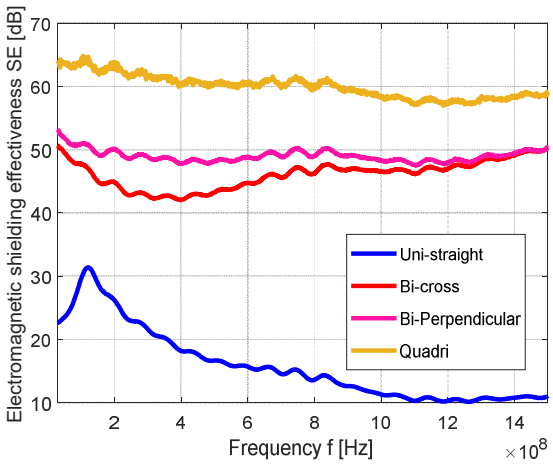

Figure 11. EM SE versus frequency (30 MHz to 1.5 GHz) graph of carbon fabrics [64].

There are some differences in the coating of conductive materials on the fabric surface and the coating on the yarn core. In the study [65], the MWCNT-COOH/ polypyrrole/ Fe_3O_4 were coated in the yarn core and yarn surface, as seen in Figure 12(c,d), and weaved as plain fabric. The core yarn was coated initially and spun with uncoated sheath yarn, as in Figure 12(a). The SE results of the surface-coated yarn fabric have 8 dB, and the core yarn-coated fabric has 5.8 dB at the frequency range of 8 – 12.5 GHz in Figure 12(b). The surface coating has a better effect compared to core coating in the yarn stage for EM SE applications. The core-coated fabric has good breaking strength and better comfort than surface-coated fabric. Electrically conductive polymers are used for textile and materials applications because of their special properties.

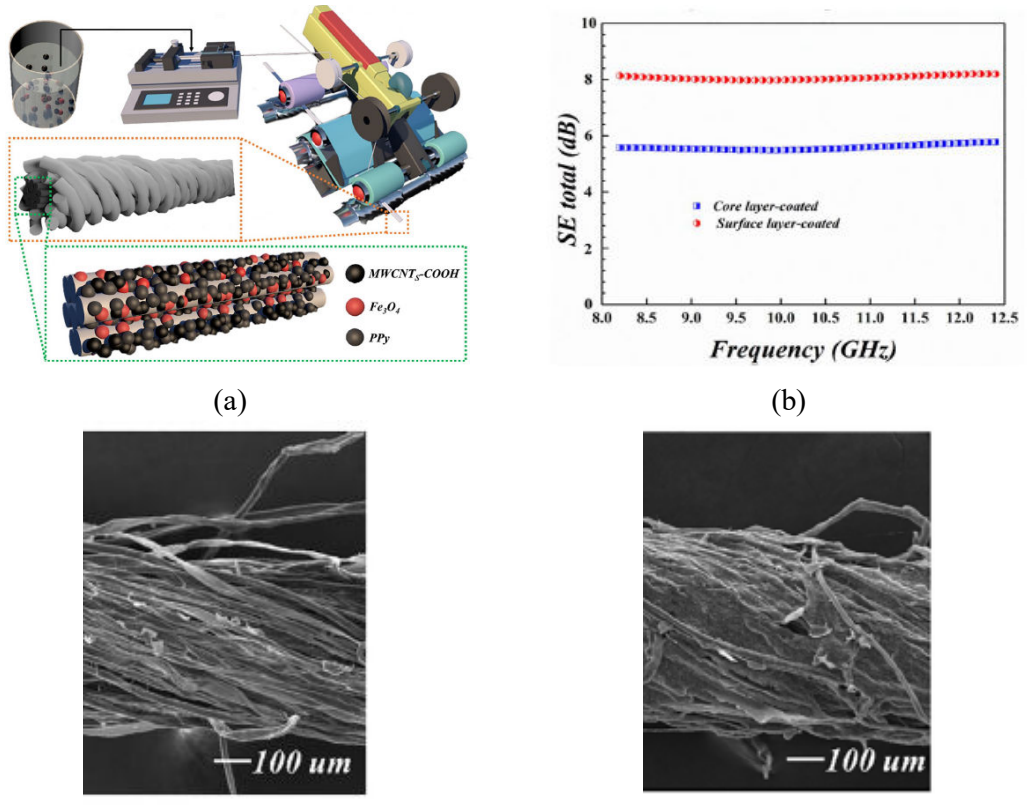

(a) (b)

(c) (d)

Figure 12. (a) Process of MWCNT-COOH/ polypyrrole/Fe_3O_4 coating of core yarn, (b) dependence of SE on frequency of MWCNT-COOH/ polypyrrole/ Fe_3O_4 core coated yarn and MWCNT-COOH/ polypyrrole/ Fe_3O_4 surface coated plain weave fabrics, (c) core MWCNT-COOH/ polypyrrole/ Fe_3O_4 coated yarn SEM image, and (d) surface coated yarn SEM image [65].

Polypyrrole (PPy) is a conductive polymer suitable for coating textiles, composites, metals, and glass materials. It is biocompatible with human tissue and has the advantage to use in medical applications. Textile substrates are easily covered with a PPy layer by immersion of the fabric in the polymerization solution containing pyrrole, an oxidant, and a doping agent [66]. The EMI SE of cotton fabric coated with PPy polymer (chemical polymerization) has 35 dB at a 1.5 GHz frequency, and electrical conductivity of 5.8 S/cm was recorded [67]. The polyester woven fabric is chemically coated with PPy, and the SE test results are around 28 dB at 1.5 GHz frequency, and absorption is higher than a reflection of EM radiation found in this work [68]. Polyaniline (PANI) is a conductive polymer that is biocompatible. In the study [24], PANI is coated on cotton, polyester, and nylon fabric with a chemical oxidation polymerization method. The coated cotton, polyester, and nylon have SE of 1.62, 2.78, and 1.5 dB, respectively, at 8-12 GHz frequency. The PANI is grafted on a nanohybrid structure with emulsion graft polymerization in the study [69]. The electrical conductivity of 0.4 S/cm and SE of 24 dB at the X-band frequency range was observed.

Palanisamy et al. [70] developed polypyrrole-coated cotton and polyester fabric for electrical conductivity applications. The pyrrole monomer was polymerized by the chemical oxidation method with ferric chloride as an oxidizing agent and tetra-ethyl ammonium p-toluene-sulfonate as a doping agent. The polypyrrole polymer was prepared by in-situ chemical polymerization method to coat polyester and cotton fabric samples. Figure 13 shows the dependence of electrical resistivity, ρ on monomer concentration, C of PPy-coated polyester and PPy-coated cotton knitted fabric samples. The electrical resistivity, ρ of polyester-coated fabric, decreases with increasing monomer concentration, C, until 0.7 C; after that, it increases shown in Figure 13(a). The electrical resistivity, ρ of cotton-coated fabric, decreases with increasing monomer concentration, C, and then increases after 0.7 C, as shown in Figure 13(b). The optimal C value is 0.4 and 0.7 for polyester and cotton fabrics material. Those PPy-coated fabrics will shield EM radiation moderately because the PPy coat has less conductivity.

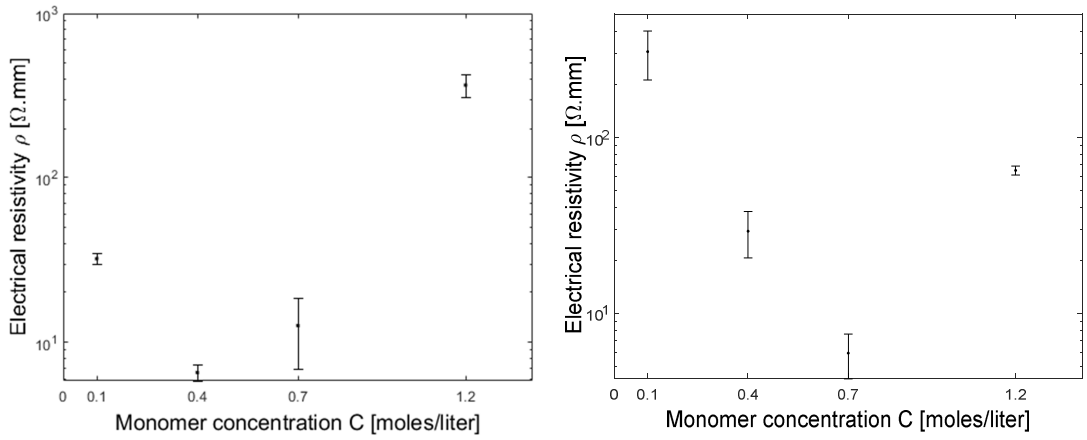

(a) (b)

Figure 13. Electrical resistivity versus monomer concentration of (a) polyester coated fabric and (b) cotton-coated fabric samples [70].

3.3.4. Effect of moisture content on EM SE

It follows from the conducted literature research that very few studies have evaluated the moisture content on EM shielding property, and there are fewer in textile materials. The moisture content on textiles varies from material to material; for example, the moisture content (%) of linen, cotton, viscose, wool, PES, and glass are 10.5, 7.5, 10, 14, 0.3, and 0%, respectively, at $T = 21\pm2$ °C and a relative humidity $RH = 65\pm5$ % [71]. Specifically, there is no work showing the effect of the moisture content of non-conductive textile materials on EM SE. Palanisamy et al. [2] studied the effect of moisture content using different liquids on the SE of non-conductive fabrics. Greater attention is dedicated to shielding of frequencies around 1 – 1.5 GHz because these frequencies are close to the operating frequencies of many electronic devices (cell phones, radars, and wireless routers). Identical methodology, more precisely, the coaxial transmission line method, according to the ASTM D4935-10, was applied to the whole sample set to avoid difficulties when comparing data gained by different measurement methods.

Distilled water, acidic sweat, and alkaline sweat solutions are three liquid mediums used in the study, and their measured electrical conductivity was 0.0016, 9.29, and 10.29 mS/cm, respectively. The sweat solutions had 50 times higher electrical conductivity than distilled water. The cotton and polyester fabric samples were treated with distilled water and artificial sweat solutions for 1 hour. The sample was then squeezed using three different pressures, and three different drying times were used to determine the moisture content (MC) [%] for the tested samples. The SE results depending on MC are shown in Figure 14.

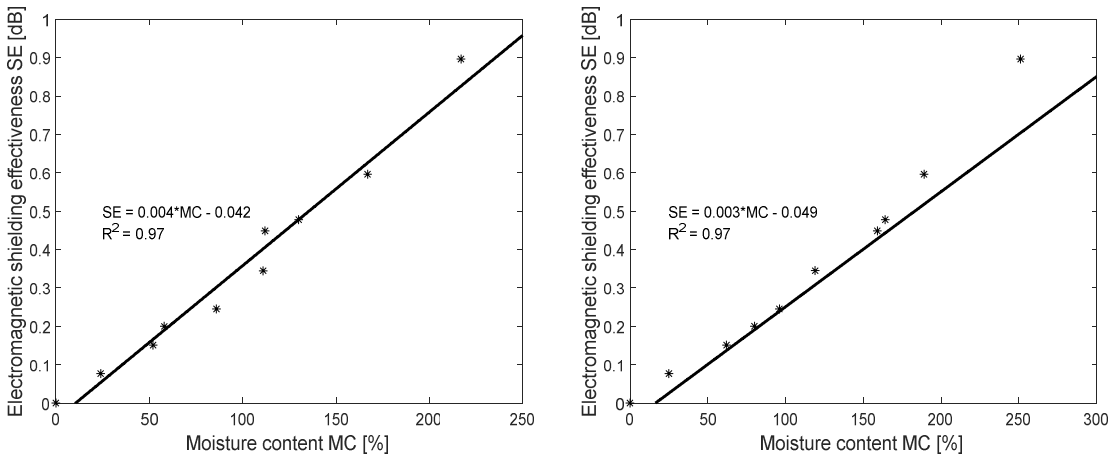

(a) (b)

Figure 14. Dependence of EM SE (*f*=1.5 GHz) [dB] on moisture content [%] of sweat solution treated (a) cotton fabric and (b) polyester fabric [2].

Figure 14 shows the EM SE [dB] at 1.5 GHz frequency versus moisture content (MC) in percentage graph of the artificial sweat-treated cotton and polyester knitted samples. Figure 14(a) shows the SE increases with increase in MC for cotton (COT) fabric sample treated with sweat solution. The linear dependence of SE on MC was noticed and its R^2 is 0.97. The sweat-treated samples containing MC [%] of 217, 111, and 24 have a SE of 1.1, 0.3, and 0.1 dB, respectively, at 1.5 GHz. Figure 14(b) shows the SE versus MC graph of the polyester (PES) fabric sample treated with sweat solution. The SE at 1.5 GHz increases with increase in MC in the polyester samples. The linear dependence of SE on MC was very good and its R^2 is 0.97. The sweat-treated samples have higher SE values at 30 MHz compared with 1.5 GHz. The sweat-treated samples containing MC [%] of 251, 119, and 25 have a SE of 0.9, 0.3, and 0.1 dB, respectively, at 1.5 GHz.

During the measurement, it was also found that the PES has a faster evaporation rate of the liquid medium at room temperature (RT) than COT; because the PES is hydrophobic and COT is hydrophilic. PES initially holds more moisture than COT because PES holds more fluid in-between yarns. The hydrophobic nature of PES tends to adsorb fluid on its surfaces, which leads to more moisture. The PES and COT MC at RT were also 0.3 % and 7.5 %, respectively. The sweat solution treated PES and COT samples have slightly higher SE (at all frequency ranges) than distilled water treated samples because the sweat solution contains 5 g/l of Na+ Cl− and it acts as a semi-conductor, which is why the sweat solution treated samples has a higher SE than distilled water treated samples at a higher frequency range.

EM shielding versus frequency results shows that the cotton treated with sweat has the highest shielding, e.g., 1.1 dB at 1.5 GHz. At all liquid media, the lowest MC in the material has a higher SE at 30 MHz, and the higher MC in the material has a higher SE at 1.5 GHz. The rate of drying of polyester is faster than cotton because of its hydrophilic nature. However, the SE of moisturized non-conductive textile materials was very low compared with electrically conductive textile materials. A limitation of this work is that only the variability of SE within the material was considered. The textile structures made of conventional fibres are in a dry state, practically transparent to the EM field. EM SE of nonconductive samples is less than 0.1 dB at a frequency range from 200 MHz to 1500 MHz, regardless of material composition. This statement was supported by very high measured electrical resistance values of traditional fabrics lying in the range of insulators. This study proved that by wetting the sample it is not possible to increase the ability of the sample to shield the electromagnetic field to the level of specially created samples containing, for example, electrically conductive fibers.

3.3.5. Comparison of SE of different conductive textiles materials

There is a large amount of information to be found in the literature on the development of new electromagnetically shielding textiles. The authors use different electrically conductive additives and create electrically conductive textiles of different structures. In addition, authors often use different measurement approaches to evaluate the electromagnetic shielding efficiency, while it is known that it is not possible to compare the SE of samples evaluated by different methods.

In this context Palanisamy et al. [1] compared the different conductive textile materials for EM SE. The comparative study helps to identify the best suitable material and structures for the area of use. That is why a relatively broad spectrum of samples (with different material compositions and structures) was used. The conductive textile samples were based on the usage of several types and quantities of the conductive component (metal-coated fibres, metal-coated fabrics, and metal fibre-containing yarns) and different structural approaches (woven, knitted, nonwoven) and were evaluated by the identical measurement method. The influence of fabric structure (woven, knitted, nonwoven), electro-conductive techniques (metal coating and metal-coated fibres), and conductive components on SE were studied. Different types of industrially produced materials having woven (W), knitted (K), and nonwoven (NW) structures were compared. Two categories were distinguished among the

19 samples based on similar types of material: metallic coating on fibre (Mf) and metallic coating on yarn or fabric (Mc).

In the Mf category, there are eleven samples which consist of two nonwoven fabrics produced with copper (Cu) / silver (Ag) coated on acrylic (PAN) fibre (brand name Eurostatic) blended with PES fibre in the ratio of 20:80 and 14:86 respectively; a nonwoven fabric with the composition of 20 % stainless steel (SS) fibre (d = 8 μm, trade name Bekinox) and 80% PES staple fibre and a plain weave woven fabric fully made-up of 100% Ag coated PES fibre spun yarn (trade name X-Static). Four different types of metal-coated fibre fabrics are included in the Mf category, which consists of five woven fabric samples made of hybrid yarns (H) consisting of SS fibre (d = 8 μm, Bekinox) and polypropylene (PP) fibre blended in different compositions of SS fibre (% of 10, 20, 40 & 75) blended with PP fibre (% of 90, 80, 60 & 25) respectively. Three knitted samples of single jersey (Ks/j) fabrics were produced by a hybrid yarn with different ratios of SS fibre: PP fibre is 10:90, 15:85, and 20:80. All the hybrid (H) yarn fabric samples were made-up of 50 tex yarn for woven fabrics and 25 tex yarn for knitted fabrics. The Mc sample set represents eight metal-coated samples which consist of two woven rip stop fabrics, one fabric having Ag plated nylon yarn (trade name Breman) and another fabric having Cu/Ag plated nylon yarn (trade name Kassel); three warp knitted fabrics made up of Ag plated nylon yarn with elastane filament (trade name Ballinger and Technik-Tex); two wefts knitted sample made up of Ag plated nylon yarn with modal and elastane blend (trade name Modal knit and Jersey Modal). The carbon (Ca) woven fabrics, knitted double jersey (Kd/j), SS yarn woven grid (WG), CuS-Ag coated PAN fiber yarn (Eu) NW and Aluminum foil (F Al) are other samples tested for EM SE. Some of the microscopic images of conductive fabric with its codes are shown in Figure 15.

Figure 16 shows the EM SE values measured at 1.5 GHz frequency of all the electro-conductive samples in ascending order for easier comparison. The textile materials are classified into five grades to rate the EM shielding [13]; see Table 1 and Table 2. Detailed information about sample set can be found in paper [1].

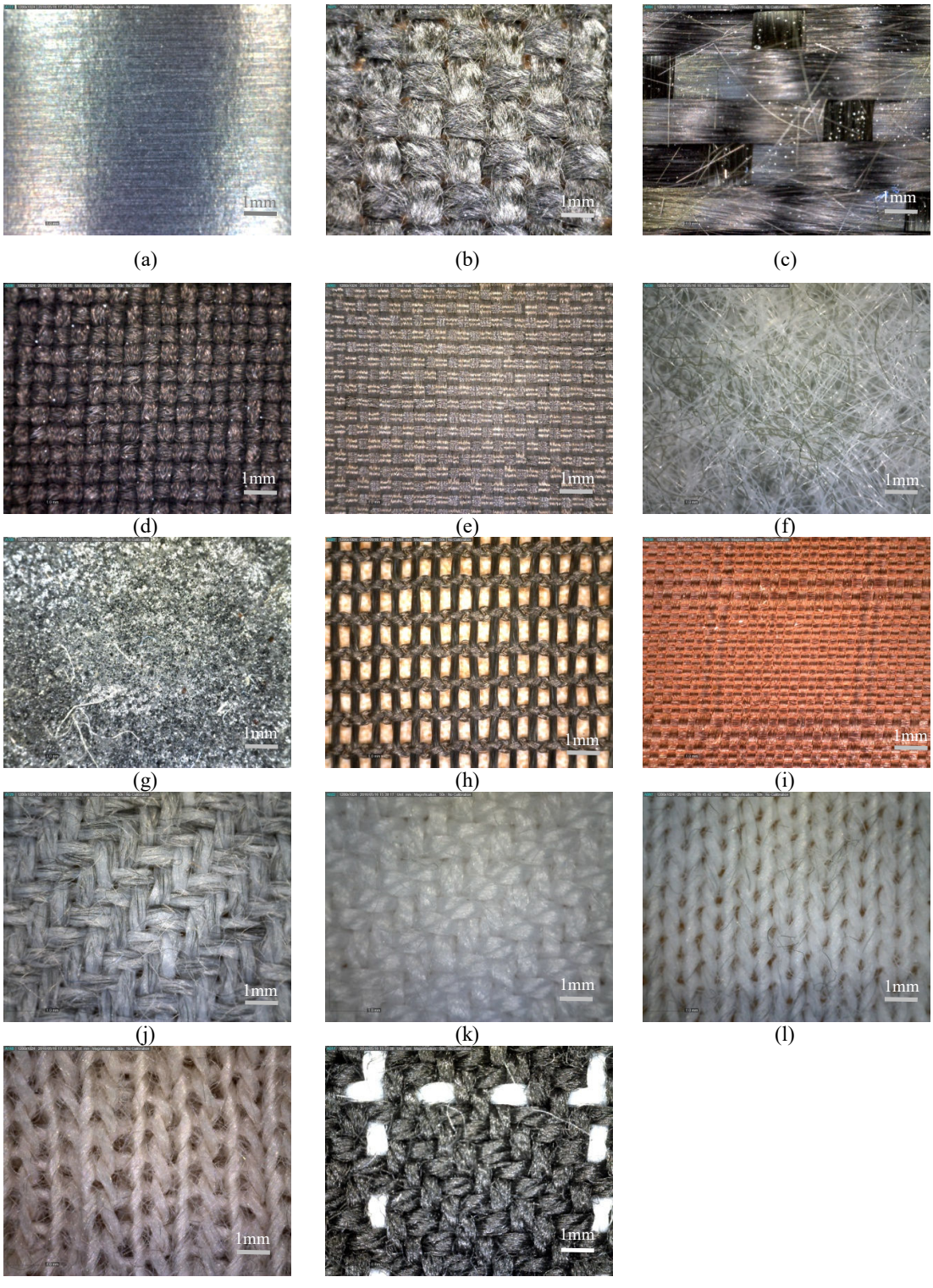

Figure 15. Microscopic images at 50x magnification of electrically conductive sample set. (a) Aluminum foil, (b) "Ca W 1", (c) "Ca W 2", (d) "PPy/PES W", (e) "Mf Ag W", (f) "Mf 20Eu NW", (g) "Mc Al NW", (h) "Mc Ag K", (i) "Mc Cu/Ag W", (j) "H 20SS W", (k) "H 1SS W", (l) "H 15SS Ks/j", (m) "H 10SS Kd/j", (n) "H 10SS WG" [1].

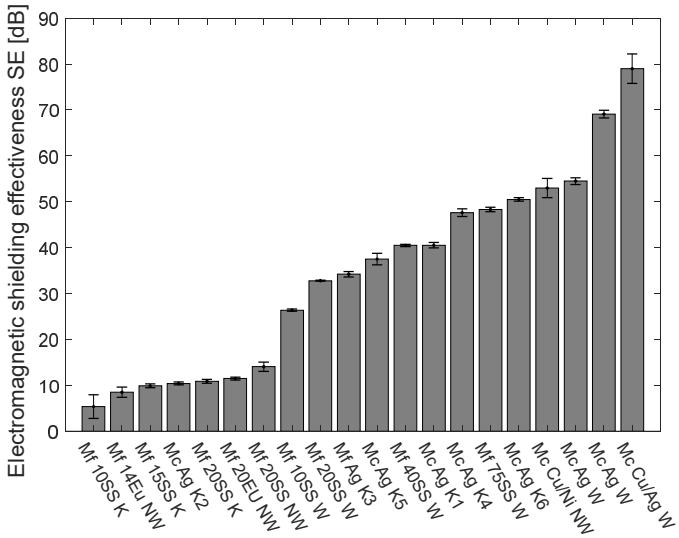

Figure 16. Comparison of mean values of the EM SE at 1.5 GHz frequency for electro-conductive samples in ascending order [1].

It can be observed that a very low shielding (< 10 dB) is provided by the knitted sample where the electro-conductive mesh is created by the hybrid yarn containing only 10 % of the SS (Mf 10SS K) and by the nonwoven samples blended with Eurostat fibre of 14% (Mf 14Eu NW). In the case of the hybrid fabric containing only the conductive mesh, the portion of the SS fibre is too low to get over the percolation threshold of the conductive component and also for nonwoven. Electromagnetic shielding effectiveness ranging from 10 to 20 dB is provided by the knitted samples with 20 % content of stainless-steel fibres (Mf 20SS K), by the knitted sample with 21 % of Ag fibres (Mc Ag K), by the nonwoven sample which containing different stainless-steel fibre content (Mf 20SS NW), by the nonwoven fabrics containing up to 20 % of Eurostatic fibres (Mf 20Eu NW). Mentioned values of shielding effectiveness match to the Good grade in case of general use, but it is unsatisfactory for professional use. Electromagnetic shielding effectiveness within the range of 20 to 30 dB (accordant with a Very good grade for general use, Fair grade for professional use) can be reached by the woven samples made of 10 % SS hybrid yarn. Electromagnetic shielding effectiveness within the range starting from 30 to 60 dB (corresponding with Excellent grade for general use, from Moderate to Very good grade for professional use) can be achieved by the woven fabric samples totally made of hybrid yarn with the SS fibre content higher than 10%, fabric with 85 % to 95 % silver coated knitted and woven fabrics. Electromagnetic shielding higher than 60 dB (satisfying an Excellent grade for both general and professional requirements) is guaranteed by usage of the coating of traditional fabric by a combination of 10% Ag/Cu or Ag and the woven (Mc Cu/Ag W).

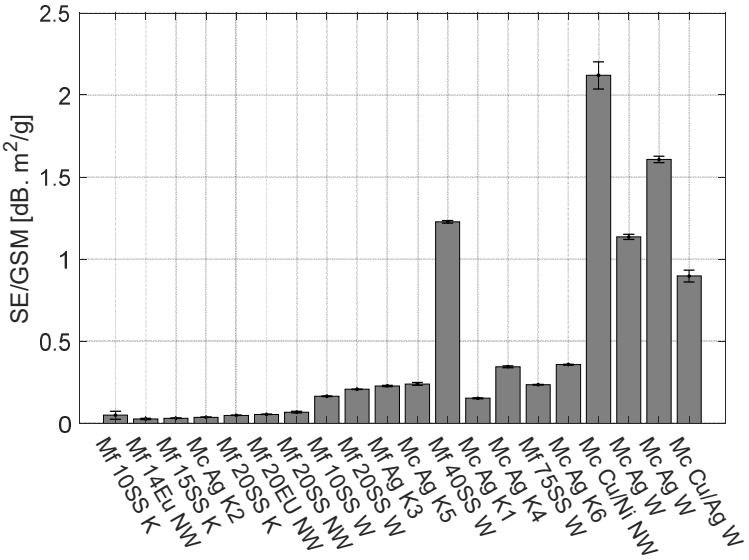

Figure 17. Comparison of the EM SE/GSM at 1.5 GHz frequency for electro-conductive samples [1].

Figure 17 shows the electromagnetic shielding divided by mass per unit area for the whole sample set at 1.5 GHz frequency. The SE/GSM gives exactly the electromagnetic shielding effectiveness per weight of the sample. Sample Mc Cu/Ag W is showing the highest SE from the sample set, namely 79 dB at 1.5 GHz frequency, but its relatively high GSM degrades its SE/GSM value to 0.9 dB m^2/g. For knitted and nonwoven fabrics, the SE/GSM is lower because the fabric mass per unit area is higher and also because of its structure. Sample Mc Cu/Ni NW has the highest SE/GSM value, namely of 2.12 dB m^2/g due to its low GSM (25 g/m^2).

Effect of electrical resistivity on SE

It is well known that the SE increases as electric conductivity as well as permittivity of shielding material increases based on the EM shielding theory, but there is a lack of experimental verification and exploration of this dependence for heterogeneous fibre-based structures with different material compositions and structures. In addition, direct measurement of fabrics EM SE needs special devices compared to measurement of electrical properties, and therefore, utilization of the presumption that the electrical part of the EM field dominates for sufficiently high frequencies seems to be helpful. Knowledge of the electrical characteristics, which are easily measurable, could be therefore used for the prediction of sample shielding ability. That is why the correlation between surface and volume resistivity on EM shielding efficiency is studied. The dependence of EM SE on

surface and volume resistivity for the whole sample set studied in [1] is shown in Figure 18(a,b). It is possible to observe a trend that says that a decrease in the electric resistivity of the sample (i.e. increase in the electric conductivity) is connected with an increase in its electromagnetic shielding ability. However, a few outliers behaving differently from this trend are traceable. One of them is an aluminum foil sample (marked "F Al") having a very high surface and volume resistivity (due to lamination on both sides of the sample by a nonconductive layer) but showing EM SE of 78 dB at 1.5 GHz frequency (due to high conductive aluminum foil core). Out of the trend are also sandwiched woven samples ("H 1SS Ws2", "H 1SS Ws3", "H 1SS Ws4" and "H 1SS Ws5") created by multiplying the same woven fabric. They show no change in surface resistivity and uneven changes in volume resistivity values accompanied by an increase in shielding effectiveness caused by the increased thickness of the sandwich.

Figure 18(a,b) shows the dependence of electromagnetic shielding effectiveness on electric resistivity for the sample set (outlying samples described above were removed) approximated by the power function shown (solid line in the graph). When observing coefficient of determination $R^2 = 0.84$ and $R^2 = 0.48$ for the dependence of electromagnetic shielding effectiveness on surface and volume resistivity, it can be concluded that the surface resistivity has better prediction ability compared to volume resistivity and, therefore, for sufficiently high frequencies are adequate to measure only the electrical characteristics especially based on surface conductivity. The prediction ability of this model is restricted to samples without an insulating layer.

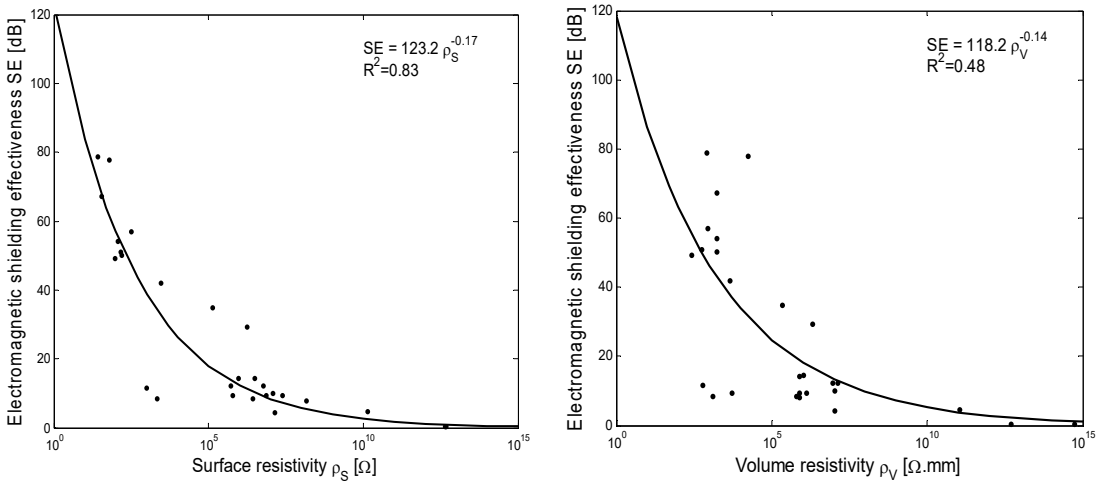

(a) (b)

Figure 18. Dependence of SE (f = 1.5 GHz) on: (a) surface resistivity [Ω], (b) volume resistivity [Ω. mm] [1].

Air permeability of the conductive samples

Besides functionality (electromagnetic shielding ability), air permeability of the sample is very important property for various applications like the development of protective clothing, breathable garments, curtain cloths, seat or interior covers, and electronic devices covers to be able to transport heat or air humidity out etc. Figure 19 shows the bar chart of air permeability values [l/m^2/s] for conductive samples set plotted in ascending order together with information about their functionality – electromagnetic shielding ability. The air permeability parameter is mainly dependent on the structure and porosity of the sample. In general, the nonwoven and knitted structures are more open (more porous, having lower packing density) than woven structures. It is notable that even if Al foil samples have very high shielding ability, they show no air permeability (A = 0 l/m^2/s) because of the presence of no gaps in the foil. This fact is very limiting for many applications. For hybrid yarn woven samples ("H 10SS W", "H 20SS W", "H 40SS W" & "H 75SS W"), with an increase in the percentage of metal fibre content (10, 20, 40 & 75 %), air permeability increases (from 130 to 1200 l/m^2/s) due to higher density of metal fibre and therefore lower yarn diameter containing metal fibres compared to the diameter of yarn totally made of polypropylene fibres. Copper and aluminum painted nonwoven ("Mc Cu NW" & "Mc Al NW") samples are less permeable to air (A < 80 l/m^2/s) than the metal fibre incorporated nonwoven samples ("Mf 20Eu NW", "Mf 14Eu NW" & "Mf 10SS NW"), where A~ 1000 l/m^2/s. Metal particle paint coating on the surface of nonwovens fills the pores of the sample, and therefore paste coated samples become less permeable to air. Metal-coated yarn knitted sample ("Mc Ag K") shows the highest air permeability value (A = 4820 l/m^2/s) of all samples, because of its low thickness, more open structure, and also by that metal coating is applied onto the yarn surface, which is not reducing the porosity of the sample significantly. As expected, with the increasing number of layers of sandwich samples (H 1SS Ws1, H 1SS Ws2, H 1SS Ws3, H 1SS Ws4 & H 1SS Ws5), air permeability decreases because of higher thickness and also because of the fact that one layer above the other can cover the pores of preceding layer and blocks the direct path of air.

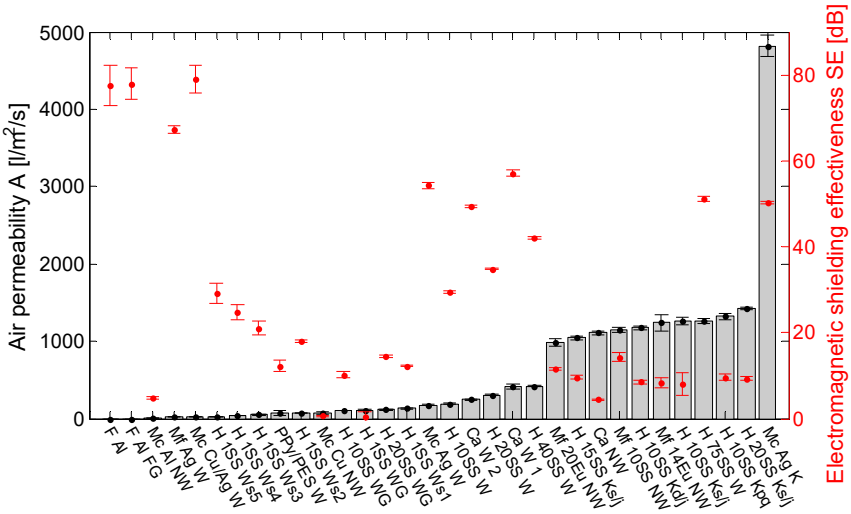

Figure 19. Combined graph of air permeability and EMI SE of conductive samples [1].

Figure 20 shows the dependence of mean values of air permeability (A) on the metal fibre content percentage (P) for woven samples totally made of hybrid yarns. Results show that air permeability increases linearly (from 134 to 1262 l/m^2/s) with the increase of metal fibre content (from 1 % to 75 %). The dependence of A on P can be simply approximated by line. The solid line in the graph corresponds to the linear regression model with parameters obtained by the minimizing sum of squared differences. Correlation coefficient of 0.96 refers to a very good positive fit, and therefore air permeability increases as metal fibre content in the hybrid yarn increases. It should be mentioned that, the proposed model is valid for a given metal fiber content. This phenomenon is becaused of the metal fibres are finer compared to polypropylene fibres and yarns with higher metal fibre content have lower diameters compared to yarns with lower metal fibre content. By using yarns with lower diameters while remaining other parameters of woven fabric constant, larger pores are created in the structure of the fabric, which allows easier penetration of both air (air permeability) and water vapor (water vapor permeability).

EM SE of textile structures containing different content and different type of conductive components ranges from 1 to 79 dB at a high-frequency range. The ability of the material shield EM field can be controlled by the proper choice of conductive component type, its content, and placement. That‘s why the best results are provided by samples made of metal-coated yarns or fibres (even if the GSM and air permeability are taken into account) having SE in the range of 50 to 80 dB, which means “very good” grade even for professional use according to specific requirements for EM shielding textiles.

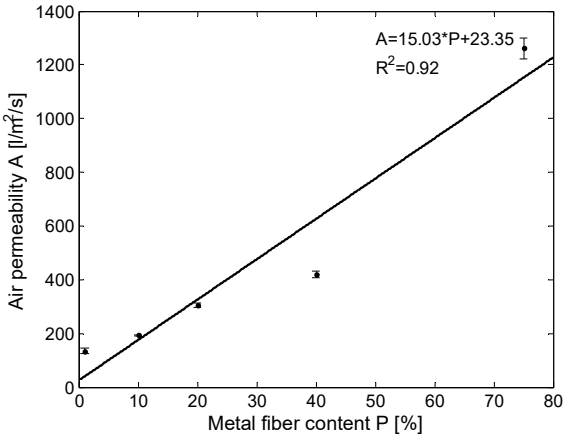

Figure 20. The dependence of air permeability A [l/m^2/s] on metal fibre content P [%] for woven samples: "H 10SS W", "H 20SS W", "H 40SS W" and "H 75SS W" [1].

Almost frequency-independent SE of metal-coated textile structures is also very favorable, which guarantees constant shielding on a given frequency range. The only drawback is their metallic appearance and handle. Aluminum foils offer very good shielding ability having 78 dB, but the zero air permeability, together with their handle and mechanical properties, is very restrictive for many applications. Samples made of hybrid yarns (containing staple stainless steel fibre), especially woven fabrics, also represent a promising approach. EM SE of these hybrid fabrics varies between 10 dB and 50 dB depending on their structure and metal fibre content which ranks them up to "Good" grade for professional use [13]. Woven fabrics made of carbon roving also show very good performance and sufficient air permeability, but they are not appropriate for usage like traditional fabrics at all. Their usability can be seen as reinforcement for composites.

Other material approaches such as coatings of nonconductive substrates with conductive polymers, treatment of nonconductive substrates by metal particle filled pasts, incorporation of carbon particles in the nonwoven structures, or incorporation of conductive fibres in bulky nonwoven structures do not seem promising, especially in the light of their lower functionality (EM SE). The shielding ability results of the material were supported by measuring the ability of a material to conduct electric current. It was found that surface resistivity can be used for the prediction of sample EMI shielding ability due to a strong indirect relationship (R^2 = 0.83) between these two parameters. The power function model can be used for the prediction of electromagnetic shielding effectiveness of newly developed material based on the knowledge of its surface resistivity.

3.3.6. Effect of apertures on EM SE

From the theoretical analysis, it follows that SE can be easily estimated based on the knowledge of the electrical conductivity of the material, the thickness of the sample and the frequency [72]. These relations apply assuming the compact sample without the presence of any discontinuities. In reality, however, this condition is very difficult to achieve. In the textile area, these discontinuities are caused by the open porous structure of the fabric, in addition this phenomenon can be also caused by for example connections, incl. seams. All the mentioned holes and pores significantly reduce the SE of the product. For high frequencies the shielding efficiency of the material itself is even less important than the attenuation caused by discontinuities (holes, cracks).

That is why, Palanisamy et al. [3] studied structural parameters of samples affecting the EM SE. Instead of using the textile structures directly, the copper-coated nonwoven fabric was cut into strips and samples with different pore types were created to evaluate the effect of the contact points, pore size, and pore shape described by laying angle on EM SE. Hence, the strips are laid like the yarns intersection in woven and knitted structures to simulate the textile structures. The nonwoven strips are formed with three factors: strip thickness, the gap between the stripes, and the angle between the two layers of strips at three levels (low, medium, and high). Two-layer strips were formed perpendicular to each other at three angles, similar to textile woven and knit structures for the EMI shielding test. Findings from this work could help construct the textile materials with minimum material use as per the required level of EM shielding.

Many studies are about the effect of EM SE on the gap between the conductive material in textile structures, but there are very few studies for the gap between and angle of laying conductive material in textile structures [36] [73]. In the study [3], the 'Cu/Ni NW' sample is cut into strips at 3, 6 & 9 mm thick and laid with 3, 6, & 9 mm gaps between each other. Each thickness of strips was laid at the above gaps and formed a single layer of the sheet, as shown in Figure 21, and with the help of CREO® CAD, the graphical model of strips was created. For example, the single layer 3 mm thick strip was laid at 3, 6, & 9 mm gap as shown in Figure 21(a-c). Likewise, 3 mm thick strips, 6 mm and 9 mm thick strips were laid at 3, 6, & 9 mm gaps. Two-layer strips were formed by laying two single-layer strips at 90˚, 45˚ & 30˚ angles with the same gap; 9 mm thick strips of 3 mm gap laid at 90˚, 45˚ & 30˚ angles are shown in Figure 21(d-f). Also, 9 mm thick strips of 6 mm and 9 mm gap are laid at 90˚, 45˚ & 30˚ angles to form two-layer strip samples. Likewise, 9 mm thick strips, the 3

mm and 6 mm thick strips were formed as two-layer strip samples with various gap and laid angle. The two-layer samples were taken for the EM SE test as per ASTM D 4935 method to analyze the effect of gap between and angle between the conductive strips' material on the total SE. Each thickness of the strips was laid in 9 different ways and tested for EM SE. So, a total of 27 samples were prepared from the combination of strip thickness, gap between the strips, and angle between the two layers of strips for testing EMI shielding and the sample codes or names are given in Table 3. The overlaying of the strips at various angles is prepared with the same strip thickness as well as the same gap between the strips as shown in Figure 21(d-f).

Table 3. Cu/Ni NW sample and its code.

No. of layers	Angle of layers [˚]	Strip thickness [mm]			Gap between the strips [mm]
		3	6	9	
One	0	SS30	SM30	SL30	3
		SS60	SM60	SL60	6
		SS90	SM90	SL90	9
Two	30	TS330	TM330	TL330	3
	45	TS345	TM345	TL345	
	90	TS390	TM390	TL390	
	30	TS630	TM630	TL630	6
	45	TS645	TM645	TL645	
	90	TS690	TM690	TL690	
	30	TS930	TM930	TL930	9
	45	TS945	TM945	TL945	
	90	TS990	TM990	TL990	
Single-layer of fabric				SLF	
Two-layers of fabric				TLF	

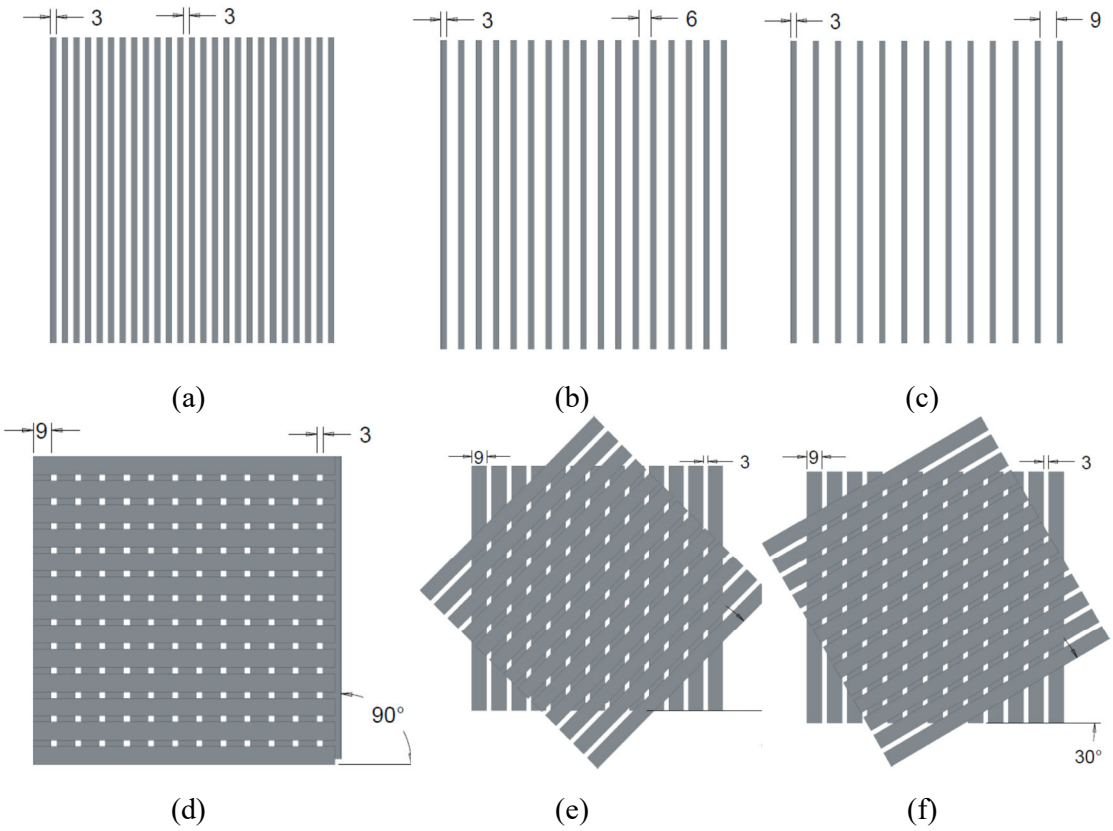

Figure 21. A graphic image of the single-layer Cu/Ni NW strips of 3 mm thickness at a distance (a) 3 mm, (b) 6 mm, and (c) 9 mm and two-layer Cu/Ni NW strips of 9 mm thickness laid at (d) 90˚ (e) 45˚ and (f) 30˚ angles [72].

Screening factorial design (SFD) was chosen to completely and systematically study the interaction between factors in addition to identifying significant factors. In this experiment, there are three variables and three levels used to design an experimental study. The factors and levels of the factorial design are listed in Table 4. The factorial experimental design was analyzed using Minitab® software.

Table 4. Factors and its levels used for SFD.

Factors	Levels			Response
Strip thickness (A)	-1	0	+1	EMI SE [dB]
Gap between the strips (B)	-1	0	+1	
Angles of layers (C)	-1	0	+1	

The variable levels are mentioned in '-1' as lower, '0' as a medium, and '+1' as a high value for response. The strip thickness and gap between the strips level are 3 mm, 6 mm, and 9 mm, mentioned as lower, medium, and higher. For laid angles of strips at 30˚, 45˚, and 90˚ are mentioned as lower, medium, and higher levels.

Effect of the cover area of strips on EM SE

The cover area of the two layers of strip samples was calculated using models (see Figure 21). Figure 22 shows the EM SE [dB] versus the percentage area covered by the strips (A_c) [%] for all two layers of strip samples. The SE versus A_c of the TS samples is shown in Figure 22(a), in which the strips laid at an angle of 90˚ have higher SE values than 30˚ and 45˚. Figure 22(a) shows the coefficient of determination (R^2) above 0.99 of linear model, which means the predictability of SE value is highly accurate with the cover area (A_c). Variation in SE for the same coverage area occurred because of the higher area per aperture for 30˚ and 45˚ laying angle of strips compared with 90˚ angle. For example, the calculated area per aperture for 30˚ and 45˚ laying angles of the TL9 series sample has 93.42 mm^2 and 114.48 $mm^{2,}$ and for 90˚ laying, the angle has 81 mm^2 per aperture. In the same case of TS samples, SE value variation is seen for the TM and TL samples, but the SE of the TL series has a higher value compared with the TM series and TS series for the same angles. At all angles, the TL series samples have higher A_s compared with TS and TM series samples; TL390 samples have 93 % cover area compared with TS390, and TM390 has 75 % and 88 % cover area. Also, the cover area increases by a decrease in the gap between the strips; TL990 has a 75 % cover area compared with TS390 having a 93 % cover area. Figure 22(b) shows the combined graph of EM SE versus the percent cover area of TS, TM, TL series, and SLT samples. SLT sample has a 100 % cover area, and it has the highest SE of 53 dB. In general, the SE increases with an increase in the cover area, but for the same coverage area, there can be different SE values. This is because of the aperture area variation. In this case, the higher aperture area has slightly less SE than the lower aperture area, and it can be seen in all the readings in Figure 22. From the linear regression analysis shown in Figure 22(b), SE increases with increasing cover area, and the R^2 is 0.75. The prediction of SE with respect to the cover area for this model is average.

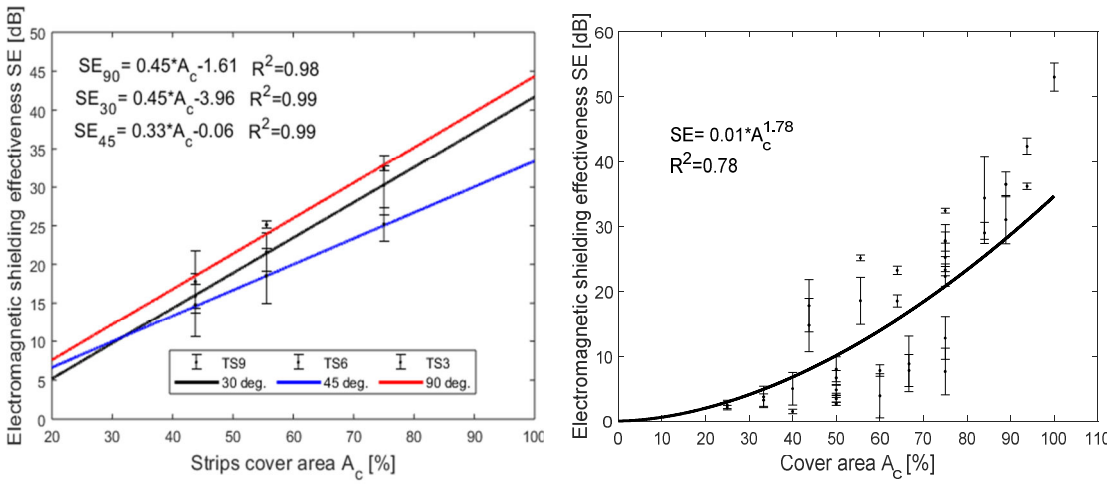

Figure 22. Dependence of EM SE [dB] at 1.5 GHz frequency on cover area (A_c) [%] of (a) TS samples and (b) one-layer, two-layer strip samples, and SLF samples [72].

Area per aperture at different laying angles and its effect on SE results

Beyond the cover area of the strip samples, another factor that influences the SE value is the area per aperture (A_a) or open space in the samples. The cover factor graph (Figure 22) shows that the same percent cover area has different SE values. After analyzing the images (Figure 21), the number of aperture and area of aperture vary for each angle of layering. So, the EM SE at 1.5 GHz frequency versus area per aperture was plotted and statistically analyzed, and it is shown in Figure 23. SE versus A_a of TS samples is shown in Figure 23, whereas SE is increasing with a decrease in area per aperture, and the regression model has a coefficient of determination of 0.91 for the exponential trend line. Regression analysis proves that SE is also influenced by area per aperture. Irrespective of the thicknesses of the two layers of strip samples, the laid angle varies the area per aperture; at 90˚ angular laid strips have very less A_a compared with 45˚ and 30˚ laid angles. The maximum A_a is achieved at a 45˚ laid angle of strips, and it registered lower SE compared with other laid angles. Other results noted in the study show that the increases in the gap between strips also decrease the SE value.

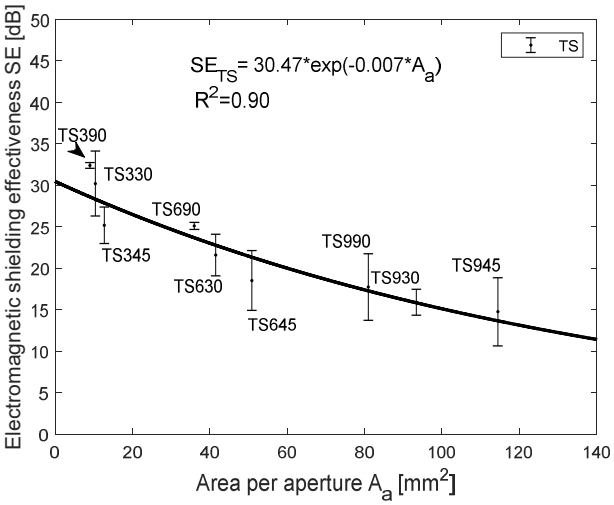

Figure 23. Graph of shielding effectiveness (SE) [dB] at 1.5 GHz frequency versus area per aperture (A_a) [mm^2], two-layer strips [72].

Equation 10 shows the regression equation in terms of uncoded units of the SFD model, SE value is predicted with the help of this regression equation, and R^2 for prediction is 92.23% which proves that the predictability of SE is highly possible.

$$SE = 23.29 + 4.331\ A - 6.498\ B + 2.231\ C - 0.780\ A*A + 0.901\ B*B + 4.464\ C*C + 0.323\ A*B + 1.016\ A*C - 0.544\ B*C \quad \text{Eq. 10}$$

The standardized effects and Pareto chart of the factors and their combinations are represented in Figure 24 at a 5% significance level ($\alpha = 0.05$) for SE at 1.5GHz frequency. In the Pareto chart (Figure 24(b)), standardized effect values of the significant factors and their interactions are higher than the critical value. Although; the Pareto chart is helpful in comparing the absolute value of the effects of each factor and its interactions with the considered SFD, a normal plot of the standardized effect is used to determine the significance and insignificant of each effect of factors more accurately. The factors with a significant difference in SE value are plotted in red marks, and factors without significant difference are plotted in blue marks, as seen in the graph (Figure 24(a)). In a normal probability plot of effect (Figure 24(a)), factors A, C, AC, and CC have a significant positive effect on SE, and factor B has a significant negative effect on SE. Among positive effects, the thickness of the strips (A) has the most significant difference in SE value, i.e., SE increases with the increasing thickness of the strip. The negative effect is saying that the SE increases with a decrease in the gap between the strips (B). The factors AA, BB, BC, and AB show no significant difference in SE value which are all very close to the straight line, *i.e.,* normal distribution.

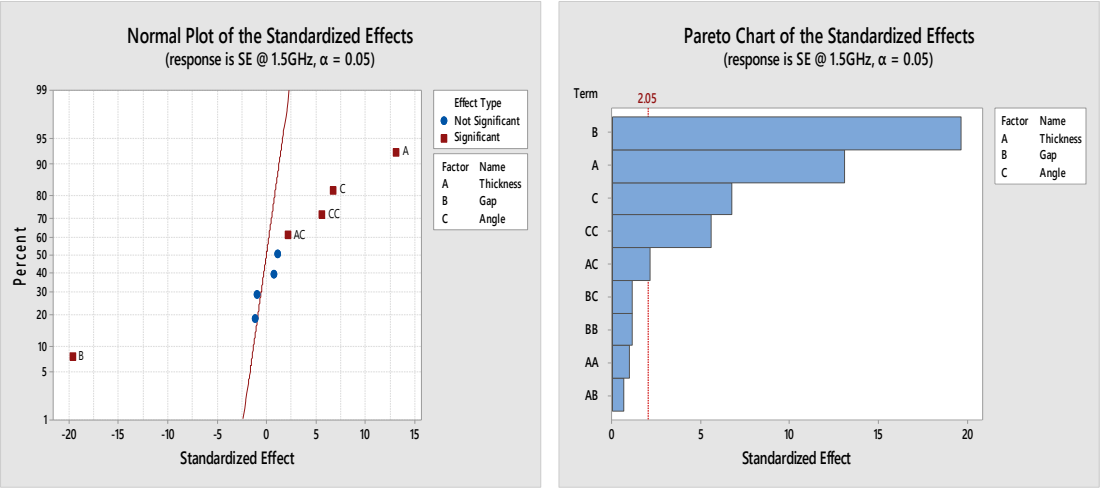

(a) (b)

Figure 24. The normal plot of the (a) standardized effects and (b) standardized Pareto chart [72].

Hence, the higher percent cover area and lower area per aperture structure have been recommended for achieving higher EM SE. By the SFD it can be concluded that the combination of the larger strip thickness, the lower gap between the strips, and the higher laid angle of the strips provides higher EM SE. This model reported that it is helpful to construct the optimal fabric or composite structures based on the required level of shielding for EM shielding application.

3.4. Textile structure as sensors

Force sensing resistors (FRS) are developed for precise pressure sensor applications. The FSR works by measuring the change in resistance by an increase in force. It detects physical pressure, squeezing, and weight by a change in resistive value. The applications of FRS are in the medical field [74], shoe insoles to detect the pressure of our foot [75], video games, electrical automobiles, sporting equipment, etc. The textile spacer fabrics coated with silver on both sides act as a capacitor, whose capacitance helps measure snowboarding sock pressure during skiing [76]. The highly elastic fabric was coated with polypyrrole (PPy) polymer to measure strain in urinary bladder dysfunction. The resistance is influenced by stretching the fabric and measuring strain variation [77]. A conductive PPy-coated electrospun poly (vinylidene fluoride) (PVDF) fibre mat is developed for pressure sensor application; the compression stress is significantly changing the relative conductivity of PVDF/PPy mat [78]. The SS yarn knitted fabric was tested for strain sensing application, the elongation of the fabric decreased 90% of electrical resistance, and time-dependent

resistance decreased by 30%. The full cardigan with a medium stitch has the best result for elongation-dependent resistance in the course direction [79].

3.4.1. Electrical resistance of textile structures

It is known from theory that the electrical resistance of a wire increases with the increasing distance of the probes in a relaxed state. The same phenomenon can be observed in textile structures containing a conductive component continuously throughout the length of the yarn. As per Ohm's law ($R=\rho L/A$), the resistance (R) is directly proportional to the yarn length (L) and indirectly proportional to the cross-section area of the yarn (A), and ρ is the resistivity [37].

The electrical properties of yarns were studied in several papers[80][81][82][83]. In paper [84], the antistatic yarn (containing bi-component fibres with carbon part) was studied, and a linear relationship between the electrical resistance and clamping length was confirmed. On the other hand, the nonlinear behavior of the electrical resistance on the clamping length was observed for yarns containing 20 % of stainless-steel fibres of staple length in their structure. Therefore, the method of conductive yarn production influences the length-resistance results. During extension, the length of the conductor (wire, single fibre, or single yarn) increases its diameter decreases and the resulting electric resistance increases.

Contact resistance is another interesting phenomenon that may affect the resulting electrical conductivity of the textile structure. The contact resistance is generated at yarn – the yarn interface. According to the contact resistance theory [85], contact resistance factors are material resistivity, material hardness, number of contact points, and contact pressure between yarns.

The stretching of the knitted fabric is influencing the structure of the knit. The courses and wales were disturbed, as seen in Figure 25. During wale way stretching (Figure 25(a)), the expansion of wale at maximum (Wmax) and contraction of course, to a minimum (Cmin), was noticed. During the course-wise stretching (Figure 25(b)), the course extension until maximum (Cmax) and wale contraction to a minimum (Wmin) was noticed. During biaxial stretching of the knitted fabric, both the course and wale were expanded and represented as course bias (Cb) and wale bias (Wb). The yarn contact points are shifting, while a biaxial stretching of the fabric is seen in Figure 25(c) [86][87]. The 1x1 rib fabric is the highest elastic textile structure, easily stretching in uniaxial and biaxial directions. This structure has more easily stretched in the course-wise direction because of loosely constructed courses. In

wale-wise stretching, the elongation occurs in the side limbs of the loop and contraction in the head and sinker loop, as noticed in this work [88]. In a study [89], the glass and polypropylene yarns were co-knitted with a 1x1 rib structure, and the fabric was stretched in uniaxial and biaxial directions to test its tensile, bending, and impact. The wale-wise stretching has more stress compared with the course-wise stretching. In bias (biaxial) stretching, the wale-wise exhibited more stress than the course-wise.

From the above, it can be assumed that the length-related resistance will increase with increasing uniaxial force, whereas the contact resistance will decrease with increasing contact points and contact force [37].

A survey of the electro-mechanical behavior of electro-conductive fabrics can be found in several professional publications. For example, in paper [84], three different forms of conductive yarn, single yarn, two overlapped yarn, and knit stitch yarn, were taken for study. Unidirectional tensile force is applied to those samples, and the electrical resistance reading is taken. It was observed that the single yarn and overlapped yarn have an increase in electrical resistance with increasing tensile, but the knit stitch yarn has a decrease in electrical resistance during increasing tensile. A study [75] noticed that the contact resistance in knit stitch form has decreased with an increase in unidirectional stretching. The conductive yarn in knit form has lesser resistance values than single-strand and overlapped yarn. In fabric form, the contact resistance affects the total resistances more than the length resistance.

The electrical conductivity of the CNT-coated nylon6/spandex yarn was investigated in the study [90]. It was reported that the CNT yarn can elongate until 100 percent lengthwise, whereas it was noticed that the yarn's electrical resistance increases with elongation.

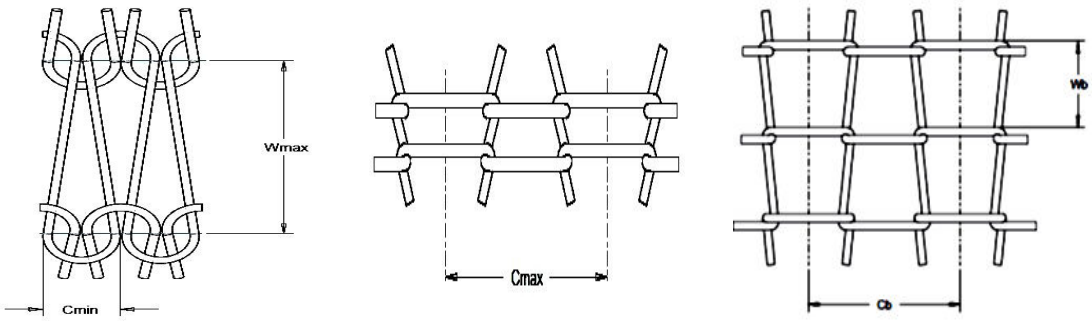

(a) (b) (c)

Figure 25. Yarn contact point shifting during (a) wale-wise stretching, (b) course-wise stretching, and (c) biaxial stretching or both ways stretching [90].

The linear relationship between the electrical resistance and the elongation was noticed until 70 percent elongation. After that, the electrical resistance was increased drastically, up to 100 times at 100 percent elongation. Authors reported that the drastically increased resistance after 70 % elongation is because of rupture and break in the CNT coating.

Another study [91] explains the contact resistance of the knit stitch made of silver-coated yarn. It was found that electrical resistance decreases while an increase in elongation and force. The authors reported that the linear fitting of the dependence of electrical resistance on elongation has a R^2 of 0.90; therefore, the statistically significant linear relationship between electrical resistance and applied force was proved. So, the contact resistance of the yarns plays an important role during fabric extension.

Three different silver-coated threads were studied for electrical resistance versus extension in work [92]. The electrical resistance of all studied threads increased with increasing elongation. Studied threads were used to sew chain stitches and zig-zag stitches on the fabric substrate, and the electrical resistance was measured against the elongation of the fabric. The author noticed that the stitch electrical resistance was decreased with the elongation of the fabric because of multiple contacts in the stitch. Most of the studies confirmed that the multiple contacts of conductive yarns in the fabric structure cause a decrease in electrical resistance during fabric elongation.

The unidirectional stretching of the Ag-coated PA yarn intarsia knit fabric at wale way was studied in work [37]. It was noticed that the electrical resistance was decreased with increasing extensile force. An increase in the number of wales caused a decrease in the fabric's electrical resistance values. Another study [93] also proves that the contact resistance and contact force on knitted fabric have an influence on electrical fabric resistance. The hexagonal resistance model for knitted structure validates the simulation of the resistance sensing mechanism. An increase in contact force decreases the contact resistance of the knitted fabric, which was proved by Holm's electric contact theory.

Article [79] shows knitted fabric's elongation-dependent and time-dependent electrical resistance in course direction. It was reported that the full cardigan with medium stitch density is more suitable for resistance stretch sensors among various knit structures.

The Ag-coated nylon 66 blended with merino wool yarn single pique knitted structure was taken with a tuck stitch to study the resistance of the knitted fabrics in work [94]. The

increase in the number of courses with constant wales and increases in the number of wales with constant courses leads to decreased electrical resistance. Also, the tuck stitch reduces the electrical resistance of the single-pique fabric. Both the theoretical model and practical model confirmed the electrical resistance results.

A study [98] developed the copper-coated Lyocell plain-woven fabric with an electroless deposition method. The developed conductive fabric was tested for flex testing until 6000 cycles, and the resistance was measured with two probes and four probes. It can be concluded from both measuring methods that the fabric resistance increases with increasing flexing cycles. The change in resistance was explained by the partial damage of copper coating on the fabric surface after 6000 flex cycles. The decrease in resistance is caused by the damage to the copper coating due to swelling and expansion of the fabric. So, the elongation and flex of fabric cause damage to surface coating, leading to reduced electrical resistance.

From above, it is visible that the major portion of developed textile sensors is based on the change of electrical conductivity of the textile structure during external stimulus using traditional wired methods. Only a few papers describe wireless strain sensing mechanisms using electromagnetic radiation, but usually, those are for the civil engineering field. In the study [95], the wireless measurement of the strain gauge for large metal structures is presented with the radio frequency method. It was presented that the wireless radiation measurement method's accuracy is higher than wired measurement by the traditional resistance method.

There are lots of studies about the electrical resistance on stretching of textile conductive fabrics [79][37] and conductive thread stitch fabrics [92], but very few studies about the conductive yarns on electro-mechanical behaviors are reported [96]. Especially, the yarn resistance has the main influence on the fabric resistance, so it is necessary to analyze it.

It follows from the performed literature search that the influence of contact and longitudinal resistance on both electrical conductivity and electrical resistance, as well as on electromagnetic shielding, especially during mechanical stress, needs to be further investigated to create wireless strain sensor technology using electro-conductive fabrics.

Electromechanical property of the conductive knitted fabric

Ohm’s law states that the voltage, V is directly proportional to the current, I (amp), passes through the circuit and resistance, R (Ω), created by the circuit.

$$\boldsymbol{V = IR}, \quad \text{Eq. 11}$$

The electrical resistance (R) of the conductive material is written as

$$\boldsymbol{R = V/I}, \quad \text{Eq. 12}$$

R depends on the length, L [m], cross-sectional area, A [m^2], and resistivity, ρ [Ω/m] of the conductor.

$$\boldsymbol{R = \rho L/A}, \quad \text{Eq. 13}$$

The surface-coated conductive material has an exponential constant, k, for its effective area written as:

$$\boldsymbol{R = \rho L/A^k}, \quad \text{Eq. 14}$$

As per the contact resistance theory, the contact resistance as:

$$\boldsymbol{R_c = \frac{\rho}{2}\sqrt{\frac{\pi H}{nP}}}, \quad \text{Eq. 15}$$

where H [N/m^2], n, and P [N] are material hardness, number of contact points, and contact pressure between the conductive yarns, respectively. The hardness and resistivity are related to the material properties, and it is constant. Contact resistance is indirectly proportional to the contact pressure and the number of contact points.

During the extension of the knit structure, the resistance of the fabric varies with related to yarn length, R_l and yarn contact points, R_c.

Conductive yarn extension mechanism

During the stretching of the yarn, the cross-section area, A, decreases, and the length, L, of the yarn increases, so the length resistance, R_l is not linearly proportional to the yarn length. Conductive yarn length and cross section are a function of applied tensile force, F [N]. The force, F included in Equation 16, with initial length, L_0 is written as:

$$\boldsymbol{R_l = f(F, L_0) = \frac{L(F,L_0)}{A(F,L_0)^k}}, \quad \text{Eq. 16}$$

The nonlinear length-related resistance is dependent on extensile force and yarn length. The Nth order effect and cross-correlation effect between the yarn length and extensile force to the resultant resistance as in the model equation below.

$$\boldsymbol{R_l = \sum_{n=0}^{N} \sum_{m=0}^{N} C_{mn}\, F^n\, L_0^m},$$ Eq. 17

where, C_{mn} is the coefficient to be determined in the experiment.

Extension mechanism of the overlapped yarns

The overlapped yarn contact resistance decreases with the increase in length or extension of the yarn or fabric. The decrease in contact pressure during the extension is due to torsion in the yarn twist releasing. The relationship between the tensile force, F, and contact pressure, P as follows:

$$\boldsymbol{P = P_0 + a_0 F},$$ Eq. 18

Where, P_0 is the initial contact pressure, and a_0 is a constant coefficient. The contact resistance, R_c, is indirectly proportional to the contact pressure, P. P is required to reflect the resistance arising from the twist of the yarn. The equivalent resistance on overlapped conductive yarn is as follows:

$$\boldsymbol{R(F, L_0) = \sum_{n=0}^{N} \sum_{m=0}^{N} C_{mn}\, F^n\, L_0^m + \frac{a_1}{P_0 + a_0 F}},$$ Eq. 19

From Equation 19, the contact resistance increases with the initial stretch, and thereafter, the length-related resistance plays an important role in total resistance. These constants will be determined in the experiment.

3.4.2. Yarn resistance model

The yarn's electrical resistance R changes with increasing tensile, elongation, or strain; the conventional resistance law is used to calculate the change in resistance as [93][97]

$$\boldsymbol{\frac{dR}{R} = \frac{d\rho}{\rho} + \frac{dl}{l} - \frac{dA}{A}}$$ Eq. 20

Where ρ, l, and A are the yarn resistivity, length, and cross-sectional area, respectively. Here, the elongation (ε) of the conductive yarn in the longitudinal and radial directions with a cylindrical structure with an initial radius of r can be written as

$$\boldsymbol{\varepsilon_l = \frac{dl}{l}}, \text{ and } \boldsymbol{\varepsilon_r = \frac{dr}{r} = -\nu \frac{dl}{l} = -\nu \varepsilon_l}$$ Eq. 21

Equation 11 uses the Poisson's ratio is *v*. Using this equation, the changes in the volume (*V*) and cross-sectional area (*A*) of the yarn can be written as

$$\frac{dV}{V} = \frac{dl}{l} + \frac{dA}{A} = \varepsilon_l - 2v\varepsilon l + v^2\varepsilon_l^2 = v^2\varepsilon_l^2 + (1-2v)\varepsilon_l \quad \text{Eq. 22}$$

and

$$\frac{dA}{A} = (1+\varepsilon_r)^2 - 1 = 2\varepsilon_r + \varepsilon_r^2 = -2v\frac{dl}{l} + v^2\left(\frac{dl}{l}\right)^2 \quad \text{Eq. 23}$$

By assuming the electrical resistivity, $\rho = cV$ for the conductive material, where *c* is the number of free electrons per atom constant and the atomic density, then

$$\frac{d\rho}{\rho} = c\frac{dV}{V} = c\,v^2\varepsilon_l^2 + c(1-2v)\varepsilon_l \quad \text{Eq. 24}$$

From Equations (20) to (24), the change in resistance of the conductive material is written as

$$\frac{dR}{R} = v^2(c-1)\varepsilon_l^2 + [2(1-c)v + c + l]\varepsilon_l \quad \text{Eq. 25}$$

For the resistance of the yarn is written as

$$R = v^2(c-1)\varepsilon_l^2 R_0 + [2(1-c)v + c + l]\varepsilon_l R_0 + R_0 \quad \text{Eq. 26}$$

Where R_0 is the yarn resistance at no strain. For a given material, the strain sensitivity, or gauge factor *K*, can be written as

$$K = \frac{dR/R}{dl/l} = v^2(c-1)\varepsilon_l + [2(1-c)v + c + l] \quad \text{Eq. 27}$$

For a small change in strain values, the electrical resistance

$$R = 2(1-c)v + c + l]\varepsilon_l R_0 + R_0 \quad \text{Eq. 28}$$

The yarn's electrical resistance is the main factor in the fabric's total electrical resistance; the distance between the yarn's contact points in the fabric structure also influences the fabric resistance. During the elongation of the fabric sample, the change in electrical resistance is noticeable, especially in knitted structures, as shown in the literature search above.

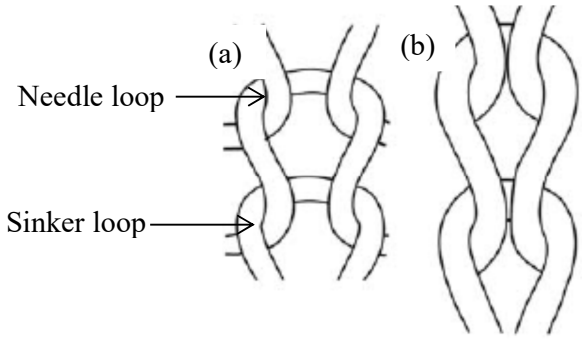

Figure 26. Knitted loops with sinker loop and needle loop at (a) relaxed state and (b) extended state [88].

3.4.1. Fabric resistance model

The knitted loop consists of a needle loop, which has one head, two limbs, and a sinker loop in its natural state, as shown in Figure 26(a). While unidirectional tension is applied on the conductive knitted fabrics, the contact points are tightened and moving. The length of the head, limbs, and sinker loop has extended and may change the contact point. The increase in tensile force has further extended the contact point, and pressure creates between the head and sinker loop. The shape of the loop extended during the tensile force is shown in Figure 26(b). The breaking of the fabric occurs when the tensile force exceeds the breaking force of the yarn.

The resistance of the conductive fabric among wale direction extension is modeled by superposition of the length-related resistance and contact resistance with the fabric length, L. Resistance is inversely proportional to the total number of wales (Equation 29) as:

$$\boldsymbol{R(F, L_0) = \frac{1}{W}\left(\sum_{n=0}^{N}\sum_{m=0}^{N} C_{mn}\, F^n\, L_0^m + \frac{a_1}{P_0 + a_0 F}\right) + W.b_0}\ , \qquad \text{Eq. 29}$$

where b_0 is an offset coefficient to account for the terminal resistance between the connector and the fabric under test, W is the total number of conductive yarn wales of knitted fabric.

The electrically conductive knitted and woven fabric structures can be assumed as resistance circuits, meaning the woven fabric is similar to a square circuit with four resistors and contact points. The plain weft knitted fabric matches to hexagonal resistance circuit model (see Figure 27(a)). There are two types of electrical resistance in this fabric structure: contact resistance (Rc), representing the contact points of overlapped yarn loop, and intrinsic resistance (RL), representing resistance between two contact points (Figure 27(b)). The fabric structure is described by one sinker loop (La), two-loop legs (Lb), and two interloped contacts (c). Based on the fabric structure, the resistance circuit is represented

with RL, Rc, resistance at needle loop and sinker loop (RLa), and two-loop leg resistance (RLb) [93]. Kirchhoff's rule is used to model the network for deriving equivalent resistance of the fabric. While applying tension to the fabric, the knit structure is disturbed, as seen in Figure 26. In this case, the Rc and RL values change according to the applied tension, and Equation 28 also explains the single yarn resistance change during stress.

As per the pierce model [88], the La and Lb under no strain are represented as $La_0 = \pi\, {}^{w}/_{4}$ and $Lb_0 = {}^{l - 2La_0}/_{2} = {}^{2l - \pi w}/_{4}$. Where l is loop length, and w is single loop width. The fabric under strain ε_w in course direction, loop length, $l = La_0(1 + \varepsilon_w)$; RLa and RLb in Equations 30 and 31 as

$$\boldsymbol{RLa = \rho_l La = \frac{\rho_l \pi w(1+\varepsilon_w)}{4}}, \qquad \text{Eq. 30}$$

$$\boldsymbol{RLb = \rho_l Lb = \frac{\rho_l [2l - \pi w(1+\varepsilon_w)]}{4}}, \qquad \text{Eq. 31}$$

Where ρ_l is the yarn resistivity per unit length, the contact resistance is eliminated because of complications in measuring under stress.

Figure 28 shows the electrical resistance circuit for 2x1 unit loops of knitted fabric, and it shows the interior loop current. Equation 32 is obtained from Kirchhoff's voltage law and the loop current method. I_1, I_2, I_3, and I_4 are total current and equivalent resistance $Re = V/I_1$, and V is voltage.

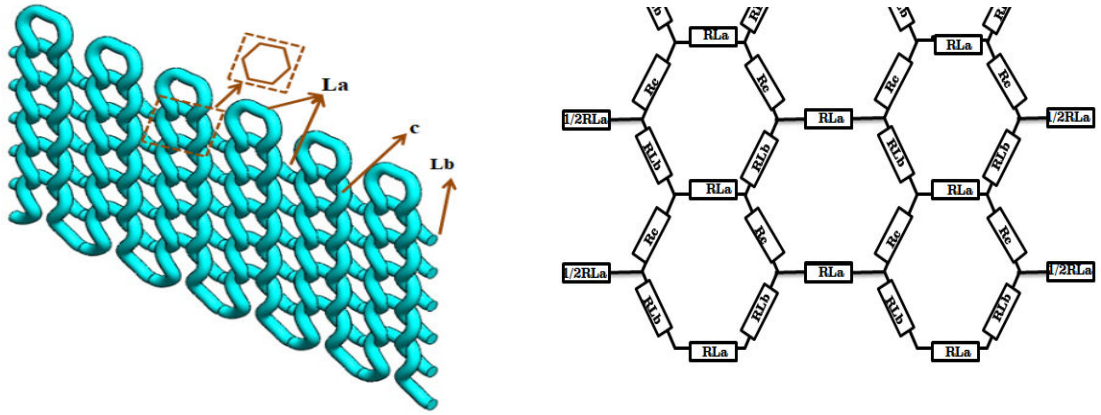

(a) (b)

Figure 27. Graphical images of (a) plain knitted fabric structure and (b) the hexagonal resistance circuit model [97].

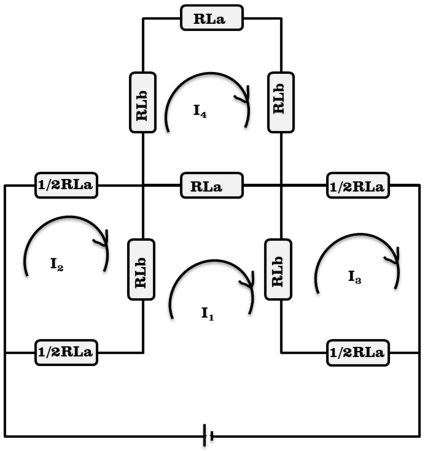

Figure 28. Electrical resistance circuit for 2x1 unit loops for knitted fabric [97].

$$\boldsymbol{R_e(2,1)} = \frac{\boldsymbol{V}}{\boldsymbol{I_1(2,1)}} = \frac{\boldsymbol{RLa(RLa+2RLb)}}{\boldsymbol{RLa+RLb}} \qquad \text{Eq. 32}$$

3.5. Research gaps

The literature review revealed some studies with different conductive textile materials, and their structure. Mostly the same material with different structure or different material with the same structure was studied separately. So, to fulfill the research gap in the comparative study, the various textile materials and different structures were taken and tested for electrical resistivity, electromagnetic shielding, and fabric parameters in the initial work of this thesis and recommendations for the creation of electromagnetically shielding textiles for different applications with different requirements were summarized. A survey of the effect of moisture in the textile material on its shading ability was carried out.

Effect of structural parameters including amount and size of pores on SE was evaluated using the copper-coated nonwoven strips simulated as textile structures and using the design of the experiment methodology. The final part of the review is based on the elongation of the textile fabric and its electrical resistance and EM SE.

There are many studies on changes in electrical resistance concerning changes in fabric elongation, but there are very few studies on EM SE against fabric elongation. In such studies, the difference in SE against the elongation of fabric is not exactly studied. No research reported on deformation sensing using conductive textiles with EM waves as a detector, so that is also considered and studied.

4 EXPERIMENTAL PART

Main goal of this work is to develop a wireless sensor based on the principle of changing the electromagnetic shielding of the textile during its tensile stress. Both the yarn from which the knitted fabrics are created and the knitted fabric itself are investigated. Knitted structures were chosen for their easy deformability. In order to understand the electromechanical behavior of knitted fabric, simple structures made of yarns are examined. This is followed by an electromechanical survey of knitted fabrics.

The conductive yarn was taken, and measured its electrical resistance with various gauge lengths; then, the yarn was formed as a single strand, single loop, and chain loop to check its resistance during elongation. The chain loop form is similar to the knitted fabric structure, so this result is important for further fabric development. Once the results of yarn forms showing the change in resistance with elongation, then further knitted fabric with single jersey and rib structure was developed for strain sensing ability. The knitted fabrics were developed at three different densities for detailed analysis. The fabric properties like stitch density, porosity, thickness, electrical resistance, and EM SE were analyzed during the fabric elongation. SE is a crucial technique used for measuring strain sensing as a wireless technology. Statistical analysis is used to find out the significant change in the results.

4.1. Electrically conductive silver-coated yarn

Since the goal was to prepare and study the mechanically deformable, highly electrically conductive knitted structures with a relatively high EM shielding ability, the silver-coated yarn was chosen. The silver-coated polyamide (AgPA) yarn with linear density 60 tex was procured from Statex Inc., Bremen, Germany. The yarn's main parameters are shown in Table 5. The SEM images of the yarn at longitudinal and cross sectional views are shown in Figure 29(a) and Figure 29(b) respectively. This yarn was used for three types of experiments where the length-related electrical resistance and contact resistance were studied under unidirectional extension forces applied.

Table 5. Yarn parameters and their mean values with a 95% confidence interval.

Yarn parameters	Values
Double yarn count raw [dtex]	476 ±6
Single yarn count raw [dtex]	235
No. of filament per yarn	36
Double yarn count - silverized [dtex]	602 ±5
Single yarn count – silverized [dtex]	301 ±10
Double yarn - twist per meter ('Z' twist)	457 ±8
Single yarn - twist per meter ('S' twist)	614 ±4
Electrical resistivity [ohm/m]	68 ±14
Tensile strength [N]	28 ±4
Elongation at break [%]	28 ±10
Tenacity [cN/tex]	47 ±2
Yield [m/kg]	Min. 16600
Double yarn dia. [µm]	426 ±30
Single yarn dia. [µm]	273 ±30

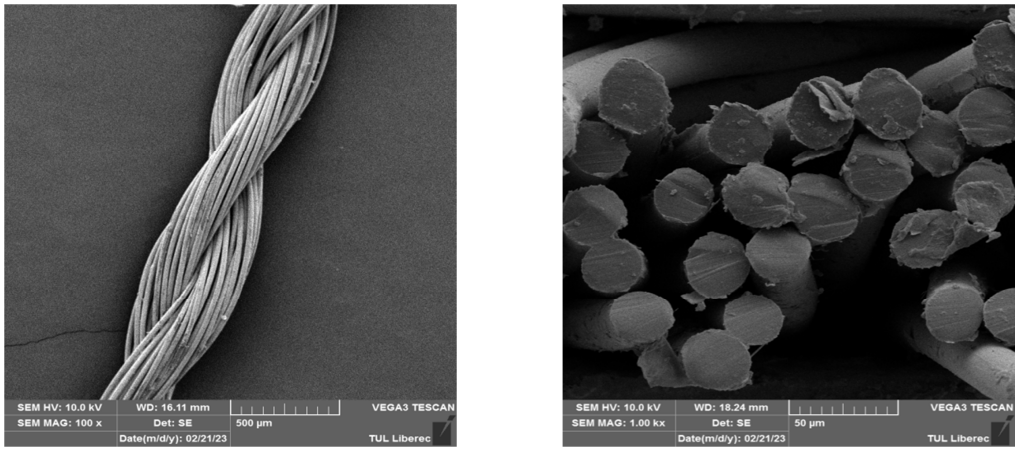

(a) (b)

Figure 29. SEM images of AgPA yarn, (a) longitudinal view at 100x magnification and (b) cross sectional view at 1000x magnification.

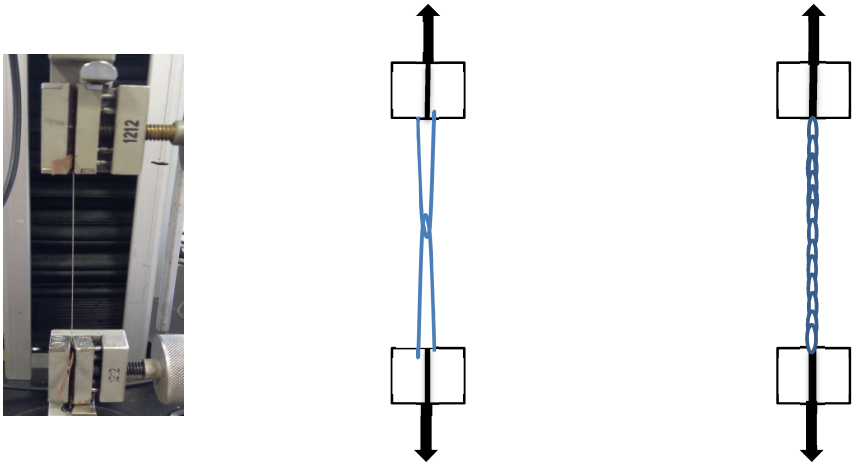

(a) (b) (c)

Figure 30. Experimental setup of (a) SY, (b) SLY, and (c) MLY samples (with chain loop formation by crochet hand knit needle) clamped in the tensile instrument for the measurement.

To explore length related resistance and the effect of contact resistance, three experiments were conducted with three different yarn forms: single yarn (SY), single-loop yarn (SLY), and multi-loop yarn (MLY), and its experimental setup is shown in Figure 30.

SY sample is prepared with a single strand of yarn (see Figure 30(a)), which is clamped between two jaws of a tensile instrument. The SLY sample is formed by overlapping the two AgPA yarns to form a single loop, as shown in Figure 30(b). The MLY sample is formed by a hand-knitted continuous chain loop with a crochet needle, and it is shown in Figure 30(c).

4.2. Mechanical properties of yarns

The mechanical properties (stress-strain curves, ultimate characteristics) of silverized yarn were tested with Lab test 2.010 instrument (Labor tech Inc., Czech Republic) as per ISO 2062 standard using 50 mm clamping length and 50 mm/s speed.

4.3. Electrical properties of yarns

The yarn resistance is measured with two probes as per ASTM D257, and as stated by [71] the yarn irregularity makes the measurement complicated. A mass-specific resistance R_s is defined as the resistance in ohms between the ends of a specimen 1 m long and of mass 1 kg, giving units of $\Omega.kg/m^2$.

The two quantities are related in Equation 33

$$\boldsymbol{R_s = \rho d,} \qquad \text{Eq. 33}$$

where, d = density of the material in kg/m^3. In practice, it is more convenient to express R_s in Ω.g/cm^2, when the numerical values for most fibres will differ by less than 50 % from the values of ρ expressed in Ω.cm. With these units, the resistance R of an arbitrary specimen is given in Equation 34

$$\boldsymbol{R = R_s \frac{1}{NT} \times 10^5} \quad , \qquad \text{Eq. 34}$$

where, l = distance between the ends of the specimen in cm, N = number of ends of yarn or fibre, and T = linear density of yarn or fibre in tex.

Because of the wide range of resistance values, results are frequently expressed in terms of the logarithm of resistance.

4.4. Electromechanical properties of yarns

The electrical resistance of the yarn was measured using the Arduino® circuit with two probes, and its experimental setup with circuit diagram is shown in Figure 31. By this setup direct recording of the electrical resistance varying with the tensile stress of the sample is possible. The Arduino circuit with breadboard was connected to a laptop, as shown in Figure 31(a); two probes from the circuit were connected with a copper plate extended from two jaws, as seen in Figure 31(b). The circuit diagram of the Arduino is shown in Figure 31(c).

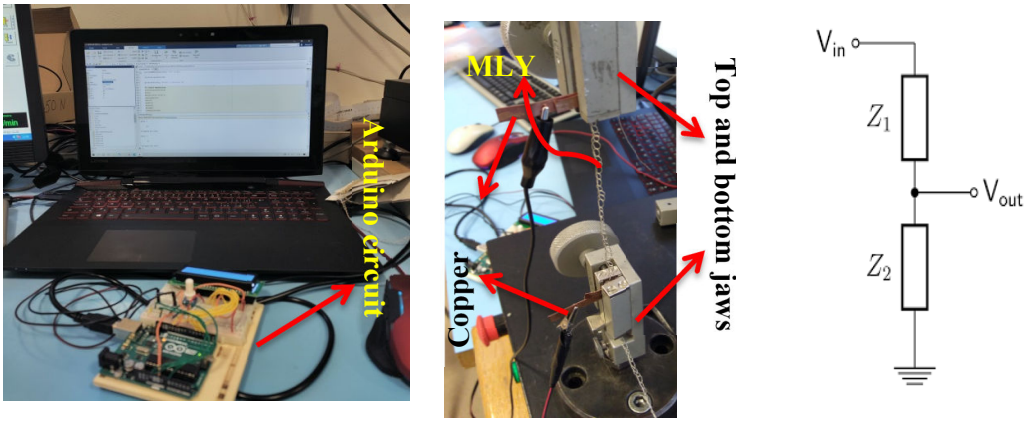

(a) (b) (c)

Figure 31. Experimental setup for measuring electrical resistance during elongation of yarn (a) Arduino circuit board attached with MATLAB software in laptop, (b) two probes in the tensile machine along with MLY sample, and (c) circuit diagram of Arduino board.

The resistance of the yarn is measured with the formula given in Equation 35, and the MATLAB program script is written and runs to record continuous electrical resistance measurement.

$$\boldsymbol{Z_2 = Z_1\left(\frac{1}{\frac{V_{in}}{V_{out}}-1}\right)} \quad \text{Eq. 35}$$

where, Z_1= known resistance, Z_2= unknown resistance, V_{in} = input Voltage, and V_{out} = output voltage. The contact between the yarn and the metal part of the jaw could affect the electrical resistance reading so that the nonconductive polymer gripper is placed between the yarn and the metal layer of the jaws. The copper plate electrode with a 3 mm width is placed on the gripper and connected with an Arduino circuit (see Figure 31) to measure the electrical resistance of yarn during unidirectional tensile measurement. Resistances of the yarn strands are recorded at a speed of 0.2 sec per reading. For recording the minute changes in resistance during tensile strain on yarn, the resistor sensitivity of 0.02 Ω is used for the measurement. Each measurement was repeated five times for each yarn category to be able to describe the variability of each measured quantity.

Table 6. Flat knit fabrics parameters and their mean values.

Test parameters	SJL	SJM	SJH	DJL	DJM	DJH
Structure	Single Jersey			1x1 Rib		
Thickness [mm]	0.85	0.83	0.84	1.52	1.48	1.37
Courses per [inch]	20.39	25.40	32.38	24.04	27	32.67
Wales per [inch]	18.29	19.30	20.46	18.62	19.05	19.27
Areal density [g/m^2]	230.79	261.66	314.46	442.01	456.02	538.96
Stitch density [per sq. inch]	361.26	475.00	641.54	447.62	514.35	680.72
Loop length [mm]	5.79	5.22	4.77	5.37	5.26	4.92
Porosity [%]	33	27.9	25.9	19.4	8.5	6.5

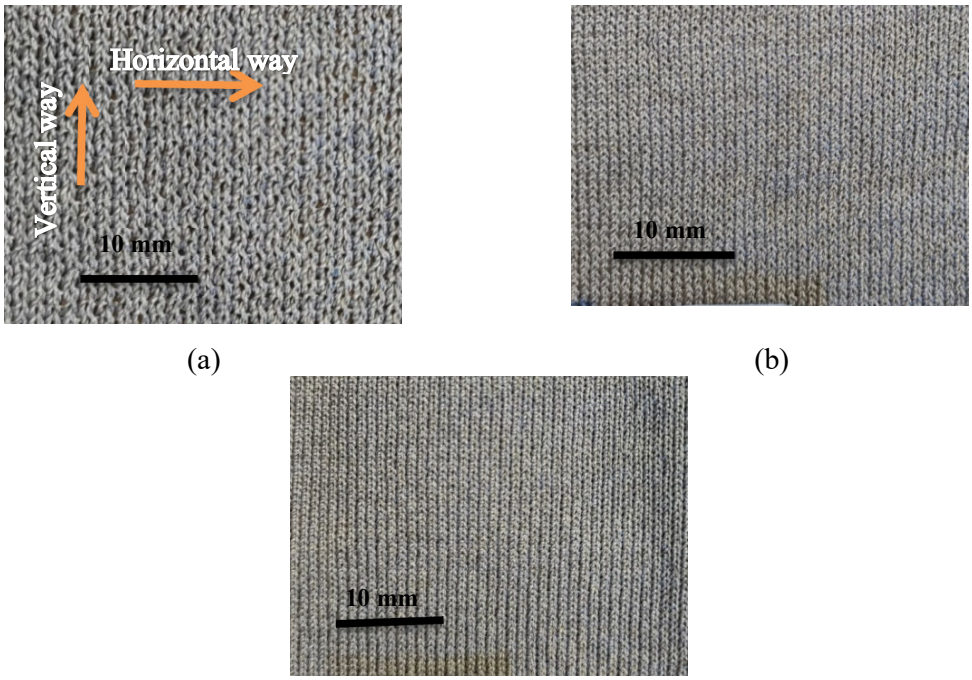

(a) (b)

(c)

Figure 32. Images of (a) SJL, (b) SJM, and (c) SJH.

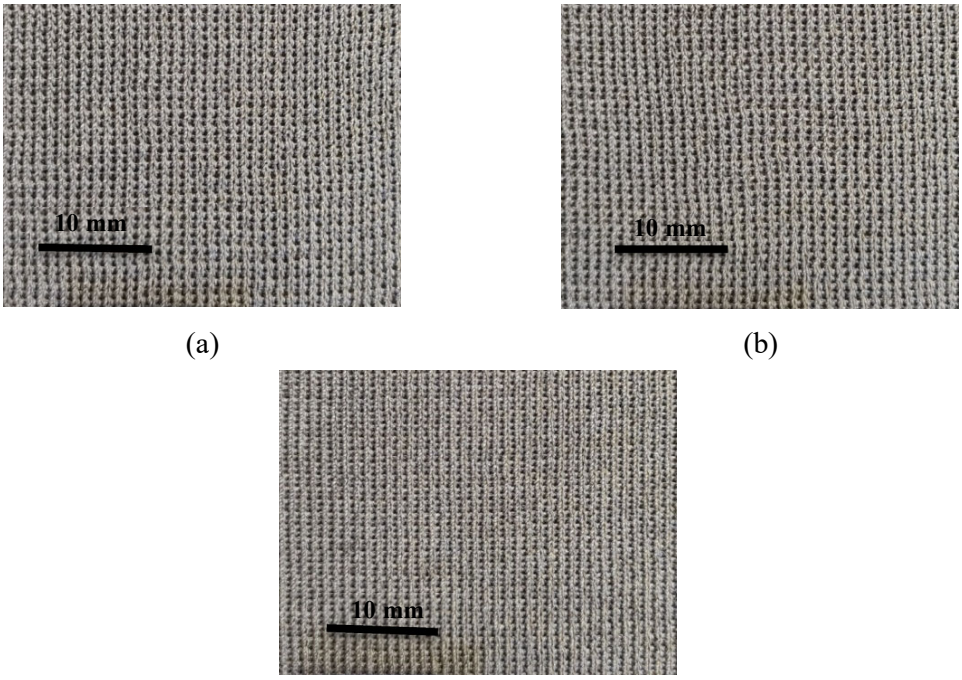

(a) (b)

(c)

Figure 33. Images of (a) DJL, (b) DJM, and (c) DJH.

4.5. Electrically conductive fabrics

Conductive silver AgPA yarn was used to knit single jersey (SJ) and double jersey rib (DJ) on a 14 gauge flat needle bed knitting machine (Shima Seiki Ltd., Japan, and Model SRY 123LP). These two structures were chosen as they are the basic ones, rib knit fabric stretches more than single jersey. In addition, these two structures of the fabric are widely in use of wearable applications. The knitted fabrics are prepared at three different densities; low (L), medium (M), and high (H). The basic parameters of knitted fabrics are shown in Table 6. Flat knit fabrics parameters and their mean values. and their images are shown in Figure 32 and Figure 33. All the images are captured as per ISO 125 with 4.73 focal lengths and a 64 MP camera. The knitted fabrics were used for the examination of electrical resistance and electromagnetic shielding under unidirectional as well as biaxial extension.

4.6. Basic properties of fabrics

The fabric mass per unit area (w) [g/m^2] was measured using the standard ASTM D 3776, and the sample size was 100 cm^2. Fabric thickness (t) was measured using the thickness gauge [mm], as per the standard ASTM D1777 (knitted samples). The loop length of the fabric samples was calculated with the Dalidovich method [98]. Ten readings per each test was taken to statistically analyze measured data sets.

4.7. Electrical properties of the fabrics

The surface resistance of the sample set was measured according to the standard ASTM D257, under a DC power supply, using two probe electrodes at the temperature T = 21°C and the relative humidity RH = 54 %. Sample resistance is measured by applying a voltage potential between two probes of specified configuration, which are in contact with the same side of the tested material. Sample resistivity ρ [Ω.mm] was calculated from the below-mentioned equation:

$$\boldsymbol{\rho = R(A/L)}, \qquad \text{Eq. 36}$$

Where, R [Ω] is the sample resistance reading, A is the area of the sample [mm^2], and L is the distance between the two probes [mm]. Ten readings per each test were taken to statistically analyze measured data sets.

4.8. Electromagnetic shielding effectiveness of fabrics

SE of the sample set was measured according to the ASTM D4935-18 for the planar materials using a plane wave, the far-field EM wave at the temperature T = 21°C, and the relative humidity RH = 54 %.SE of the samples was measured over the frequency range of 30 MHz to 1.5 GHz. The set-up consisted of a sample holder with its input and output connected to the network analyzer. A shielding effectiveness test fixture (Electro-Metrics, Inc., model EM-2107A) was used to hold the sample. The design and dimension of the sample holder follow the ASTM method mentioned above. A vector analyzer, Rohde & Schwarz ZN3, was used to generate and receive the electromagnetic signals. The standard mentioned above determines the shielding effectiveness of the fabric using the insertion-loss method. A reference measurement for the empty cell was required for the shielding effectiveness assessment. A "through" calibration with the help of the reference sample was made first. A load measurement was performed on a solid disk shape sample subsequently. The reference and load specimens must be of the same material and thickness. Both the reference and load samples geometries are according to the ASTM D 4935-18. The measurements were performed at five different places of the textile samples because of the subsequent statistical analysis. The mean values and 95% confidence intervals for means of the *SE* for 1.5 GHz frequency are summarized.

4.9. Electromechanical properties of fabrics

To study the effect of fabric strain on ER and SE, a biaxial device was used. Figure 34 shows the experimental setup of the biaxial stretching device with fabric to measure electrical resistance using two probe method (Figure 34(a)), and electromagnetic shielding measuring apparatus as per ASTM D4935-18 method (Figure 34(b)). Figure 34(b) shows the knitted fabric image marked with horizontal and vertical ways; the horizontal way represents the coarse wise, and the vertical way represents the wale wise. This designation (horizontal, vertical) will be used later in the text to show which direction of loading was used.

The continuous measurement of the electrical resistance of the knitted fabric sample is done with an Arduino resistance setup, as seen in Figure 34(a). The edges of the fabric samples were connected with two probes from the resistance circuit board at a distance of 14 cm, and the sample was stretched at a speed of 3.5 mm/sec to measure electrical resistance until 30 % fabric elongation. It was found that the elongation of the fabric until 30 percent was not

causing any damage to the knit structure. The fabric structure was disturbed by unraveling and breaking after exceeding 30 % elongation. While uniaxial stretching, the probes are connected to the stretching direction for a measurement. During biaxial stretching, the probes are connected in the vertical direction of the sample, and only wale way resistance is measured. The resistance readings were recorded online using MATLAB software and then saved in a data file for further analysis.

The electromagnetic shielding effectiveness (EM SE) of the sample was measured using the coaxial transmission line method, as seen in Figure 34(b). The coaxial holder is placed on the surface of the fabric sample and attached with a biaxial device. The stretching cycle is programmed with Fabris 5K software. The stretching speed was 3.5 mm/sec, and for every 5% elongation of fabric, the holders were paused for 30 sec to measure the EM SE. The stretching process is continued until 30% elongation of the sample.

The pore area of the fabric sample during the biaxial stretching process is measured using the Nikon NIS element software as per internal standard number 23-107-01/01. The fabric's total open pore area value, called porosity, was obtained by the NIS element image analysis and used for plotting graphs.

All three types of experiments were conducted on the sample set: uniaxial deformation at both ways and biaxial deformation. Output values were: electrical resistance, EM SE, and sample porosity. All tests were performed at the temperature T = 21°C, and the relative humidity RH = 54 % and three readings were taken for each test.

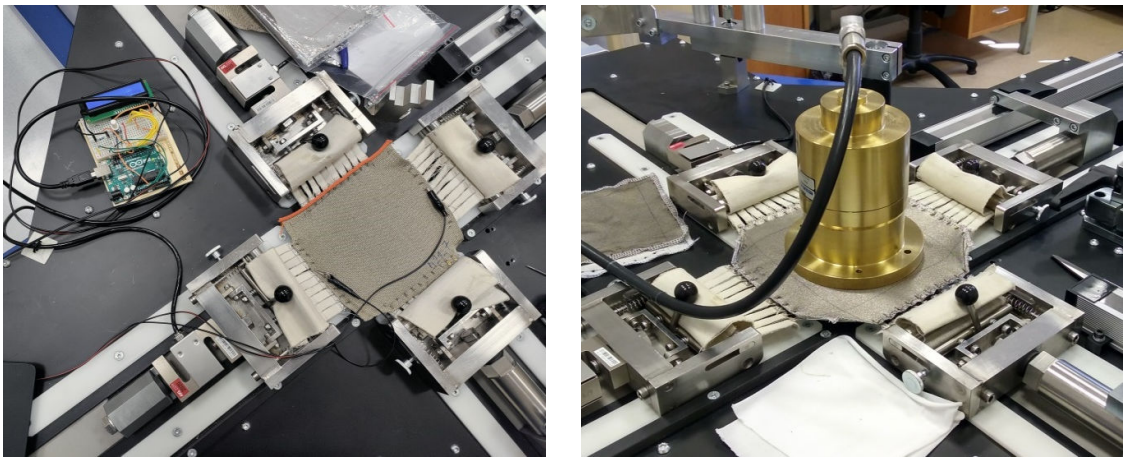

(a) (b)

Figure 34. Experimental setup of fabric attached in the biaxial device to measure (a) electrical resistance and (b) electromagnetic shielding effectiveness.

5 RESULTS AND DISCUSSIONS

In this chapter, the conductive yarn and conductive knitted fabrics test results are evaluated deeply and discussed statistically as well as logically for strain sensing applications.

5.1. Conductive yarn and its forms

The three forms of the yarns were tested for electrical resistance, resistance during elongation, tensile strength, and in addition SEM images after yarn break are discussed here.

5.1.1. Electrical resistance analysis of yarn and its forms

As the electrically conductive yarn is the basic element used in this work, it was investigated in detail in terms of their electrical properties. Measured was electrical resistance using different gauge lengths. In the next step, the following characteristics were calculated: length resistances for all yarn forms, electrical resistivity together with electrical conductivity for the single yarn.

The single yarn (SY), single loop yarn (SLY), and multi-loop yarn (MLY) are tested for electrical resistance at 1, 3, 5, 10, 15, and 30 cm distances between the two probes, and the results are given in Figure 35. It is visible that electrical resistance (R) increases with increasing gauge length (GL), and this relationship can be approximated by a straight line (Equation 37) with a very high coefficient of determination ($R^2 > 0.98$). Slope of the line represents length resistance R_L and y-intercept represents the sum of resistances at the interface between measured material and probe. Comparing R_L shown in Figure 35 and Table 7, it is visible that the SLY has the lowest length resistivity, and the highest length resistivity shows a sample marked as SY. The resistance value changes because the SY has single length related resistance, SLY has four length related resistances and one contact resistance between yarns, whereas MLY has multiple length related resistances and contact resistances at yarn-yarn interface within the same length. Based on measured electrical resistance and gauge length dependence of single yarn, mass specific resistance of single yarn was calculated according to Equation 39, which is 0.29 $m\Omega.g.cm^{-2}$.

$$\boldsymbol{R = R_L . GL + R_C} \qquad \text{Eq. 37}$$

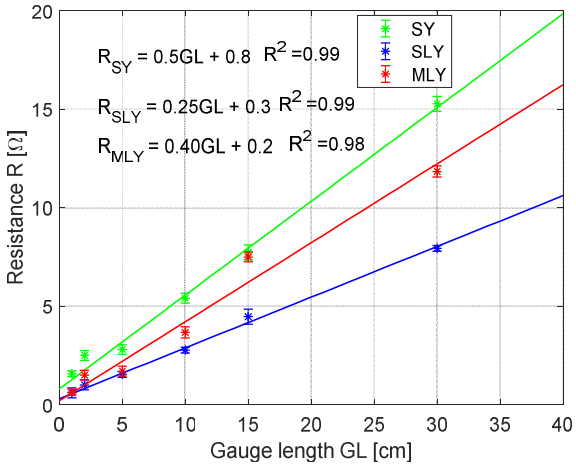

Figure 35. The gauge length of two probes versus the resistance of single yarn (SY), single loop yarn (SLY), and multi-loop yarn (MLY).

5.1.2. Mechanical properties of yarn and its forms

The stress-strain or tensile property of the yarn is the main characteristic to identify whether the yarn is suitable for apparel applications or not. When doubling the yarn, the tensile strength also increases. In this part, yarns' single-strand, single-loop, and multi-loop forms were tested for tensile strength properties.

The single yarn was tested for its tensile strength as per ČSN EN ISO 2062 and its gauge length is 15 cm and speed is 150 mm/min. Reading of 30 samples and their result are given in Figure 36. The maximum strength of 38.72 cN/tex and breaking elongation of 20% was obtained from this experiment and the 95 % confidence interval was plotted in dotted line.

The tensile strength of the yarns was measured at 5 cm gauge length and 50 mm/min traverse speed. The results of SY, SLY, and MLY stress–strain curves are shown in Figure 37, and the average of five readings was used for this plot; the average yarn breaking strength and breaking elongation values with a 95% confidence interval (CI) are shown in Figure 37.

Table 7. Electrical length resistance of different yarn forms with 95% CI**.**

Yarn form	Electrical length resistance R_L [Ω/cm]	
	Mean	CI
SY	0.45	0.03
SLY	0.25	0.02
MLY	0.40	0.09

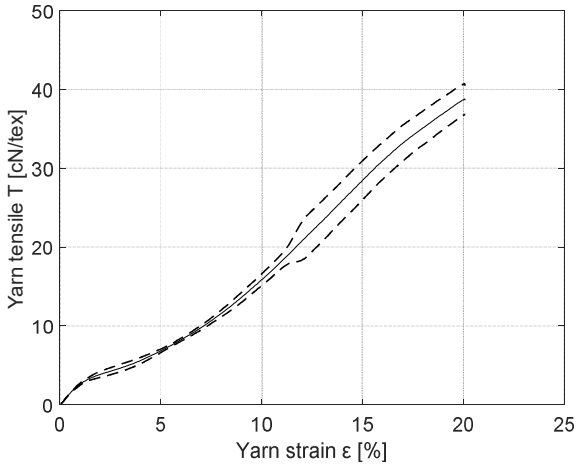

Figure 36. Stress-strain curve of the single yarn.

The mean values of breaking force and elongation at the break of yarn forms with 95% CI are given in Table 8.

Figure 37(a) shows the results of the single yarn at 5 cm gauge length test at 50 mm/min speeds. The rapid increase in single yarn tensile was noticed between 5% and 22%; after that, the yarn break at 34.7 % strain with 42.4 cN/tex force. Apart from SY behaviors, the SLY was initially zero stress until 3% strain; after that, the stress acted on it (see Figure 37(b)). The SLY breaking strength is 40 % higher compared to SY. The SLY sample is constructed with two threads of SY (see Figure 30(b)), which means the yield strength of SLY is double that of SY, which is why the strength and elongation at the break of the samples also increase.

In MLY results (Figure 37(c)), the load is acting after a certain percentage of occurred strain which is because of the loosely constructed loops structure (see Figure 30(c)). Once the loops get in contact with each other, then the load is acting. The MLY has 70% higher breaking strength compared with SY.

Table 8. Tensile strength and strain of yarn forms with 95% CI.

Parameters	SY		SLY		MLY	
	Mean	CI	Mean	CI	Mean	CI
Yarn tensile, T [cN/tex]	42.40	1.51	61.25	4.59	73.08	12.60
Yarn strain, ε [%]	34.79	2.56	29.19	2.22	73.32	10.48

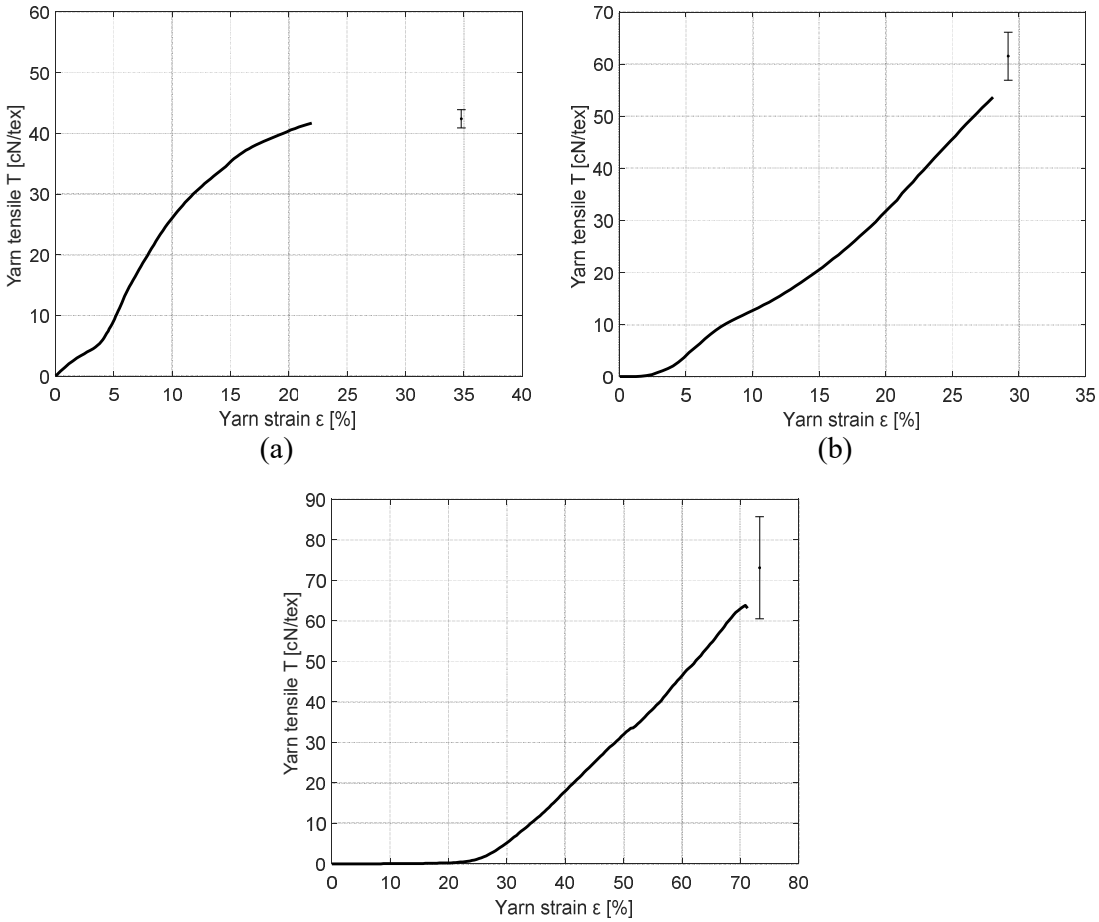

Figure 37. Yarn strain ε [%] versus tensile, T [N] of (a) SY, (b) SLY, and (c) MLY.

The yarn strain at break is higher for MLY, but SY has higher than SLY; this is because of more rupture occurs at the SLY contact point. The higher the number of loops, the higher the breaking strength was noticed.

5.1.3. Electromechanical properties of yarn and its forms

The conductive yarn is used to develop the conductive fabric for strain-sensing application. The fabric property is mainly based on yarn properties, so testing the electromechanical properties of different yarn forms is helpful in determining the fabric results. In this part, the strain or stress versus electrical resistance of yarn forms was studied.

The dependence of electrical resistance on tensile for SY, SLY, and MLY samples at 5 cm gauge length using 50 mm/min test speed is shown in Figure 38. When observing this dependence for the SY sample (see Figure 38(a)), it is visible that during the initial tensile process (T < 3.34 cN/tex), for this gauge length and test speed), the resistance increases

slightly. After a certain point, resistance increases steeply. A single linear model may not adequately describe the relationship between electrical resistance and yarn tensile. In this case, a segmented or piecewise linear regression allows multiple linear models to fit the data for different ranges of x. In our case, piecewise linear regression with two segments was used when the breakpoint (the point where the slope of the linear function changes) was unknown. The breakpoint was found as the minimum of the sum of RSS (residual sum of squares) of the two linear models. Figure 38(a) shows two straight lines with a very high coefficient of determination defining the breakpoint.

It was confirmed that there are two phenomena during the tension process: length-related resistance and contact resistance. The contact resistance occurs during the initial tension due to the twist of conductive yarn and the increasing number of contacts between fibres, reducing total length-related resistance. After the changing point, only length-related resistance occurs. It could also be assumed that the continuous conductive layer on the fibre surface during large deformations may be disturbed, and therefore the electrical resistance will increase.

The dependence of electrical resistance on the tensile force for single loop yarn (two overlapped yarns, SLY) is shown in Figure 38(b). It is visible that the resistance decreases until 3.34 cN/tex, which is caused by contact resistance dominating at the initial stressing. After reaching the change-point, the resistance increases steeply due to length-related resistance, and contact resistance has little effect on this region. Also, in this case, it is possible to fit two regions by straight lines to find a change-point. It is observable that the length-related resistance and contact resistance behave as competing factors which confirms that the electrical resistance of knitted fabric can be modeled by the superposition of the length-related resistance and the contact resistance, see Figure 25. When comparing the initial resistance and also the rear area of measured resistances of SY and SLY, the resistances in Figure 38(b) are almost half of that in Figure 38(a) because, in the case of SLY, two conductive yarns were connected in parallel.

The dependence of electrical resistance on the tensile force for multi-loop yarn (multiple overlapped yarns, MLY) is shown in Figure 38(c). It is visible that the resistance decreases until 8.35 cN/tex, which is caused by contact resistance between the yarn loops dominating at the initial stressing. After reaching the change point, the resistance increases steeply due to length-related resistance, and contact resistance has little effect on this region.

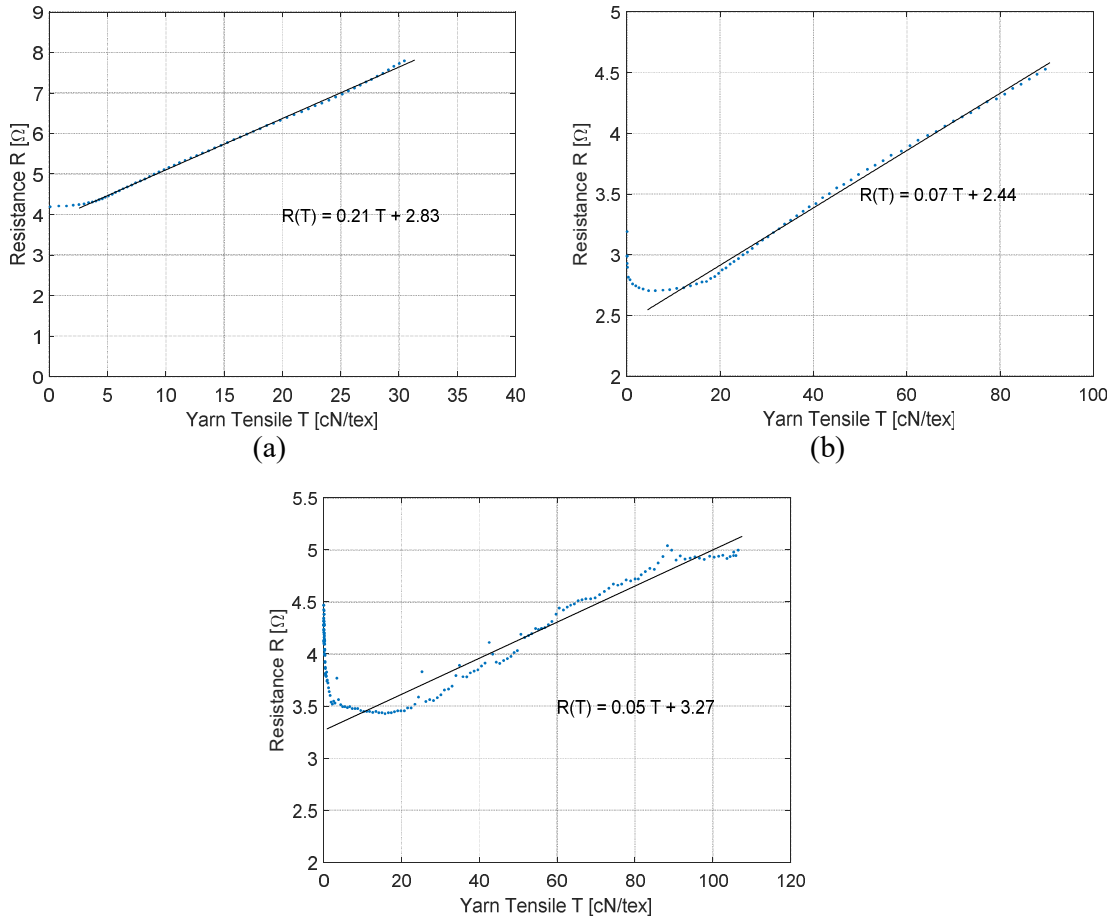

Figure 38. Dependence of resistance, R [Ω] on yarn tensile, T [cN/tex] for (a) SY, (b) SLY, and (c) MLY.

Also, it is possible to fit one region by a straight line to find the change point in this case. This multiple loops model helps to model the knitted fabric for electrical resistance change during elongation. When comparing initial resistance and also a rear area of measured resistances of SY, SLY, and MLY, resistances in Figure 38(c) are almost half of that in Figure 38(b) and a quarter of that in Figure 38(a); due to the case of MLY, multiple loops of conductive yarn were connected in parallel. When comparing the slope of the increasing linear models of all yarn-type structures, the highest slope (the steepest growth of R) has the SL sample, and the lowest slope has the MLY sample.

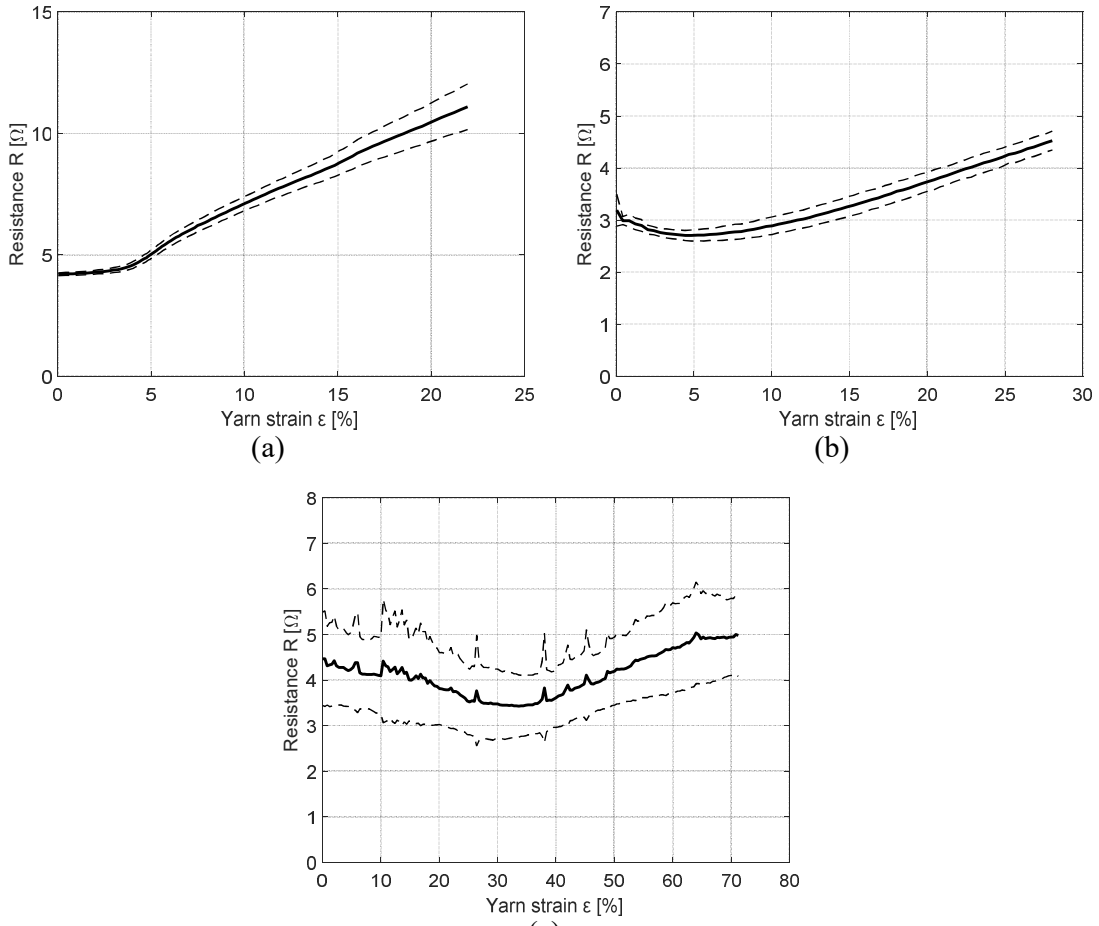

Figure 39. Dependence of electrical resistance, R [Ω] on yarn strain, ε [%] of (a) SY, (b) SLY and (c) MLY.

The dependence of yarn electric resistance R on yarn elongation ε is shown in Figure 39(a-c). Mean values together with 95 % confidence intervals of means displayed by dotted lines, are presented for SY, SLY, and MLY. The breaking strain is marked as a point with errors, as shown in Figure 39; MLY has a higher value following SY and SLY.

When observing R versus ε dependence, two regions of the tension process corresponding to length-related resistance and contact resistance are also visible, whereas the contact resistance has the smallest effect for SY samples and the highest effect for MLY samples. This phenomenon is connected to the number of contact points in the yarn-forming structure. For example, contact resistance is dominating factor of up to 30 % elongation for the MLY sample. The single contact point has a smaller effect on the R-value in Figure 39(b); SLY resistance decreases initially and then increases. Once the yarn rupture increases, the R-value also increases. Due to the multiple connecting points, the curve in

Figure 39(c) has wave formation; throughout the graph, there are many waves indicating the sudden rupture and slip between the contact points occurred.

5.1.4. SEM analysis of yarn

SEM analysis of yarn in Figure 40 shows the surface coating on filaments. Before the elongation of the yarn, the coating on the surface of the filament covers most of the part (Figure 40(a)), and after the elongation, the filament surface coating is a wear-off and uneven break of filament, as clearly seen in Figure 40(b). The surface coating of Ag on the filament surface came out after the yarn break, as seen in Figure 40(b), which confirms that the conductive particles on the surface are no longer in contact, the conductive network is not formed, and the electrical resistance increases during the larger tension process. The SLY yarn break occurred by abrasion in the loop, whereas one part of the loop was completely broken and another part was broken partially, as seen in Figure 40(c). The partial break of filaments is more clearly seen in Figure 40(c); the abrasion of yarn leads to the break of the surface coating and completely cuts the conductive network. Higher tension applied on the yarn leads to wear-off and breaks the filament surface coating, which is the reason behind the increase of resistance on SY samples during stress-strain analysis.

5.2. Electro-conductive knitted fabrics

The study of EM SE against fabric stretching is a new approach to measure strain sensitivity applied in the present thesis. In this way, the strain is measured with wireless technology, and it takes sensor technology to the next level of development. Woven and knitted fabrics are widely used for sensor applications. Those fabrics are widely used in clothing and technical textile applications. Knitted fabrics have higher elongation properties, and a balanced structure is suitable for sensor applications.

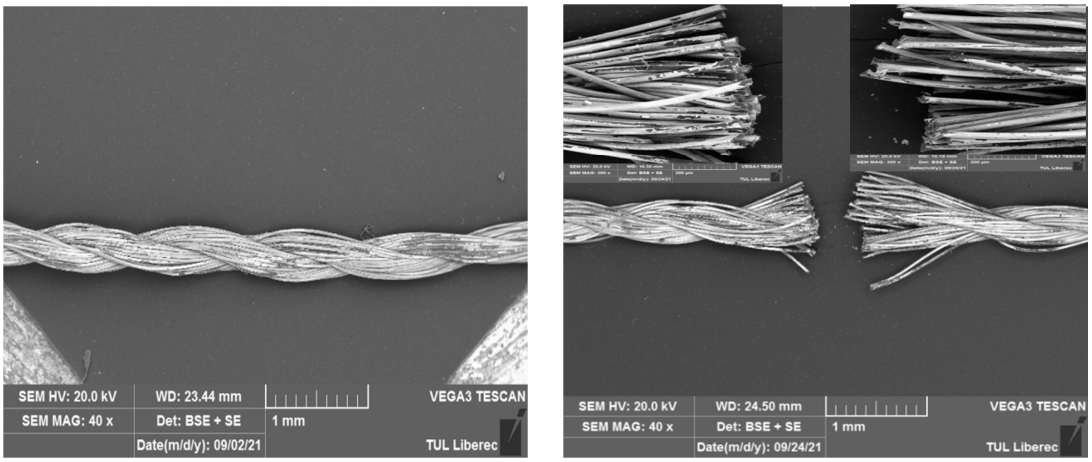

(a) (b)

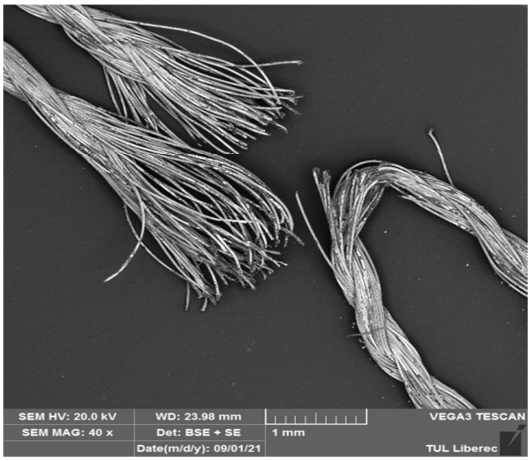

(c)

Figure 40. SEM images of silverized filament yarn surfaces (a) SY before break (x40) , (b) SY after break (x40), and (c) SLY after break (x40).

This work produces the plain jersey and rib knitted fabric using silver-coated yarn to analyze its sensing properties. The biaxial device is used to elongate the fabric in uni-axial and bi-axial directions to find its sensory features. The single jersey and double jersey fabrics are knitted with a flat knitting machine and tested for EM SE, electrical resistance, and porosity during stretching with a biaxial device. This work is based on preparing the wireless sensor fabric, and most of the preliminary examinations are done in this chapter.

5.2.1. Electromagnetic shielding effectiveness of the knitted fabrics

As mentioned above, the SJ and DJ samples, developed at three different densities, L, M, and H, were tested for electromagnetic shielding effectiveness at a frequency range from 30 MHz to 1.5 GHz as shown in Figure 41 (mean values are shown). The average SE at 1.5 GHz frequency together with its 95 % CI of SJ and DJ samples is shown in Table 9 and Table 10.

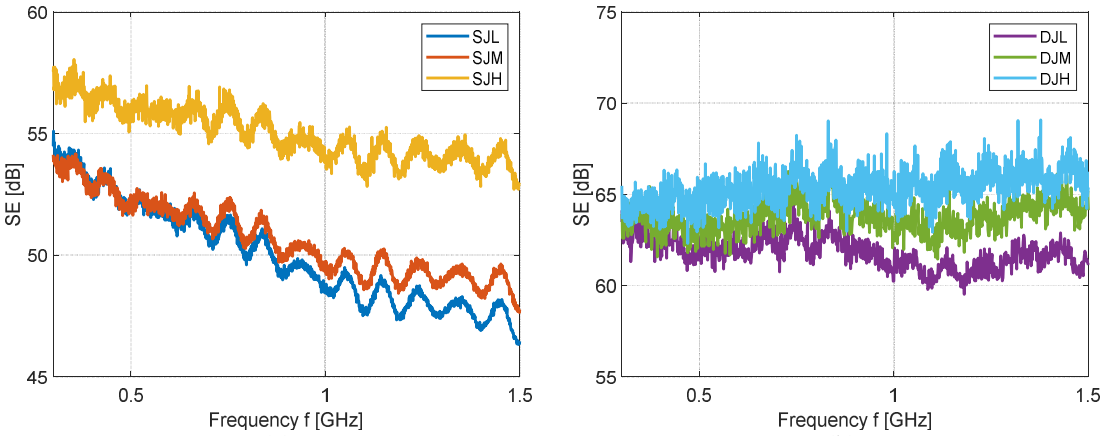

(a) (b)

Figure 41. Dependence of EM SE [dB] vs. frequency, f [Hz] (f = 30MHz - 1.5 GHz) of the (a) SJ and (b) DJ samples.

Table 9. Mean values of SJ knitted samples SE with 95% CI

Sample name	SE [dB] at 1.5 GHz frequency	
	Mean	CI
SJL	46.1	0.25
SJM	48.9	0.31
SJH	52.5	0.24

Table 10. Mean values of DJ knitted samples SE with 95% CI

Sample name	SE [dB] at 1.5 GHz frequency	
	Mean	CI
DJL	61.5	0.54
DJM	64.9	1.89
DJH	64.7	1.07

The EM SE of the single jersey fabrics decreases logarithmically with increasing frequency, as seen in Figure 41(a). Also, the density of the fabric influenced the SE value positively; SE of the SJL, SJM, and SJH fabrics is 46 dB, 49 dB, and 52 dB at 1.5 GHz frequency (see Table 9). The density of the sample influences the fabric thickness as well as the fabric porosity, increase in density increases the thickness, stitch density, and areal density but decreases the loop length (see Table 6). The EM waves are reflected by thicker conductive layers and lesser porous structures. That is the reason why higher-density fabric has higher SE than lower-density fabric. DJ fabric's SE has an ambiguous trend (SE is more or less constant) throughout the frequency range of 30 MHz to 1.5 GHz, as seen in Figure 41(b). The SE of DJ rib fabrics are close to the dynamic range of the measurement device used, therefore the shape of the curves of samples with higher SE is not smooth. This kind of structure has an identical appearance on both sides with paired curves. Also for this sample set it was confirmed that the SE value increases with increasing fabric density; the DJL, DJM, and DJH samples have 62 dB, 65 dB, and 65 dB at 1.5 GHz frequency (see Table 10). The increase in density of DJ is an increase in the amplitude of the SE readings in the graph because higher density fabric has closer loops and increased curves in structure, which creates the higher amplitude. The SJ fabric SE results also have noises, but the amplitude of the SE readings is lesser than the DJ results. This kind of wave is formed with the presence of the pore or aperture in the structure; according to plane wave theory [38], the aperture size induces the amplitude of the SE results. Overall, the DJ fabric sets have higher SE than SJ fabric sets; another reason is the DJ is thicker as well as dense than the SJ.

5.2.2. Mechanical properties of knitted fabrics

The tensile-elongation curve of sample is important to know the stress-strain behavior of knitted fabrics and it was necessary to know it in order to plan further electromechanical experiments. SJM sample was chosen for this experiment. The tensile strength of the SJM fabric is tested with a biaxial device at 3.5 mm/min holder speed, gauge length of 15 cm, and fabric width of 10 cm. SJM knitted fabric is tested for tensile strength at wale-wise and course-wise directions. Figure 42 shows the tensile strength result of the SJM fabric, whereas the wale-wise tensile strength of the sample is in Figure 42(a). The strain increases with increasing stress; after 154 mm elongation, the fabric tensile loses its strength from 115 N/m by breaking its loop structures. In the course-wise tensile shown in Figure 42(b), the strain increases with increasing stress; after 200 mm elongation, the fabric tensile loses its strength from 500 N/10cm by breaking its loop structures. The wale-wise direction strength

of fabric is higher than the course-wise direction strength. The breaking of the fabric occurs slowly that the reason the peak is not dropped suddenly, especially wale-wise. The course-wise elongation is more compared with wale-wise, which is because of loosely constructed loops in course direction, as already discussed. Based on this experiment it was decided that both knitted samples will be deformed in the range from 0 to 25% (indicated in the graph and it corresponds to 37.5 mm) so that the elastic region of the curve was explored. It is also visible from these results that the wale-wise has more elastic recovery than course-wise. The elastic recovery of the fabric is identified as 60 mm and 140 mm for wale-wise and course-wise respectively. It was noticed that the deformation of fabric in one direction is higher and it is much needed for strain sensing application.

5.2.3. Effect of knitted fabric parameters on SE

In this subchapter the comparison of SE sample set will be done with respect to different sample parameters. The comparison of the SJ and DJ fabrics with respect to the SE results is discussed in Figure 43. In a bar chart, the SE versus SJ and DJ fabrics are plotted in Figure 43(a); SE of SJ is higher than the DJ, increases in fabric density from low to high also increases the SE values was noticed. The SE/*h* versus SJ and DJ fabrics are plotted in Figure 43(b), the SJ has higher SE/h than the DJ, the thickness of SJ is lesser, and it has an effect on SE/*h* values. The SE, along with fabric parameters, represent the actual SE values of the fabric samples, which are also considered to take into account for the end use of the fabrics.

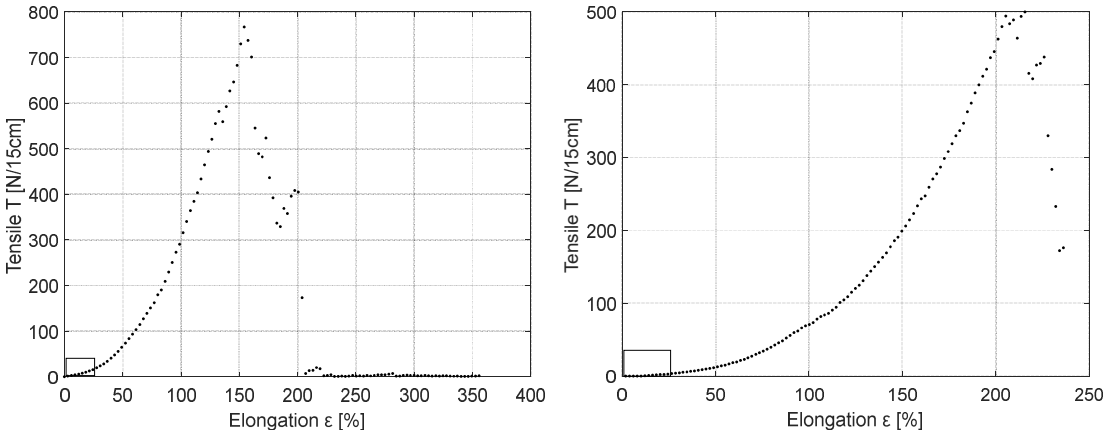

(a) (b)

Figure 42. Stress-strain curve of the SJM fabric tested with the biaxial device at (a) wale-wise and (b) course-wise directions.

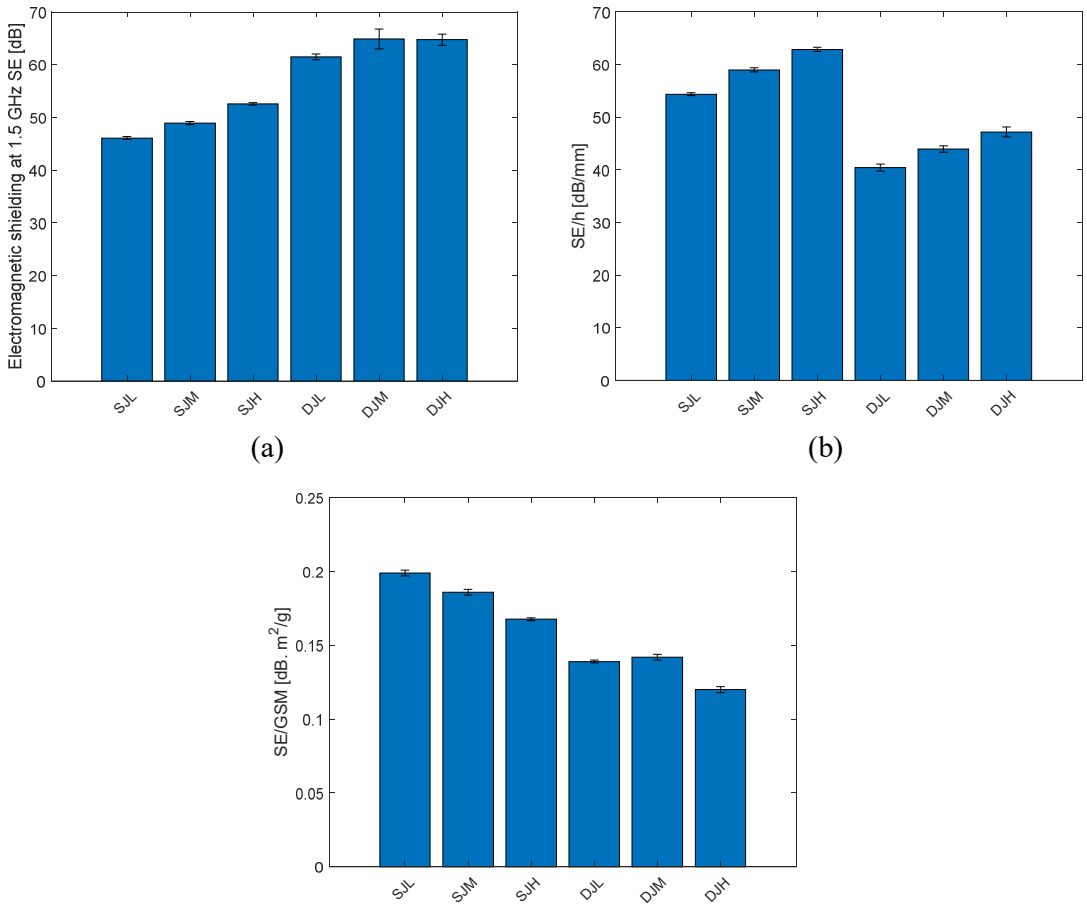

Figure 43. Comparison of (a) SE, (b) ratio of SE and thickness, *h* [mm] and (c) ratio of SE and areal density GSM, (SE [dB] measured at 1.5 GHz frequency) for whole sample set.

In a bar chart, the SE/GSM versus SJ and DJ fabrics is plotted in Figure 43(c); the SE/GSM of the SJ samples has higher than the DJ samples. The SJ has lesser GSM than the DJ, that why the SE/GSM is higher for SJ.

The basic parameters of the fabric samples are stitch density, areal density, thickness, and porosity are compared and shown in Figure 44. The SE is increase with increase in stitch density of the SJ linearly and DJ in nonlinear trend as seen in Figure 44(a). Figure 44(b) shows the SE is increases with increase in areal density for SJ and DJ fabrics, DJ has sudden increase at medium range and no change after. The increase in fabric thickness has different effects on SE, for SJ samples SE has different values but the thickness has no significant difference; DJ samples thickness increases then the SE is decreases slightly as seen in

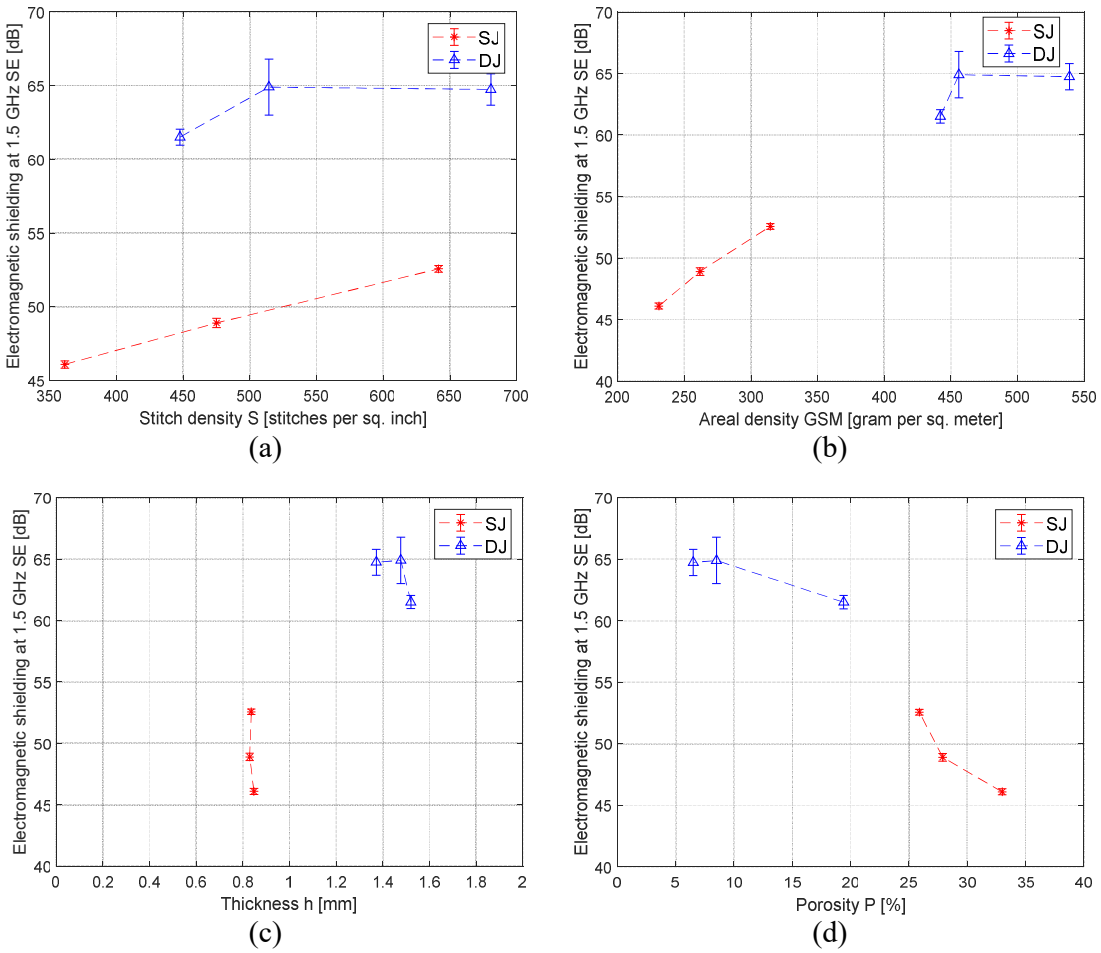

Figure 44. Dependence of SE at 1.5 GHz frequency on (a) stitch density, (b) areal density, (c) thickness, and (d) porosity of the fabric samples.

Figure 44(c). Another main parameter is the porosity of the SJ and DJ fabrics are compared with their SE values in Figure 44(d). An increase in porosity has decreased the SE of the SJ and DJ fabrics; a more open area is transmitting the EM radiation, and the reason the SE decreases with increasing porosity. Those results show the difference in SE with the fabric structure and its densities; it might be helpful to decide the suitable fabric for the sensor range. The DJ's medium density and high density fabrics has no significant difference in SE values was noticed.

The stitch density is the total knit stitches present in square inches, which is the multiplication of courses per inch and wales per inch. In the literature review, it was discussed that fabric density is mainly affecting the electrical and shielding properties. So the effect of the stitch density on SE/GSM, thickness, and porosity was compared for SJ and DJ, as shown in Figure 45, where mean values together with 95 % CI of means are shown. The two main parameters for sensing application are SE and GSM; here, SE/GSM is

compared with stitch density in Figure 45(a). SJ has a decrease in SE/GSM with an increase in stitch density, but DJ structure has increased initially and decreases in SE/GSM with an increase in stitch density (Figure 45(a)). The stitch density of the SJ fabric sample does not affect the samples' thickness, but for DJ, the thickness decreases with an increase in stitch density (Figure 45(b)). The increase in stitch density leads to compressing the structure of DJ, which leads to a decrease in thickness. Both the SJ and DJ porosity decreases with the increase in stitch density (Figure 45(c)), which is expected. An increased stitch density of the fabric causes more loops, which decreases the samples' porosity. The slight change in SE/GSM DJ result is because of the sudden drop in porosity of the medium stitch density fabric. The connecting line in the graphs is used only for better visualization of the results, and it hasn't any approximation meaning.

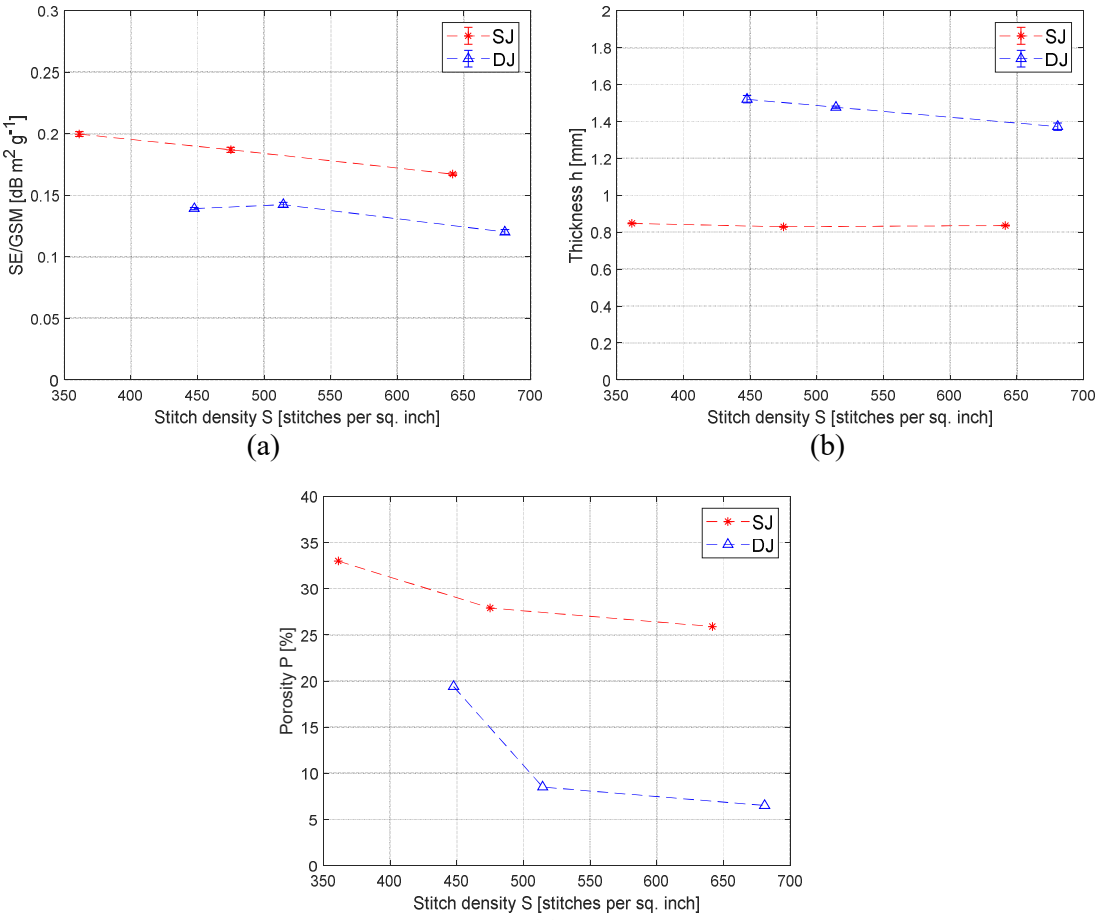

Figure 45. The graph of SJ and DJ fabric stitch density versus (a) SE/GSM in dB sq. meter per gram, (b) thickness, and (c) porosity

5.2.4. Effect of knitted fabric elongation on its electrical resistance

The electrical resistance (ER) is indirectly proportional to the electromagnetic shielding effectiveness if other variables are held constant, which means higher the resistance lowers the shielding and vice versa. EM SE is therefore related to the ER and total ER is mainly affected by the number of contact points between the conductive yarns causing a conductive path. While elongating the knitted fabric, the change in resistance with respect to the number of contact points is derived in Equation (30) and (31). During both way elongation measurements, the ER is measured in a vertical way only because the wale-wise has more influence on ER than course-wise.

The SJ sample's ER behavior is different for different densities; mostly, the ER is decreased while stretching the fabrics. ER for SJ lies between the 1 to 2.5 ohms range for all the samples and there is an observable decrease in electrical resistivity with increasing density of the knitted fabric. During the increasing horizontal way of fabric elongation, the ER is slightly decreasing for all densities of samples. When increasing vertical way fabric elongation ER is decreasing more steeply. During both ways of fabric elongation, ER is deviating moderately between horizontal and vertical ways results. ER of SJL sample has decreased with an increase in elongation at all directions of loading, as seen in Figure 46(a). At both ways of stretching of SJL, the ER increases slightly and then decreases drastically; from 2 to 5 % elongation, the ER increases suddenly because of the relaxation of fabric. SJM sample has decreased in resistance with an increase in elongation at the horizontal way; at vertical and both ways stretching, the resistance increases initially until 7.5% elongation and then decreases drastically, as seen in Figure 46(b). SJM is constructed with moderate stitch density so that the ER is increased vertically as well as both ways of elongation of the fabric and fabric loops loosen in this direction. SJH sample ER slightly decreased with an increase in elongation of the sample, as seen in Figure 46(c). SJH vertical way elongation causes increase in ER initially due to fabric relaxation or pre-tension, but in horizontal way elongation, the resistances increase after 2.5 % to 7.5 % elongation, proving the loose connection between the loops at this point. Based on the stitch densities, the ER results vary with fabric elongation. The loose structure has constantly decreased in ER, but the tight structure has slightly decreased in ER against the elongation. ER trend is somehow similar to the SE results of the SJ fabrics.

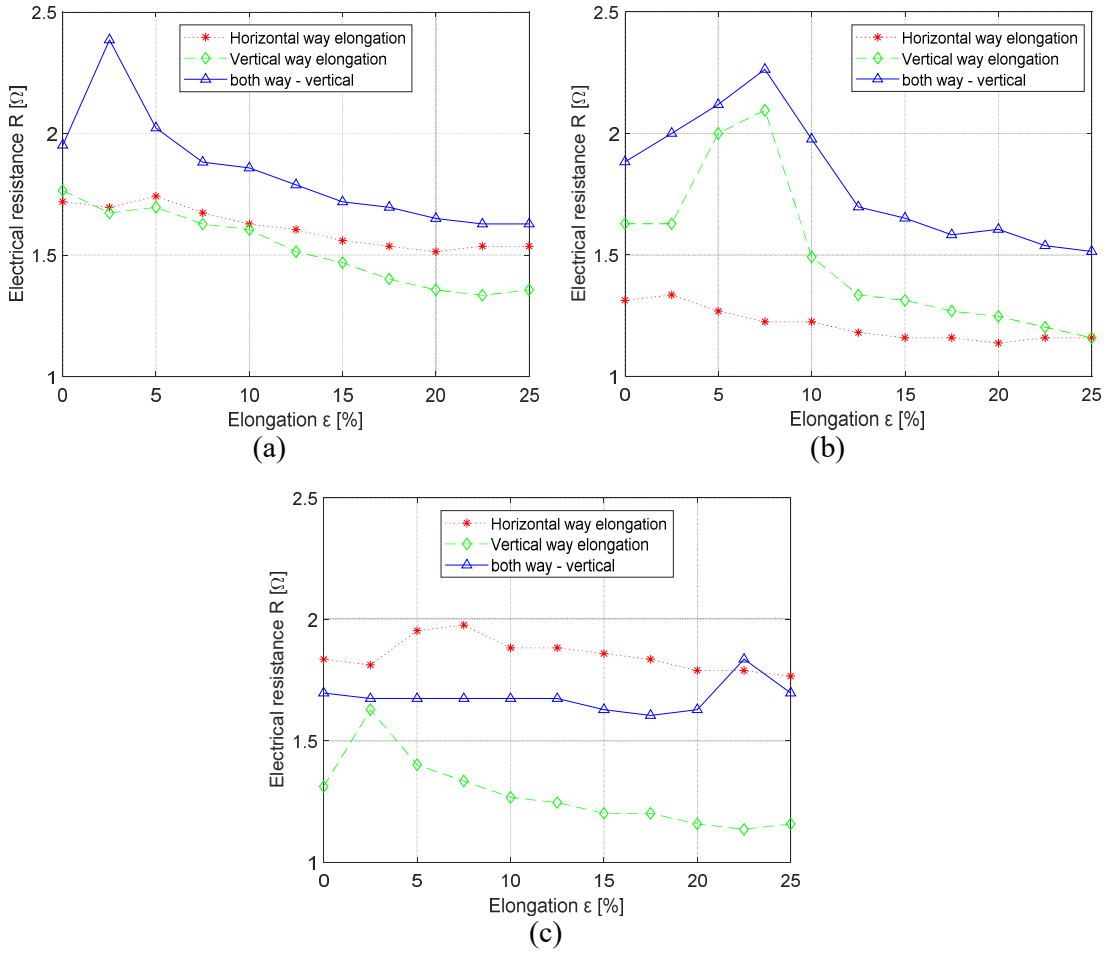

Figure 46. Dependence of electrical resistance R [Ω] on elongation of fabric ε [%] for single jersey fabrics having: (a) low, (b) medium, and (c) high density.

The DJ fabrics have different trends on ER for different densities during fabric elongation, as seen in Figure 47. An increase in fabric density is shifting the ER trend from downward to upward against the fabric elongation. DJ fabrics ERs are behaving similarly for vertical elongation. There is a peak shift in ER results related to fabric density; an increase in the density of the fabric is shifting ER peak from the initial to the final point of elongation. Such kind of shift in the peaks is due to the following reasons. In a loosely constructed structure, the pre-tension between the loops causes less connection between the loop yarn and increases the ER. In tightly constructed structures, the loop yarns surface coating was affected by abrasion after a certain point of elongation and tend to loss in electrical connection, which is why the ER increases at the final stage of elongation. The moderate structure lies between the loose and tight one; here, the wider increase in ER is because of pre-tension. In horizontal way of elongation of DJ samples, ER is almost constant. In vertical way of elongation of DJ samples, ER is decreases after 5% elongation for low and

medium densities. In both ways of elongation of DJ samples, the ER decreases after 5% elongation for low and medium densities. Compared with SJ samples, the DJ samples ER is opposite in horizontal way elongation. The SJ or plain knit structure has a moderately loose course, but the DJ or rib structure is looser. This is the reason that the DJ and SJ horizontal results vary due to structural differences. DJL has an increase in ER initially and then decreases with respect to an increase in elongation at all ways of stretching shown in Figure 47(a). DJM sample also increases ER at an initial stretch and then decreases with vertical and both ways of elongation, as shown in Figure 47(b). DJH sample follows a similar trend to others, but at horizontal way stretching, the resistance has no change with an increase in elongation (Figure 47(c)). The electrical resistivity trends are most closely related to the SE results of the DJ fabrics.

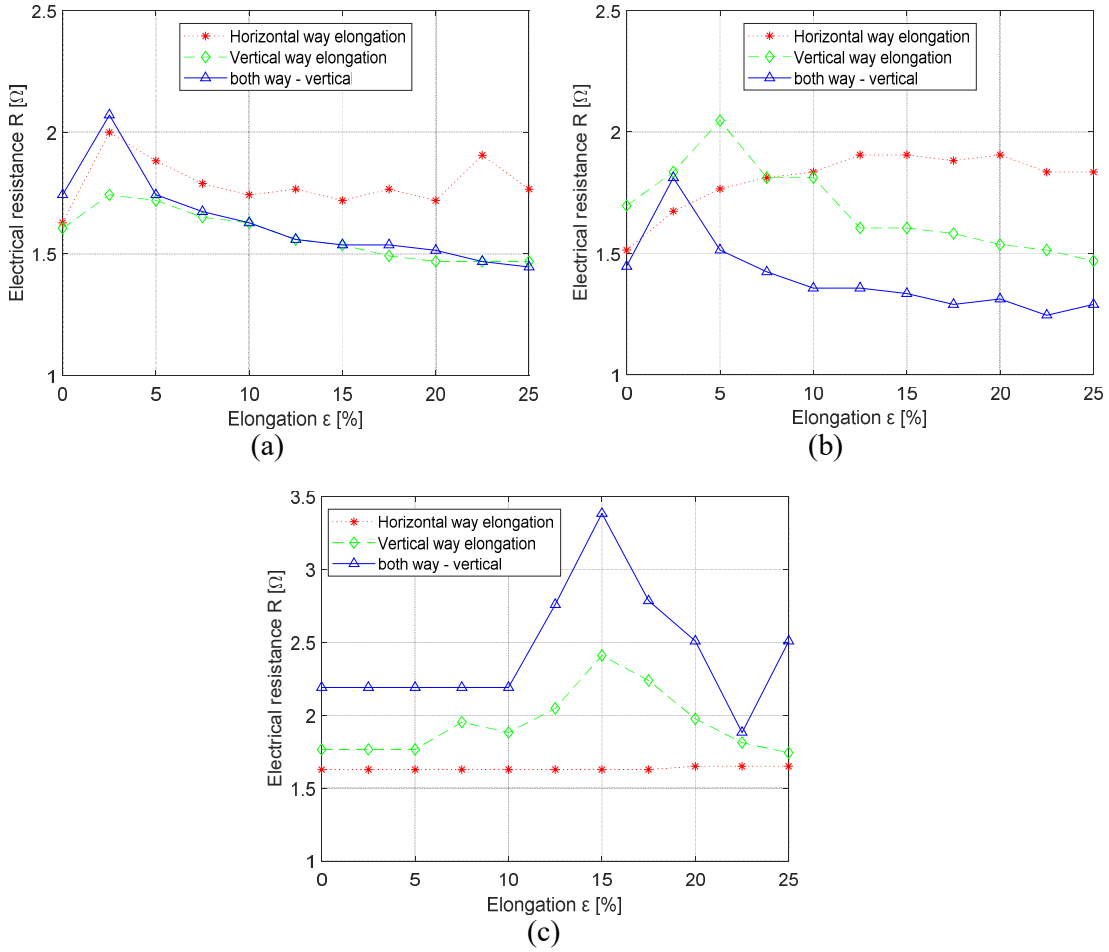

Figure 47. Elongation of fabric ε [%] versus electrical resistance R [Ω] for double jersey having(a) low, (b) medium, and (c) high density.

5.2.5. Effect of knitted fabric elongation on its porosity

The porosity or aperture of the shielding material has significantly affected the SE results, as stated by the theory and also as confirmed in the work Palanisamy et al. [3]. That is why the porosity of the fabric during elongation and its SE is studied in this part.

The elongation versus porosity of the SJ fabric is shown in Figure 48. It is visible that the porosity at 0 % loading (P_0) decreases with higher sample density. The extension of the fabric causes increase of the porosity in most cases, and increasing porosity could affect the shielding effectiveness. SJL, SJM, and SJH fabric's porosity increase with an increase in elongation at vertical, horizontal, and both ways, as seen in Figure 48(a-c), whereas the trend is almost linear. At both ways of elongation, the samples porosity increased much higher than in other ways and the slope of the approximation line would have the highest slope.

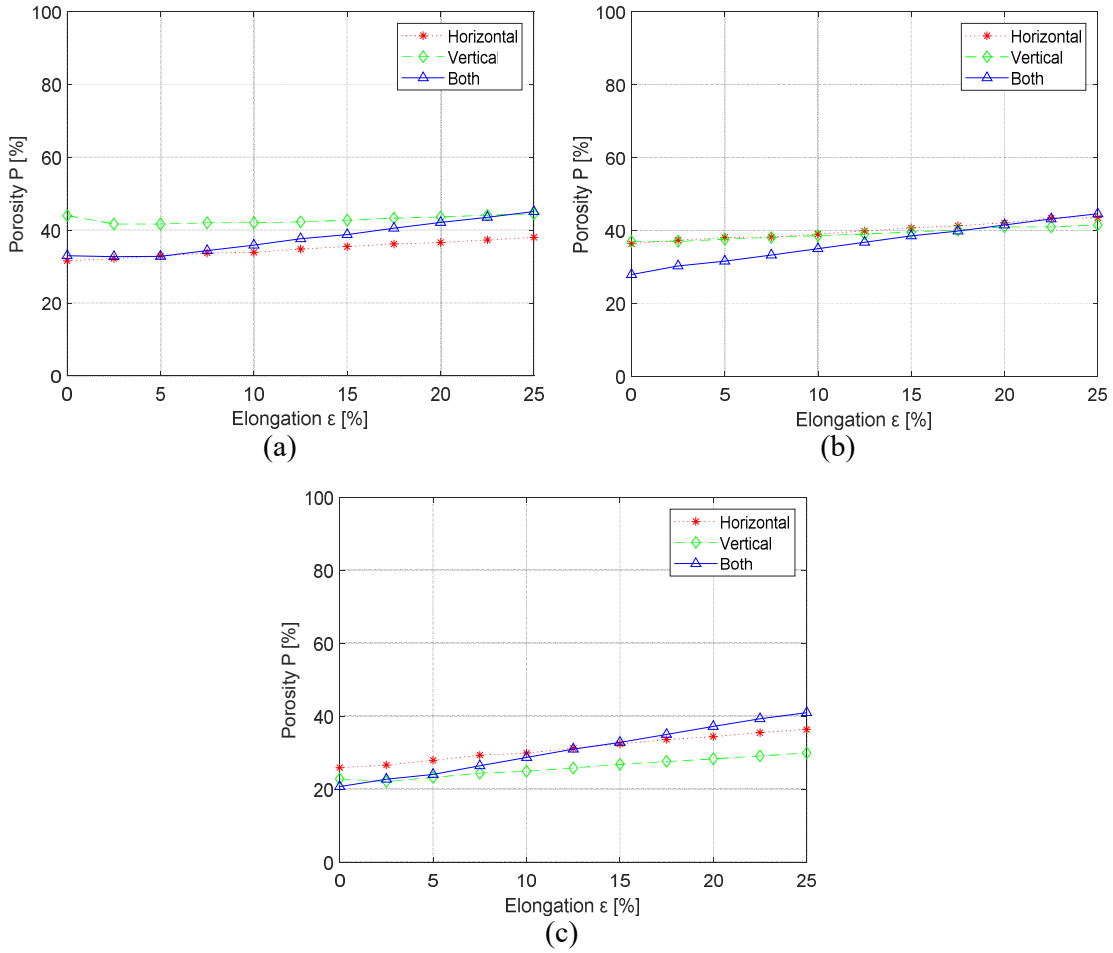

Figure 48. Dependence of open pore area P on fabric elongation ε [%] for single jersey having: (a) low, (b) medium, and (c) high density.

The second most increase in porosity during elongation was noticed at the horizontal way elongation of the fabric. The loops are tightly arranged in a vertical direction or course-wise of the SJ structure, which is not elongating much at this direction of stretch and the effect of stretch on porosity is the lowest one. The density of the fabric also affects the porosity; the higher the density, the greater change in porosity against the elongation noticed. The SJL, SJM, and SJH have a maximum difference in porosity of 16 %, 18 %, and 24 %, respectively, during both ways stretch. In a horizontal direction or wale-wise, the knit loops are arranged loosely to elongate the fabric easily, and the pores are opened wider in this direction of stretch. The knit loop structures affect the porosity with respect to the direction of the stretch. The elongation versus porosity of the DJ fabric is shown in Figure 49. DJL, DJM, and DJH fabric's porosity increase with the elongation at vertical, horizontal, and both ways, as seen in Figure 49(a-c).

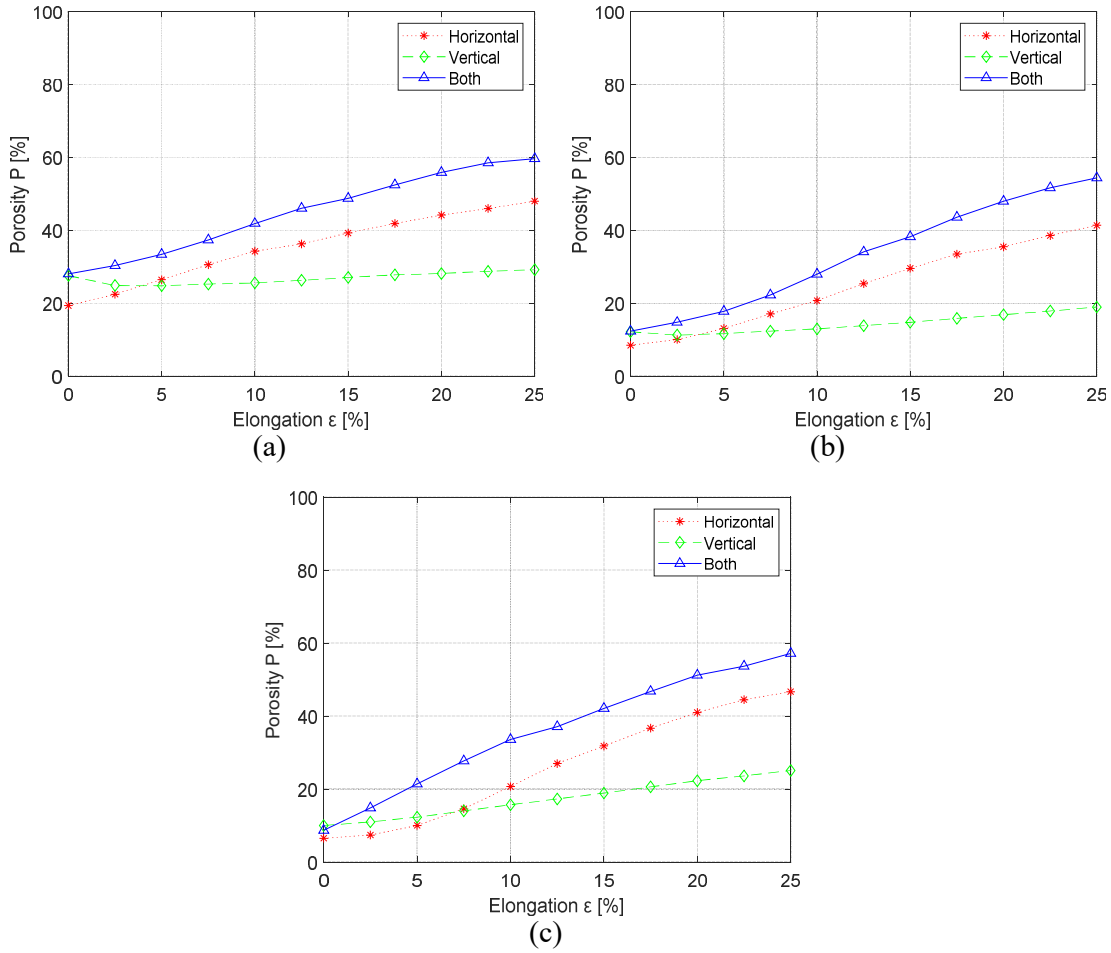

Figure 49. Elongation of fabric ε [%] versus open pore area P [%] for double jersey having (a) low, (b) medium, and (c) high density.

Also, in this case, the increase of porosity with increasing elongation is almost linear. During the both way elongation of the samples, the porosity increased significantly, the slope of the approximation line would be the highest. Significant effect of elongation on porosity can be observed also during horizontal type of elongation, the increase of P is around 40 %. The loops are tightly arranged in a vertical direction or course way of the double jersey structure and that is why samples are not elongating much at this direction of stretch. The loading in vertical direction has the lowest effect on porosity. The density of the fabric also affects the porosity; the higher the density, the greater change in porosity against the elongation noticed. The DJL, DJM, and DJH have a maximum difference in porosity of 30 %, 40 %, and 48 %, respectively, during both ways stretch. In horizontal direction or wale ways, the knit loops are arranged loosely to elongate easily. The porosity is affected by the knit loop structures with respect to the direction of stretch.

5.2.6. Effect of knitted fabric elongation on its SE

The stretching of the fabric in a uniaxial and biaxial direction changes the fabric geometry, as discussed in the literature review. Equations 30 and 31 determine the change in resistance with a change in fabric strain values. If the electrical resistance changes, then the EM SE also changes because those are indirectly proportional to each other.

In case of knitted fabric extension, the increase of electrical conductivity is expected during the initial extension process as shown during electromechanical analysis of crochet chain, which is caused by an increase in the number of contacts between the yarns in the knit structure. This phenomenon could increase the EM SE. On the other hand, it is expected that the porosity of the sample could increase with sample loading, which could have a negative effect on the SE level. That is why, SE of knitted sample set (single jersey, double jersey having 3 different densities) will be studied during all types of elongation experimentally.

The elongation of the SJ fabrics in a horizontal way, vertical way, and both ways versus EM SE at 1.5 GHz frequency is shown in Figure 50. Studied is SE response during the extension of sample to 25 % elongation. The SJ fabrics are produced at three densities: low, medium, and high, based on their stitch density. All three densities of SJ fabrics increase in SE with an increase in fabric elongation at all directions of stretches, as shown in Figure 50. In Figure 50(a), the SJL fabric SE results are shown, and SE increases with all directions of the elongation. Especially, the vertical direction of the stretch has increased the SE value higher compared with horizontal and both ways stretching with increases in elongation. Both ways, points lie in between vertical and horizontal points. The deviation in the SE is higher in the

vertical direction and lowest in the horizontal direction. For SJM and SJH, fabric samples also have higher SE differences at vertical way stretch, but at horizontal and both ways stretching of the samples also increases the SE value with increases in elongation (Figure 50(b,c)). In the vertical direction elongation of the fabric, the wales are expanding, and courses are contracting; wales are tightly constructed, and contact between the yarns increases with elongation; that's the reason why the SE increases much. The SJL, SJM, and SJH have the SE of 50 dB, 53 dB, and 57 dB at 25 % vertical way elongation. SE is higher for high-density fabric, and the difference between the initial and final elongated SE values also had more difference than other densities.

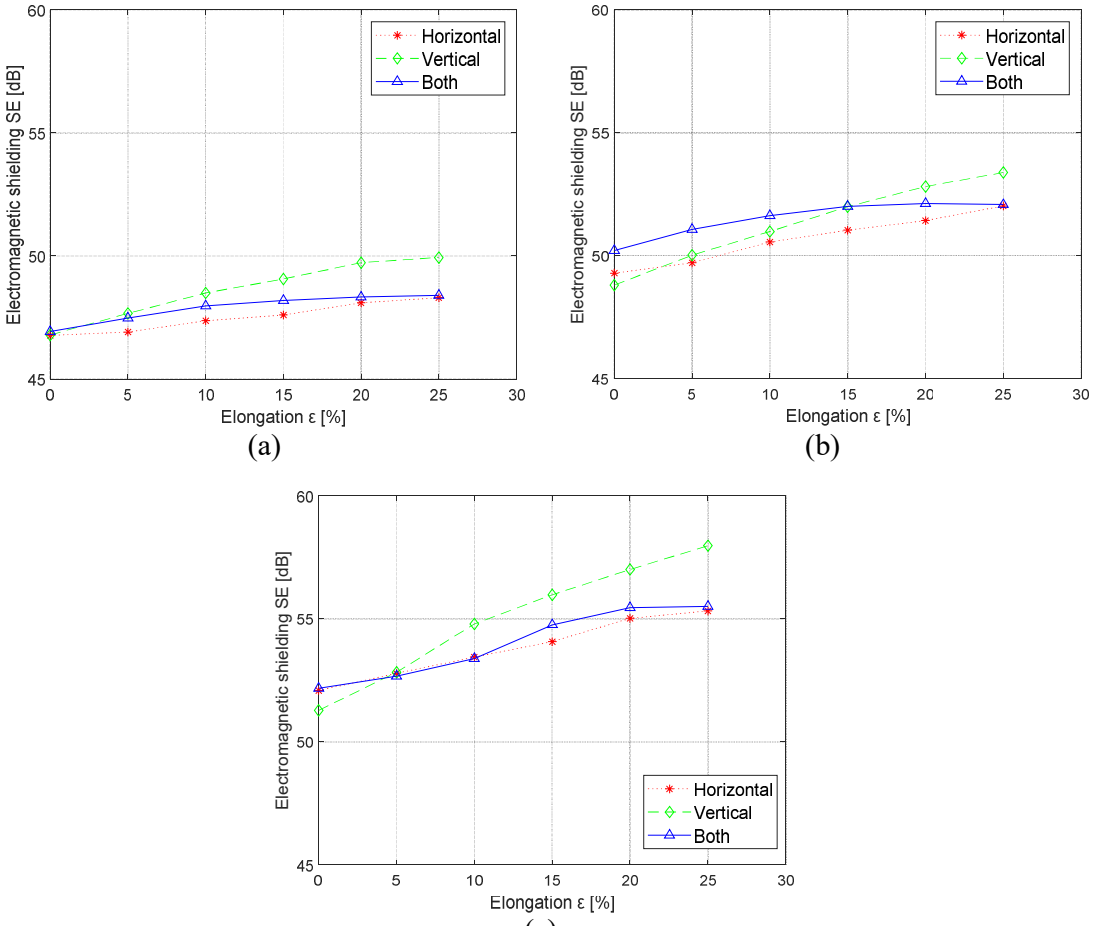

Figure 50. Dependence of SE [dB] at 1.5 GHz frequency on elongation ε [%] for sample: (a) SJL, (b) SJM, and (c) SJH.

For the creation of sensors, it seems that the most interesting stretching mode is the vertical stretching of the sample, when a linear increase in SE with elongation is observed for all densities of samples and also during vertical stretch the highest ΔSE (SE-SE_0) is achieved, namely approx. 5 dB for a sample with low and medium density and approx. 7 dB for a sample with high density.

The elongation in the percentage of the DJ fabrics in a horizontal way, vertical way, and both ways directions versus EM SE at 1.5 GHz frequency results are shown in Figure 51. The double jersey fabric was prepared also in three densities: low, medium, and high. All the fabrics have the same trend in SE versus elongation graph: the vertical way stretch of the fabric causes linear increase of SE with increasing elongation; the horizontal and both ways stretching fabrics cause first a decrease in SE followed by an increase in SE, however, SE does not exceed SE_0 at 25 % elongation. DJL, DJM, and DJH fabrics results are shown in Figure 51(a), 51(b), and 51(c); all the results follow the same trend as described above. In a vertical way, the difference in SE values at initial to final elongation increases with an increase in fabric density from low to high. Fabric stretch in a horizontal way for DJ fabrics decreases steeply until 10 % elongation and then increases by 1 dB until 25 % elongation, the SE values from 10-25 % elongation is very less changes. During the both ways stretching, the DJ fabrics SE decreases steeply until 10% elongation and then increases by 3 dB from 10 % to 25 % elongation, the SE value from 10-25 % elongation has average change. Both ways of stretching have very less change in SE values during fabric elongation. The reason for the change in SE with respect to the direction of elongation is further studied with electrical properties and porosity analysis. The main reason behind the change in SE is the changing number of contact points between the yarns; the vertical way produces more contacts, and the horizontal way loosens the structure to create lesser contact points.

If we look at the results considering the requirements for the creation of strain sensors, the use of vertical tensile stress of the samples seems to be the most interesting, where a linear change of SE with a change in elongation is observed, while the average ΔSE is about 3-5 dB.

5.2.7. Effect of knitted fabric elongation on SE sensitivity

The SE sensitivity (SES) or gauge factor is the important parameter for describing the fabrics strain sensitivity results. The gauge factor (GF) is used to indicate the strain sensitivity of the fabric and its formula is given in Equation 40.

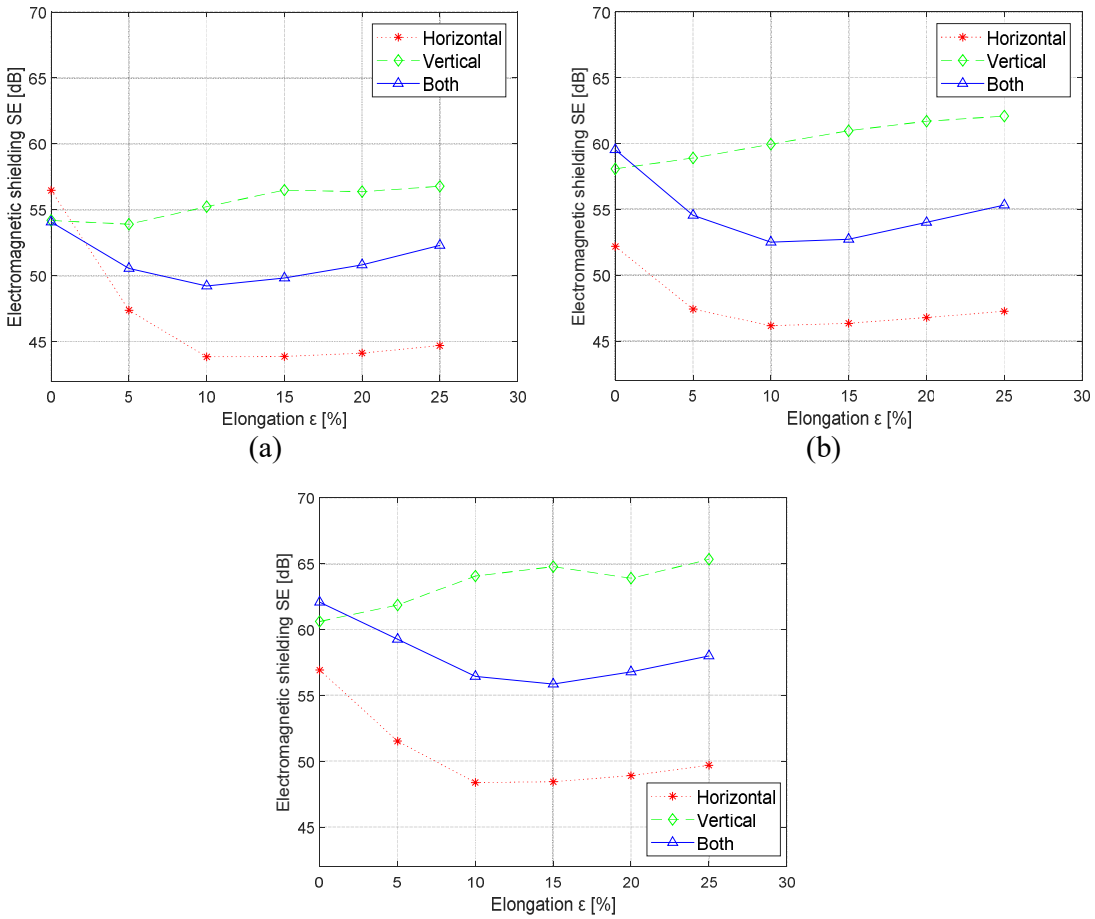

Figure 51. Dependence of SE [dB] at 1.5 GHz frequency on elongation ε [%] of (a) DJL, (b) DJM, and (c) DJH.

Here the sensitivity based on SE values is shown against the vertical elongation of the fabric samples (Figure 52); because there is one directional change was noticed at vertical elongation for SJ and DJ fabric.

$$\boldsymbol{GF = SES = \frac{SE_x - SE_0}{SE_0} = \frac{\Delta SE}{SE_0}} \quad , \qquad \text{Eq. 38}$$

where, SE_x is the SE value at x % elongation, SE_0 is SE value at 0% elongation, and ΔSE is difference between SE_x and SE_0. The elongation of the SJ fabrics versus EM SE with respect to SE at 0% elongation (SE_0) as also called as SE sensitivity (SES) was shown in Figure 52(a). The SES of the SJ fabrics increases with the increase in elongation at vertical direction. The dependence of SES on elongation has very good correlation and its R^2 is 0.80. The DJ fabrics dependence of SES on vertical elongation of fabric is shown in Figure 52(b).

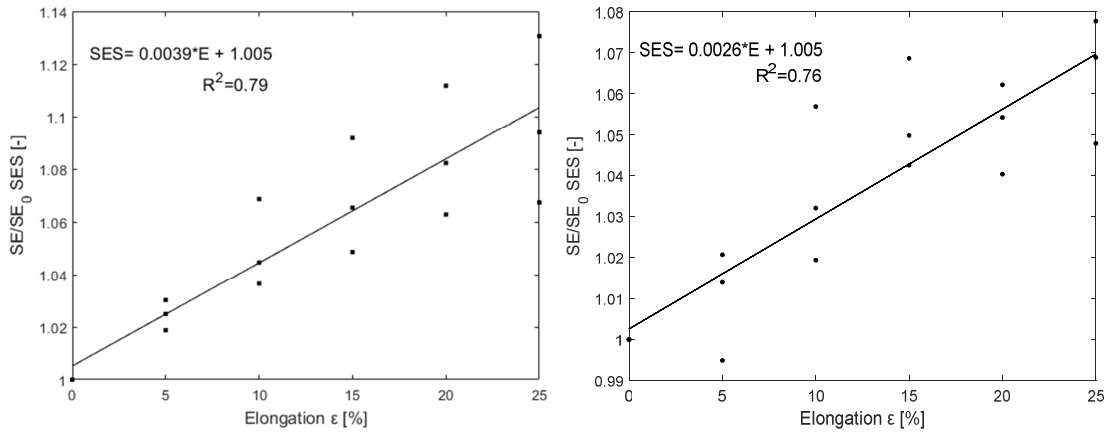

(a) (b)

Figure 52. Dependence of SE sensitivity SE/SE_0 [-] at 1.5 GHz frequency for vertical direction of elongation ε [%] of (a) SJ, and (b) DJ.

Here, the linear increase of SES with increase in fabric elongation at vertical direction was noticed. The predictability and correlation of SES on elongation for DJ fabrics is very good and its R^2 is 0.76. The vertical elongation of the fabrics results are taken further for regression analysis to find out the correlation between explanatory variables.

5.2.8. Empirical model building

As mentioned above, measurement of SE needs special devices. In addition, measurements of electrical conductivity and porosity of textiles are common tests. Another goal of the work was therefore to describe the behavior of the electromagnetic shielding parameter of knitted fabrics based on the knowledge of their conductivity and porosity in a certain degree of elongation. The aim is therefore to propose 2 prediction equations, for single jersey and for double jersey knitted fabric, valid for all 3 types of samples in terms of their density. This modeling was limited to only one type of such stress, namely in the vertical direction, which seems to be the most interesting for the creation of sensors.

A linear regression model is formed by a linear combination of explanatory variables x or their functions. A linear model generally means linear according to the model parameters. This analysis is in fact valid for all types of model where the least-squares criterion is used for model adjustments. Principal regression attacks the problem by regressing y variable on the important principal components and then parceling out the effect of the principal component variables to the original variables [99]. The linear regression model is used for analysis of the results in this part to find out the predictability of x variable with respect to y.

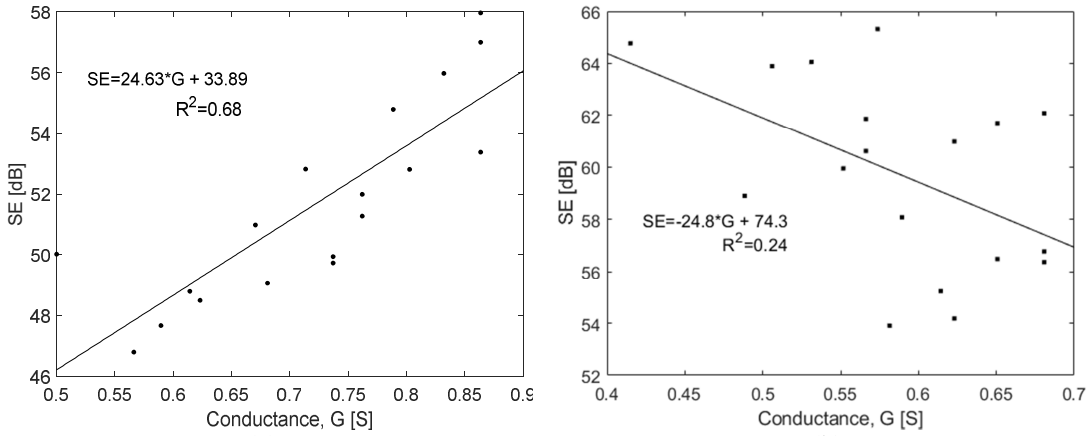

(a) (b)

Figure 53. Dependence of SE on *G* for (a) SJ, (b) DJ fabrics.

In the first step, dependence of SE on electrical conductance *G* [S] and the dependence of SE on porosity *P* [%] were plotted and investigated in order to choose a suitable approximation model. In Figure 53, the dependence of SE on *G* for both knitted structures is shown, whereas a linear relationship with a relatively high correlation coefficient between the two variables can be observed. The SE at 1.5 GHz frequency versus electrical conductance graph was plotted for wale-wise elongation of SJ fabrics (Figure 53(a)). It was noticed that the increase in fabric electrical conductance increases the SE. Some points in conductance are scattered and make a 2 dB difference in the results; this change in SE is due to the difference in fabric parameters. In Figure 53(b) the conductance, *G* versus SE at 1.5 GHz frequency graph was plotted for wale-wise elongation of DJ fabrics. It was noticed that the increases in electrical conductivity have decreased in SE, but three separate trends were noticed because of three fabric densities.

In Figure 54, the SE dependence on porosity *P* was plotted for SJ and DJ fabric samples during wale-wise elongation. In general, the porosity of the SJ fabrics increases which also increases the SE values as seen in Figure 54(a). This phenomenon is probably not caused by increasing pores in the knitted fabric only, but increasing contact between the yarns as the elongation increases. There are three different data clouds which indicate the three different densities; for higher density fabric the less porosity was noticed and the change in SE was higher and vice versa to lower density fabric. The porosity versus SE for DJ fabrics is in Figure 54(b), the porosity increases then the SE values also increase was noticed.

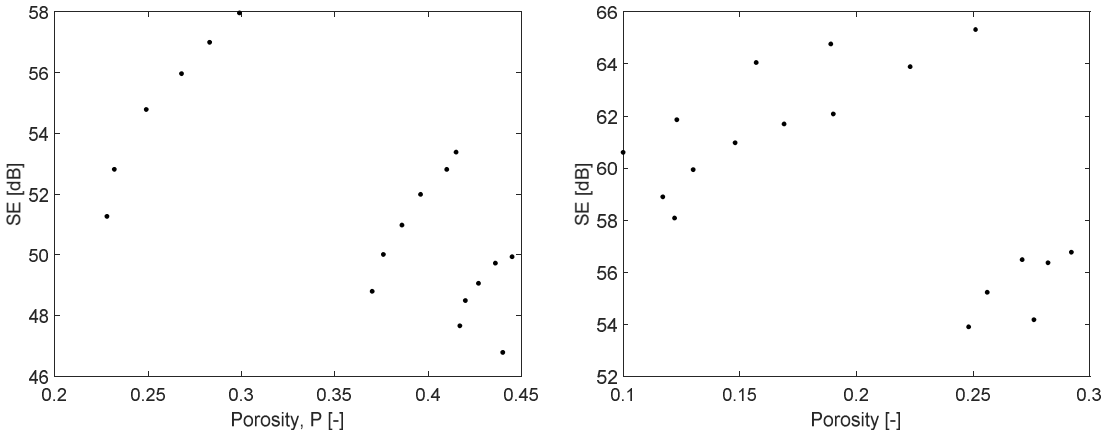

(a) (b)

Figure 54. Dependence of SE on *P* for (a) SJ, (b) DJ fabrics.

Higher density fabrics has higher SE values and changes in SE also higher, lower density fabrics has lesser SE and the changes in SE is lesser compare with medium and higher density fabrics. For exact analysis of the porosity results with irrespective of fabric densities, the gauge porosity was introduced and the results were analyzed.

Figure 55 shows dependence of SE on *P* for both knitted structures. It is visible from the SE, *P* dependence that 3 data groups are distinguishable because the samples differ in the density of rows and columns. For this reason, the relative variable P/P_0 was used (where *P* is actual porosity at actual level of extension and P_0 is sample porosity in the relaxed state, see Table 6), which describes this dependence better (see Figure 55 where dependence of SE on P/P_0 is shown and approximated by linear model with relatively high correlation coefficient) and the intended relationship will be able to be used universally for any density of knitted sample. SJ fabrics gauge porosity (*GP*) (Porosity/ P_0 (porosity at zero elongation)) was calculated and plotted against the SE at 1.5 GHz frequency in Figure 55 (a); gauge porosity (*GP*) increases which increase the SE is seen in the result. Usually, the increase in porosity increases the transmission of EM radiation. In this case, it is quite the opposite; the reason is that the yarn-to-yarn contact increases during stretching, which leads to an increase in conductivity, so porosity is not affecting the SE. The SE on GP has a high coefficient of determination of 0.86 and it indicates the GP has very good correlation with SE. DJ fabrics GP (Porosity/ P_0 (porosity at zero elongation)) was calculated and plotted against the SE at 1.5 GHz frequency in Figure 55(b).

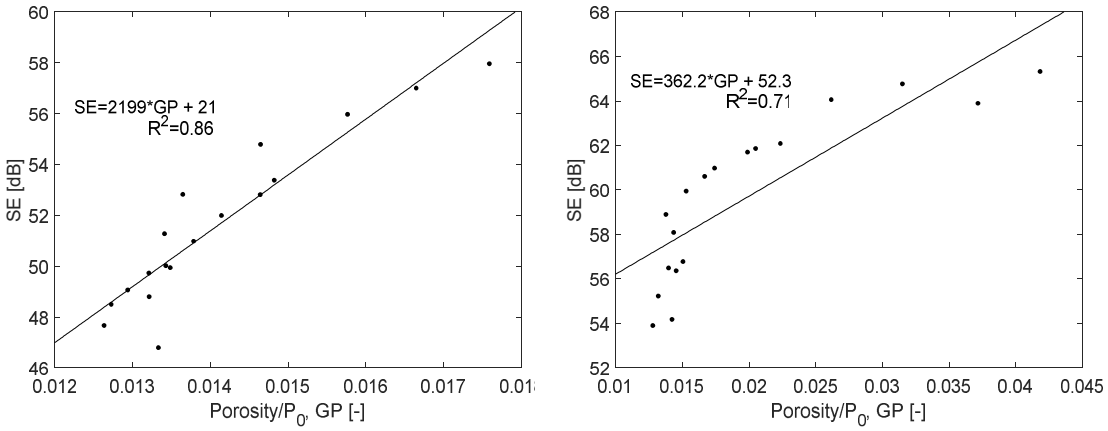

(a) (b)

Figure 55. Dependence of SE on P/P_0 for (a) single jersey, (b) double jersey fabrics.

The SE increases with an increase in GP, and its coefficient of determination is 0.71 means GP has a good correlation. The wale-wise elongation of all the fabric samples follows the linear trend for SE versus GP.

The modelling part mainly discusses the measured and calculated SE value comparison and regression analysis of the SJ and DJ fabrics elongated in vertical directions. Based on preliminary analysis, two main variables $x_1 = G$, $x_2 = GP$ were selected, see Table 11. The corresponding linear regressing has the form:

$$\boldsymbol{SE = b0 + b1.x1 + b2.x2} \qquad \text{Eq. 39}$$

The dependence between measured and predicted SE is shown in Figure 56. The linear regression between the SE predicted versus SE measured for SJ fabrics in Figure 56(a) follows a linear trend, and its coefficient of determination is 0.90, which means the linear model is acceptable for predicting the SE value. The linear regression between the SE predicted versus SE measured for DJ fabrics in Figure 56(b) follows a linear trend, and its R^2 is 0.71, which means the linear model has a good correlation to predict SE value. The coefficients for the linear regression model (Equation 41) for both types of knit are shown in Table 12. Because the dependences between measured and predicted SE are slightly curved and scattered (especially for the DJ fabric), the partial regression graphs were constructed and explored [99], see Figure 57 and Figure 58.

Table 11. Symbols and names.

Symbol	Characteristic name	Characteristic unit
G	Electrical conductance	S
P	Porosity	%
P_0	Initial porosity	%
GP or P/P_0	Gauge porosity	-

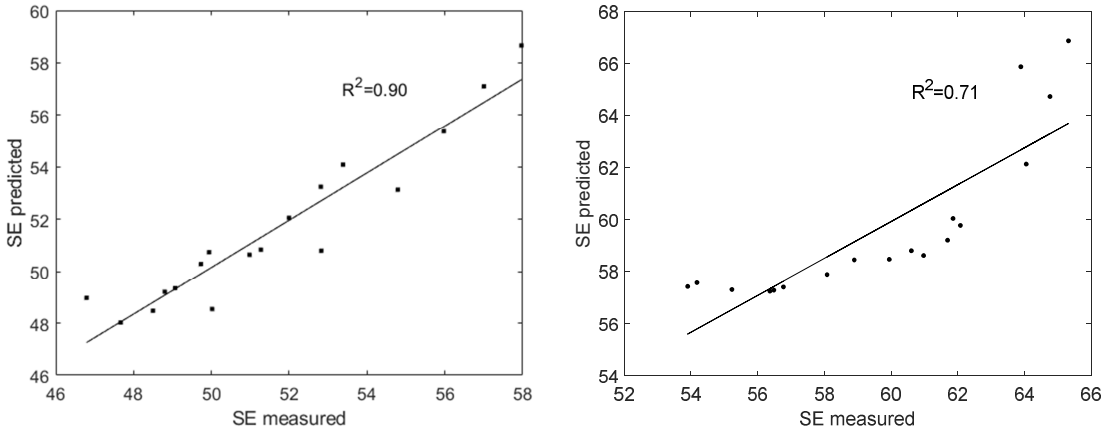

Figure 56. SE measured versus SE predicted using Equation 41 for (a) SJ, and (b) DJ fabrics.

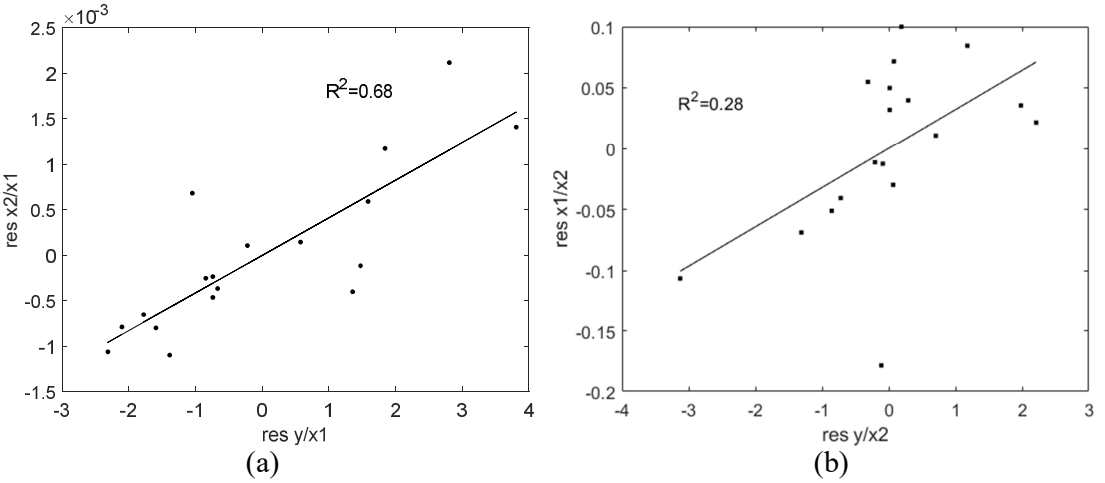

Figure 57. Partial regression graphs for model (Equation 41) (a) variable 1, (b) variable 2 for single jersey sample set.

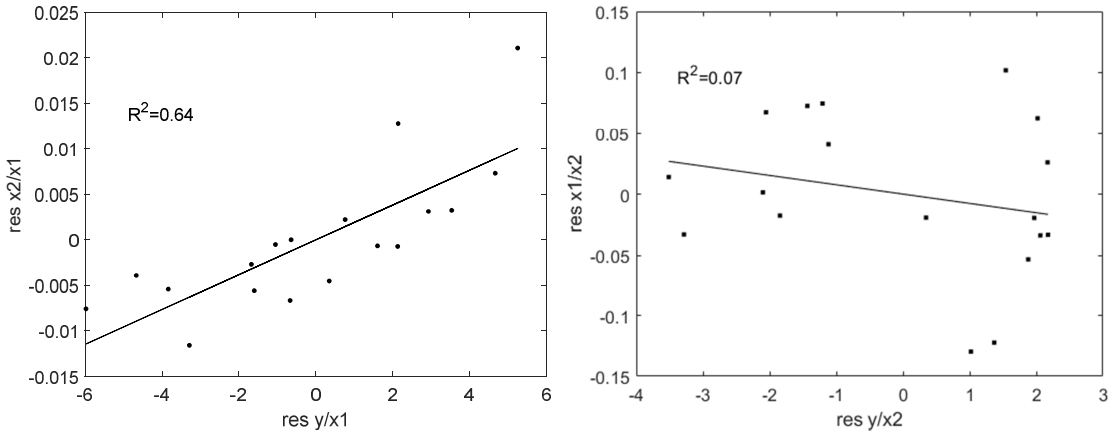

(a) (b)

Figure 58. Partial regression graphs for model (Equation 41) (a) variable 1, (b) variable 2 for double jersey sample set.

Due to nonlinearity of the x_2 variable in particular the modified regression model was created using transformation of this variable. The model has the form:

$$\boldsymbol{SE = b0 + b1.x1 + b2.\sqrt{x2}} \qquad \text{Eq. 40}$$

The corresponding coefficient of determination is 0.91 and 0.87 for single jersey and double jersey respectively. The relation between predicted and measured SE for this model is shown in Figure 59. The regression model coefficients are shown in Table 13. The model with square root for x_2 variable or P/P_0 has higher predictability and it is recommended for modelling of the sensors made of electrically conductive knitted fabrics.

Table 12. Regression coefficients for regression model (Equation 41) for SJ and DJ

Coefficients	Single jersey	Double jersey
b0	21.85	57.46
b1	8.91	-7.78
b2	1655.38	333.56
R^2	0.90	0.71
Adj. R^2	0.89	0.69

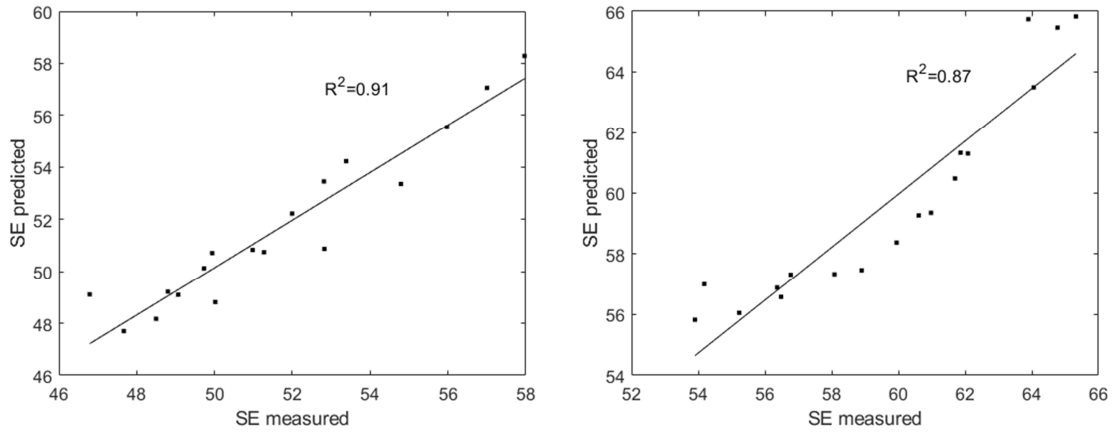

(a) (b)

Figure 59. SE measured versus SE predicted at 1.5 GHz frequency using Equation 42 of (a) SJ, and (b) DJ fabrics.

Table 13. Regression coefficients for regression model (Equation 42) for SJ and DJ

Coefficients	Single jersey	Double jersey
b0	73.57	74.05
b1	7.51	-6.7
b2	-0.76	-0.36
R^2	0.91	0.87
Adj. R^2	0.90	0.86

6 CONCLUSIONS

The conductive knitted fabrics were developed successfully for the deformation characteristic. The electromagnetic shielding during the deformation at biaxial stretching of the fabrics is measured.

In preliminary findings of this work, it was found out the traditional textile materials like cotton, viscose, polyester, and wool are insulators, totally transparent to electromagnetic waves. Additionally it was explored that imparting moisture to them also shows insignificant changes in electrical resistance as well as electromagnetic shielding capacity. It is universally known that most metals are very good conductors of electricity; copper, gold, silver, nickel, zinc, aluminum, etc., are those metals. Usage of the conductive metal and polymer coatings applied on the surface of the fibers or fabrics represents one the possibilities to increase the electrical conductivity of the fabrics. By a comparison of different conductive textile materials it was found that the electrically conductive woven and knitted structures are very good for electrical and EM shielding applications. The copper and silver-coated textile materials exhibit very good SE and conductivity. Also carbon fabrics also have very good conductivity and EM shielding. Secondly, copper nonwoven strips were prepared, laid with different aperture sizes, and tested for SE. It was found that the size of the apertures is influencing significantly with the SE results.

The main part of the thesis work focused on developing deformation sensors with knitted fabrics. The Ag coated PA yarn was used for preparing the knitted fabric was initially analyzed for its electrical properties during its extension. Three forms of yarns, SY, SLY, and MLY, were used to simulate the simple elements of knitted structure. ER against gauge length was measured proving that ER is highly correlated with gauge length, whereas it was found that SL form has the lowest electrical length resistance caused by its structure. The tensile strength of the SY, SLY, and MLY are 42.4 cN/tex, 61.3 cN/tex, and 72.9 cN/tex, respectively, and breaking elongation is highest for MLY. MLY is imitating the single column of the knitted structure. The electromechanical properties of the yarn forms were analyzed with a tensile tester connected with an ARDUINO resistance circuit, and data were recorded in MATLAB. It was found out that ER decreases initially and then increases with an increase in elongation for MLY and SLY forms, but for SY, the ER increases with an increase in elongation. The number of contact points is influencing the ER against the elongation of yarn, MLY has multiple contact points, and SY has only one contact point. ER

of MLY decreases up to 25 % during elongation, but for SLY, it decreases up to 10%; here, the electrical conductivity increases with the increase in contact points proven in yarn forms.

The SJ and DJ (1x1 rib) fabrics were knitted with a flat knitting machine with three various fabric densities, which are analyzed for deformation sensing ability. In most of the literature, ER is used for measuring the strain sensitivity but in this study, EM SE property of the fabric is used as wireless sensing measurement. It is known that the EM SE is inversely proportional to the ER functions of the fabric samples. Moreover, some additional factors like fabric porosity, number of yarn contact points in fabric, and fabric structure has singled out as influential for the SE results. In the relaxed state the EM SE of the SJ fabrics decreases logarithmically with increasing frequency, and the DJ fabric is almost constant throughout the frequency range (30 MHz to 1. 5 GHz). DJ fabrics have higher SE than SJ fabrics because of higher densities. SE difference between the low and high density DJ is 3dB at 1.5 GHz frequency. Increase in fabric density has decreases the porosity, thickness, and SE/GSM but increases the SE/*h*, and SE in SE/GSM. SJL has higher SE/GSM value among the whole set of samples which means the more efficiency of SE was obtained. In the fabrics' basic parameters, the porosity and GSM results are as expected; SE/GSM and SE/*h* are factors for developing the sensor fabrics.

The SJ and DJ fabrics' SE versus elongation results reflect deformation sensitivity. For uniaxial and biaxial elongation of the samples, the biaxial device was used equipped with four independent jaws. SE of SJ samples increased with increasing fabric elongation at all directions, and the change in SE was more significant for higher-density fabrics. DJ samples SE showed a parabolic trend during course-wise and both directional elongation and SE had an increasing trend at wale-wise elongation. On the basis of this research, for the creation of sensors, it is recommended to use SE changes in the wale wise direction of the knitted fabric, where a linear trend was observed under uniaxial tensile stress.

The electrical resistance is indirectly proportional to the SE, which also influences the fabric results. ER is decreased with an increase in elongation at all directions for SJ fabric; for DJ samples, ER increases and then decreases with an increase in elongation at all directions. It was noticed that the wale-wise elongation has a significant difference in SE values, and this way of fabric strain measurement will be suitable for sensor applications. SE increases with an increase in gauge porosity of the SJ and DJ fabric samples. The pore sizes of studied fabrics are in units of micrometers, and the wavelength of 1.5 GHz is 0.19 meters, so it expected that the electromagnetic wave of his frequency cannot penetrate through the fabric.

According to the conductance results of wale-wise elongation, the SE increases with SJ and decreases in DJ elongation, but for DJ density wise it conductance was increases. The rib structure contact points loosen by wale-wise elongation, which decreases the fabric's electrical conductivity.

During the modelling of SE depending on the uniaxial tensile stress of knitted samples, two regression models were introduced. As predictor, variables electrical conductance and gauge porosity of the sample at given elongation were chosen. In the first proposed model, only the main effects of SE were considered. Based on the partial regression graph analysis the nonlinearity in the gauge porosity was identified and that is why optimal regression model was created using transformation of this variable. The corresponding coefficients of determination R^2 of this model are shown in Table 12 and Table 13, respectively, which is satisfactory.

This deformation sensor model will be used as wireless strain sensor is mainly focused on replacing the wired strain sensors, which are already used in structural health monitoring and wearable body moment measurements; also able to use in vehicle testing, structural health monitoring, and construction applications. This wireless sensor is cost-effective based on wire-free use. The light weight and portable measuring device for SE is helpful for development of such sensor in future.

7 REFERENCES

[1] S. Palanisamy, V. Tunakova, and J. Militky, "Fiber-based structures for electromagnetic shielding – comparison of different materials and textile structures," *Text. Res. J.*, vol. 88, no. 17, pp. 1992–2012, 2018.

[2] S. Palanisamy, V. Tunakova, J. Militky, and J. Wiener, "Effect of moisture content on the electromagnetic shielding ability of non-conductive textile structures," *Sci. Rep.*, vol. 11, no. 1, pp. 1–10, 2021.

[3] S. Palanisamy *et al.*, "Electromagnetic interference shielding of metal coated ultrathin nonwoven fabrics and their factorial design," *Polymers.*, vol. 13, no. 4, p. 484, Feb. 2021.

[4] C. Christopoulos, *Principles and techniques of electromagnetic compatibility*, Second. Boca Raton, Florida, USA.: CRC Press, 2018.

[5] C. Morari, I. Balan, J. Pintea, E. Chitanu, and I. Iordache, "Electrical conductivity and electromagnetic shielding effectiveness of silicone rubber filled with ferrite and graphite powder," *Prog. Electromagn. Res. M*, vol. 21, pp. 93–104, 2011.

[6] M. H. Al-Saleh and U. Sundararaj, "Electromagnetic interference shielding mechanisms of CNT/polymer composites," *Carbon N. Y.*, vol. 47, no. 7, pp. 1738–1746, 2009.

[7] S. A. Schelkunoff, *Electromagnetic waves,* New York: D Van Nostrand Co., 1943.

[8] R. B. Schulz, V. C. Plantz, and D. R. Brush, "Shielding theory and practice," *IEEE Trans. Electromagn. Compat.*, vol. 30, no. 3, pp. 187–201, 1988.

[9] T. W. Wieckowski and J. M. Janukiewicz, "Methods for evaluating the shielding effectiveness of textiles," *Fibres Text. East. Eur.*, vol. 14, no. 5, pp. 18–22, 2006.

[10] N. Quiévy *et al.*, "Electromagnetic absorption properties of carbon nanotube nanocomposite foam filling honeycomb waveguide structures," *IEEE Trans. Electromagn. Compat.*, vol. 54, no. 1, pp. 43–51, 2012.

[11] P. Saini, V. Choudhary, B. P. Singh, R. B. Mathur, and S. K. Dhawan, "Polyaniline-MWCNT nanocomposites for microwave absorption and EMI shielding," *Mater. Chem. Phys.*, vol. 113, no. 2–3, pp. 919–926, 2009.

[12] D. Munalli, G. Dimitrakis, D. Chronopoulos, S. Greedy, and A. Long, "Electromagnetic shielding effectiveness of carbon fibre reinforced composites," *Compos. Part B Eng.*, vol. 173, p. 106906, 2019.

[13] FTTS-FA-003, "Specified requirements of electromagneticshielding textiles," *Committee for Conformity Assessment of Accreditation and Certification on Functional- Report*, New Taipei City, Taiwan, 2005.

[14] F. J. F. Gonçalves and A. Brancaccio, “Free-space materials characterization by reflection and transmission measurements using frequency- by-frequency and multi-frequency algorithms,” *Electronics.,* vol. 7, no. 10, pp. 3–6, 2018.

[15] S. Geetha, K. K. S. Kumar, C. R. K. Rao, M. Vijayan, and D. C. Trivedi, “EMI shielding: methods and materials-A review,” *J. Appl. Polym. Sci.*, vol. 112, pp. 2073–2086, 2009.

[16] L. Cheng, T. Zhang, M. Guo, J. Li, S. Wang, and H. Tang, “Electromagnetic shielding effectiveness and mathematical model of stainless steel composite fabric,” *J. Text. Inst.*, vol. 106, no. 6, pp. 577–586, 2015.

[17] K. B. Cheng, T. W. Cheng, R. N. Nadaraj, V. R. G. Dev, and R. Neelakandan, “Electromagnetic shielding effectiveness of the twill copper woven fabrics,” *J. Reinf. Plast. Compos.*, vol. 25, no. 7, pp. 699–709, 2006.

[18] H. G. Ortlek, T. Alpyildiz, and G. Kilic, “Determination of electromagnetic shielding performance of hybrid yarn knitted fabrics with anechoic chamber method,” *Text. Res. J.*, vol. 83, no. 1, pp. 90–99, 2013.

[19] Sung-Hoon Park, P. T. Theilmann, P. M. Asbeck, and P. R. Bandaru, “Enhanced electromagnetic interference shielding through the use of functionalized carbon-nanotube-reactive polymer composites,” *IEEE Trans. Nanotechnol.*, vol. 9, no. 4, pp. 464–469, 2010.

[20] S. C. Lin *et al.*, “Electromagnetic interference shielding performance of waterborne polyurethane composites filled with silver nanoparticles deposited on functionalized graphene,” *Appl. Surf. Sci.*, vol. 385, pp. 436–444, 2016.

[21] V. Tunáková, J. Grégr, M. Tunák, and G. Dohnal, “Functional polyester fabric/polypyrrole polymer composites for electromagnetic shielding: Optimization of process parameters,” *J. Ind. Text.*, vol. 47, no. 5, pp. 686–711, 2018.

[22] Z. Yildiz, I. Usta, and A. Gungor, “Investigation of the electrical properties and electromagnetic shielding effectiveness of polypyrrole coated cotton yarns,” *Fibres Text. East. Eur.*, vol. 98, no. 2, pp. 32–37, 2013.

[23] A. J. Patil and A. K. Pandey, “A novel approach for in situ polymerization of polypyrrole on cotton substrates,” *Indian J. Fibre Text. Res.*, vol. 37, no. 2, pp. 107–113, 2012.

[24] N. Muthukumar and G. Thilagavathi, “Development and characterization of electrically conductive polyaniline coated fabrics,” *Indian J. Chem. Technol.*, vol. 19, no. 6, pp. 434–441, 2012.

[25] X. Luo and D. D. L. Chung, “Electromagnetic interference shielding using continuous carbon-fiber carbon-matrix and polymer-matrix composites,” *Compos. Part B Eng.*, vol. 30, no. 3, pp. 227–231, 1999.

[26] T. Kim and D. D. L. Chung, “Mats and fabrics for electromagnetic interference shielding,” *J. Mater. Eng. Perform.*, vol. 15, no. 3, pp. 295–298, 2006.

[27] X. Liu, L. Zhang, X. Yin, F. Ye, Y. Liu, and L. Cheng, “Flexible thin SiC fiber fabrics using carbon nanotube modification for improving electromagnetic shielding properties,” *Mater. Des.*, vol. 104, pp. 68–75, 2016.

[28] R. R. Bonaldi, “Electromagnetic shielding characterisation of several conductive fabrics for medical applications,” *J. Fiber Bioeng. Informatics*, vol. 2, no. 4, pp. 237–245, 2009.

[29] V. Safarova and J. Militky, “Electromagnetic field shielding fabrics with increased comfort properties,” *Adv. Mater. Res.*, vol. 677, pp. 161–168, 2013.

[30] D. Duran and H. Kadoğlu, “Electromagnetic shielding characterization of conductive woven fabrics produced with silver-containing yarns,” *Text. Res. J.*, vol. 85, no. 10, pp. 1009–1021, 2015.

[31] L. Lu *et al.*, “Electrical conductivity investigation of a nonwoven fabric composed of carbon fibers and polypropylene/polyethylene core/sheath bicomponent fibers,” *Mater. Des.*, vol. 112, pp. 383–391, 2016.

[32] E. Sano and E. Akiba, “Electromagnetic absorbing materials using nonwoven fabrics coated with multi-walled carbon nanotubes,” *Carbon N. Y.*, vol. 78, pp. 463–468, 2014.

[33] K. B. Cheng, S. Ramakrishna, and K. C. Lee, “Electromagnetic shielding effectiveness of copper/glass fiber knitted fabric reinforced polypropylene composites,” *Compos. Part A Appl. Sci. Manuf.*, vol. 31, no. 10, pp. 1039–1045, 2000.

[34] Z. C. Yu, J. F. Zhang, C. W. Lou, H. L. He, A. P. Chen, and J. H. Lin, “Determination of electromagnetic shielding and antibacterial properties of multifunctional warp-knitted fabrics,” *J. Text. Inst.*, vol. 106, no. 11, pp. 1203–1211, 2015.

[35] K. Jagatheesan, A. Ramasamy, A. Das, and A. Basu, “Fabrics and their composites for electromagnetic shielding applications,” *Text. Prog.*, vol. 47, no. 2, pp. 87–161, 2015.

[36] Z. C. Yu *et al.*, “Functional properties and electromagnetic shielding behaviour of elastic warp-knitted fabrics,” *Fibres Text. East. Eur.*, vol. 23, no. 5, pp. 78–83, 2015.

[37] L. Li, S. Liu, F. Ding, T. Hua, W. M. Au, and K. Wong, “Electromechanical analysis of length-related resistance and contact resistance of conductive knitted fabrics,” *Text. Res. J.*, vol. 82, no. 20, pp. 2062–2070, 2012.

[38] M. Neruda and L. Vojtech, “Electromagnetic shielding effectiveness of woven fabrics with high electrical conductivity: Complete derivation and verification of analytical model,” *Materials.*, vol. 11, no. 9, p. 1657, 2018.

[39] H. Özdemir, Ş. S. Uğurlu, and A. Özkurt, “The electromagnetic shielding of textured steel yarn based woven fabrics used for clothing,” *J. Ind. Text.*, vol. 45, no. 3, pp. 416–436, 2015.

[40] M. S. Özen, “Investigation of the electromagnetic shielding effectiveness of carded and needle bonded nonwoven fabrics produced at different ratios with conductive steel fibers,” *J. Eng. Fiber. Fabr.*, vol. 10, no. 1, pp. 140–151, 2015.

[41] V. Šafářová and J. Militký, “Electromagnetic shielding properties of woven fabrics made from high-performance fibers,” *Text. Res. J.*, vol. 84, no. 12, pp. 1255–1267, 2014.

[42] V. Šafářová and J. Militký, “Multifunctional metal composite textile shields against electromagnetic radiation-effect of various parameters on electromagnetic shielding effectiveness,” *Polym. Compos.*, vol. 38, no. 2, pp. 309–323, Feb. 2017.

[43] J. H. Lin, Y. T. Huang, T. T. Li, C. M. Lin, and C. W. Lou, “Manufacture technique and performance evaluation of electromagnetic-shielding/far-infrared elastic warp-knitted composite fabrics,” *J. Text. Inst.*, vol. 107, no. 4, pp. 493–503, 2016.

[44] R. Perumalraj and B. S. Dasaradan, “Electromagnetic shielding effectiveness of copper core yarn knitted fabrics,” *Indian J. Fibre Text. Res.*, vol. 34, no. 2, pp. 149–154, 2009.

[45] R. Perumalraj, B. S. Dasaradan, R. Anbarasu, P. Arokiaraj, and S. Leo Harish, “Electromagnetic shielding effectiveness of copper core-woven fabrics,” *J. Text. Inst.*, vol. 100, no. 6, pp. 512–524, 2009.

[46] J. Veer and V. K. Kothari, “Electromagnetic shielding effectiveness of woven fabrics having metal coated zari wrapped yarns,” *Indian J. Fibre Text. Res.*, vol. 42, no. 3, pp. 271–277, 2017.

[47] K. Lai, R. J. Sun, M. yu Chen, H. wu, and an X. Zha, “Electromagnetic shielding effectiveness of fabrics with metallized polyester filaments,” *Text. Res. J.*, vol. 77, no. 4, pp. 242–246, 2007.

[48] Y. Lu, Q. Liang, and W. Li, “Fabrication of copper/modal fabric composites through electroless plating process for electromagnetic interference shielding,” *Mater. Chem. Phys.*, vol. 140, no. 2–3, pp. 553–558, 2013.

[49] W. Qin and R. Guo, “Metallization of polyester fabric by autocatalytic copper plating process using glyoxylic acid as a reducing agent,” *Fibers Polym.*, vol. 16, no. 8, pp. 1671–1675, 2015.

[50] E. G. Han, E. A. Kim, and K. W. Oh, “Electromagnetic interference shielding effectiveness of electroless Cu-plated PET fabrics,” *Synth. Met.*, vol. 123, no. 3, pp. 469–476, 2001.

[51] A. Ali, V. Baheti, M. U. Javaid, and J. Militky, “Enhancement in ageing and functional properties of copper-coated fabrics by subsequent electroplating,” *Appl. Phys. A Mater. Sci. Process.*, vol. 124, no. 9, pp. 1–15, 2018.

[52] J. Liu *et al.*, “A large-area AgNW-modified textile with high-performance electromagnetic interference shielding,” *npj Flex. Electron.*, vol. 4, no. 10, pp. 1–7, 2020.

[53] J. Y. Zong *et al.*, “A wearable multifunctional fabric with excellent electromagnetic interference shielding and passive radiation heating performance,” *Compos. Part B Eng.*, vol. 225, p. 109299, 2021.

[54] K. Kardarian *et al.*, “Sintering of nanoscale silver coated textiles, a new approach to attain conductive fabrics for electromagnetic shielding,” *Mater. Chem. Phys.*, vol. 147, no. 3, pp. 815–822, 2014.

[55] X. Wang *et al.*, “A lightweight MXene-coated nonwoven fabric with excellent flame Retardancy, EMI shielding, and electrothermal/photothermal conversion for wearable heater,” *Chem. Eng. J.*, vol. 430, no. P1, p. 132605, 2022.

[56] W. Cheng *et al.*, “Durable electromagnetic interference (EMI) shielding ramie fabric with excellent flame retardancy and self-healing performance,” *J. Colloid Interface Sci.*, vol. 602, pp. 810–821, 2021.

[57] F. Shahzad *et al.*, “Electromagnetic interference shielding with 2D transition metal carbides (MXenes),” *Science.*, vol. 353, no. 6304, pp. 1137–1140, 2016.

[58] N. Duan, Z. Shi, J. Wang, G. Wang, and X. Zhang, “Strong and flexible carbon fiber fabric reinforced thermoplastic polyurethane composites for high-performance emi shielding applications,” *Macromol. Mater. Eng.*, vol. 305, no. 6, pp. 1–12, 2020.

[59] Z. W. Fan, R. T. Liu, and X. J. Cheng, “Preparation and characterization of electromagnetic shielding composites based on graphene-nanosheets-loaded nonwoven fabric,” *Coatings*, vol. 11, no. 4, 2021.

[60] S. Ghosh *et al.*, “Fabrication of reduced graphene oxide/silver nanoparticles decorated conductive cotton fabric for high performing electromagnetic interference shielding and antibacterial application,” *Fibers Polym.*, vol. 20, no. 6, pp. 1161–1171, 2019.

[61] P. Modak, S. B. Kondawar, and D. V. Nandanwar, “Synthesis and characterization of conducting polyaniline/graphene nanocomposites for electromagnetic interference shielding,” *Procedia Mater. Sci.*, vol. 10, pp. 588–594, 2015.

[62] A. R. Sousa *et al.*, “Design of Electromagnetic shielding textiles based on industrial-grade multiwalled carbon nanotubes and graphene nanoplatelets by dip-pad-dry process,” *Phys. status solidi*, vol. 219, no. 15, 2022.

[63] K. Raagulan *et al.*, “Electromagnetic shielding by mxene-graphene-pvdf composite with hydrophobic, lightweight and flexible graphene coated fabric,” *Materials.*, vol. 11, no. 10, pp. 1803, 2018.

[64] S. Palanisamy, A. Ali, M. Ryvalova, V. Tunakova, and J. Militký, "An analysis of the carbon preforms for electromagnetic shielding, 1st International conference on polymers and composites," *1st International conference on polymers and composites*, vol. 1, no. 1. National Textile University,Faisalabad, Pakistan, 2021.

[65] D. Xu, W. W. Yang, H. M. Jiang, H. Fan, and K. S. Liu, “Electromagnetic interference shielding characteristics of a core layer-coated fabric with excellent hand-feel characteristics,” *J. Eng. Fiber. Fabr.*, vol. 15, 2020.

[66] Y. Liu, X. Zhao, and X. Tuo, “Preparation of polypyrrole coated cotton conductive fabrics,” *J. Text. Inst.*, vol. 108, no. 5, pp. 829–834, 2017.

[67] M. Lu, R. Xie, Z. Liu, Z. Zhao, H. Xu, and Z. Mao, “Enhancement in electrical conductive property of polypyrrole-coated cotton fabrics using cationic surfactant,” *J. Appl. Polym. Sci.*, vol. 133, no. 32, 2016.

[68] Y. . Hong *et al.*, “Electromagnetic interference shielding characteristics of fabric complexes coated with conductive polypyrrole and thermally evaporated Ag,” *Curr. Appl. Phys.*, vol. 1, no. 6, pp. 439–442, 2001.

[69] A. Raza, A. Nasir, M. Tahir, S. Taimur, T. Yasin, and M. Nadeem, “Synthesis and EMI shielding studies of polyaniline grafted conducting nanohybrid,” *J. Appl. Polym. Sci.*, vol. 138, no. 2, 2021.

[70] S. Palanisamy, V. Tunáková, B. Malengier, D. Karthik, L. Van Langenhove, and J. Militky, “Development of the force sensitive resistors using polypyrrole coated cotton woven fabric for pressure sensing application,” *22nd STRUTEX 2018,* Liberec, Czech Republic, 2018.

[71] W. E. Morton and J. W. S. Hearle, *Physical properties of textile fibers*, Fourth. Cambridge, England: Woodhead publishing limited, England, 2008.

[72] L. Vojtech and M. Neruda, “Design of radiofrequency protective clothing containing silver nanoparticles,” *Fibres Text. East. Eur.*, vol. 101, no. 5, pp. 141–147, 2013.

[73] V. Tunakova *et al.*, “Hybrid knitted fabric for electromagnetic radiation shielding,” *J. Eng. Fiber. Fabr.*, vol. 15, 2020.

[74] O. Akkermans *et al.*, "Application of electrodeposited piezo-resistive polypyrrole for a pressure-sensitive bruxism sensor," *Phys. status solidi*, vol. 213, no. 6, pp. 1505–1509, 2016.

[75] N. K. Rana, "Application of Force Sensing Resistor (FSR) in Design of Pressure Scanning System for Plantar Pressure Measurement," in *2009 Second International Conference on Computer and Electrical Engineering*, 2009, pp. 678–685.

[76] T. Holleczek, A. Rüegg, H. Harms, and G. Tröster, "Textile pressure sensors for sports applications," *Proc. IEEE Sensors*, pp. 732–737, 2010.

[77] S. Rajagopalan, M. Sawan, E. Ghafar-Zadeh, O. Savadogo, and V. P. Chodavarapu, "A polypyrrole-based strain sensor dedicated to measure bladder volume in patients with urinary dysfunction," *Sensors*, vol. 8, no. 8, pp. 5081–5095, 2008.

[78] C. Merlini, R. D. S. Almeida, M. A. D'Ávila, W. H. Schreiner, and G. M. De Oliveira Barra, "Development of a novel pressure sensing material based on polypyrrole-coated electrospun poly(vinylidene fluoride) fibers," *Mater. Sci. Eng. B Solid-State Mater. Adv. Technol.*, vol. 179, no. 1, pp. 52–59, 2014.

[79] A. Ehrmann, F. Heimlich, A. Brücken, M.O. Weber, and R. Haug, "Suitability of knitted fabrics as elongation sensors subject to structure, stitch dimension and elongation direction," *Text. Res. J.*, vol. 84, no. 18, pp. 2006–2012, 2014.

[80] A. A. Simegnaw, B. Malengier, M. G. Tadesse, G. Rotich, and L. Van Langenhove, "Study the electrical properties of surface mount device integrated silver coated vectran yarn," *Materials.*, vol. 15, no. 1, 2022.

[81] O. Weizman, J. Mead, H. Dodiuk, and S. Kenig, "Electrical properties enhancement of carbon nanotube yarns by cyclic loading," *Molecules*, vol. 25, no. 20, 2020.

[82] Y. J. Yun, C. S. Ah, W. G. Hong, H. J. Kim, J. H. Shin, and Y. Jun, "Highly conductive and environmentally stable gold/graphene yarns for flexible and wearable electronics," *Nanoscale*, vol. 9, no. 32, pp. 11439–11445, 2017.

[83] H. Souri and D. Bhattacharyya, "Electrical conductivity of the graphene nanoplatelets coated natural and synthetic fibres using electrophoretic deposition technique," *Int. J. Smart Nano Mater.*, vol. 9, no. 3, pp. 167–183, 2018.

[84] V. Šafářová, L. Hes, and J. Militký, "An approach to electrical resistance measurement eliminating contact resistance problem," in *International Conference on Applied Electronics*, 2014.

[85] R. Holm , Holm, Else,, "Electric contacts : theory and application." Springer-Verlag, Berlin; New York, 1967.

[86] T. Mihailovic and L. Simovic, "Geometry and deformation properties of plain loops made of spun cotton yarns," *Tekst. Ind.*, vol. 46, pp. 23–28, 1998.

[87] P. Popper, “The theoretical behavior of a knitted fabric subjected to biaxial stresses,” *Text. Res. J.*, vol. 36, no. 2, pp. 148–157, 1966.

[88] D. J. Spencer, *Knitting Technology*, Third edit. Cambridge, England: Woodhead publishing limited, England, 1998.

[89] G. Demboski and G. Bogoeva-Gaceva, “Properties of weft knitted composites affected by preform stretching,” *Appl. Compos. Mater.*, vol. 8, no. 6, pp. 371–384, 2001.

[90] A. Ali *et al.*, “Highly stretchable durable electro-thermal conductive yarns made by deposition of carbon nanotubes,” *J. Text. Inst.*, vol. 113, no. 1, pp. 80–89, 2022.

[91] J. Wang, H. Long, S. Soltanian, P. Servati, and F. Ko, “Electro-mechanical properties of knitted wearable sensors : Part 2 – Parametric study and experimental verification,” *Text. Res. J.*, vol. 84, no. 2, pp. 200–213, 2014.

[92] M. Ruppert-stroescu and M. Balasubramanian, “Effects of stitch classes on the electrical properties of conductive threads,” *Text. Res. J.*, vol. 88, no. 21, pp. 2454–2463, 2018.

[93] J. Wang, H. Long, S. Soltanian, P. Servati, and F. ko, “Electromechanical properties of knitted wearable sensors: Part 1 – theory,” *Text. Res. J.*, vol. 84, no. 1, pp. 3–15, 2014.

[94] S. Liu, J. Tong, C. Yang, and L. Li, “Smart E-textile: Resistance properties of conductive knitted fabric – Single pique,” *Text. Res. J.*, vol. 87, no. 14, pp. 1669–1684, 2017.

[95] A. Gregori, E. Di Giampaolo, A. Di Carlofelice, and C. Castoro, “Presenting a new wireless strain method for structural monitoring: experimental validation,” *J. Sensors*, vol. 2019, 2019.

[96] H. Zhang, X. Tao, S. Wang, and T. yu, “Electro-mechanical properties of knitted fabric made from conductive multi-filament yarn under unidirectional extension,” *Text. Res. J.*, vol. 75, no. 8, pp. 598–606, 2005.

[97] W. M. Murray and W. R. Miller, *The Bonded Electrical Resistance Strain Gage*. New York, USA: Oxford university press Inc, 1992.

[98] E. A. E. Eltahan, M. Sultan, and A. B. Mito, “Determination of loop length, tightness factor and porosity of single jersey knitted fabric,” *Alexandria Eng. J.*, vol. 55, no. 2, pp. 851–856, 2016.

[99] A. Majumdar, “Soft Computing in Textile Engineering,” *Soft Comput. Text. Eng.*, no. 111, pp. 1–538, 2010.

8 LIST OF PUBLICATIONS BY AUTHOR

8.1. Author's publications in impact factor journals

Journal Paper	Impact factor*	Quartile **	Citations
1. **S. Palanisamy**, V. Tunakova, and J. Militky, "Fiber-based structures for electromagnetic shielding – comparison of different materials and textile structures," *Text. Res. J.*, vol. 88, no. 17, pp. 1992–2012, 2018.	2.46	2	45
2. **S. Palanisamy** *et al.*, "Electromagnetic interference shielding of metal coated ultrathin nonwoven fabrics and their factorial design," *Polymers.*, vol. 13, no. 4, p. 484, Feb. 2021.	4.97	1	9
3. **S. Palanisamy**, V. Tunakova, J. Militky, and J. Wiener, "Effect of moisture content on the electromagnetic shielding ability of non-conductive textile structures," *Sci. Rep.*, vol. 11, no. 1, pp. 1–10, 2021.	5.00	2	6
4. **S. Palanisamy**, V. Tunakova, M. Tunak, and J. Militky, "Textile-based weft knit strain sensor: Experimental investigation of the effect of stretching on electrical conductivity and electromagnetic shielding," J. Ind. Text., vol. 52, pp. 1–23, 2022.	2.93	1	-
5. T. Yang, **S. Palanisamy** et al., "Experimental and modelling studies on thermal insulation and sound absorption properties of cross-laid nonwoven fabrics," Autex Res. J., pp. 1–8, 2021.	1.94	2	2
6. T. Yang, **S. Palanisamy** et al., "AFDeter: A MATLAB-based tool for simple and rapid determination of the structural parameters and the airflow-related properties of fibrous materials," SoftwareX, vol. 20, p. 101213, 2022.	2.69	2	-
7. M. Shahid, **S. Palanisamy** et al., "Copper-treated environmentally friendly antipathogenic cotton fabric with modified reactive blue 4 dye to improve its antibacterial and aesthetic properties," Coatings, vol. 13, no. 1, p. 133, 2023.	3.24	2	-

* – Impact factor was taken from year 2021. ** - JCR category quartile based on Web of Science.

8.2. Publications in conference proceedings

Conference paper/ abstract	Index
1. **S. Palanisamy,** V. Tunakova, D Karthik, et al., "Study on textile comfort properties of polypropylene blended stainless steel woven fabric for the application of electromagnetic shielding effectiveness," IOP Conf. Series: *Materials Science and Engineering,* pp. 254, 2017.	Web of science
2. **S. Palanisamy**, V. Tunakova, et al.. "EMI shielding of the copper/ nickel coated nonwoven," *AUTEX 2021 International conference*, pp. 410-411, 2021, Guimaraes, Portugal. (Published in Diffusion and Defect Data pt.B: Solid State Phenomena (2022, vol 333, pp 137-142))	Scopus
3. **S. Palanisamy,** V. Tunakova, et al. "Modeling of an electrically conductive nonwoven strip for electromagnetic shielding," *TBIS 2021 international conference*, pp. 37-43, 2021, Roubaix, France.	Scopus
4. **S. Palaniamy,** et al.. "An analysis of the carbon preforms for electromagnetic shielding," *International conference on polymers and composites (ICPC-2021*), 2021, Faisalabad, Pakistan	-
5. **S. Palanisamy**, V. Tunakova, et al. "Wireless sensing properties of electrically conductive knitted structures," ***4th Indonesian Textile Conference,*** 2022, Bandung, Indonesia.	-
6. **S. Palanisamy**, V. Tunakova, et al. "Impact of bi-axial stretching of rib knitted fabric on its emi shielding" *The 15th Textile Bioengineering and Informatics Symposium, 2022,* Liberec, Czech Republic.	Scopus
7. **S. Palanisamy**, et al. "Bi-axial stretching of rib knitted fabric and its EMI shielding," *23rd STRUTEX*, 2022, Liberec, Czech Republic.	-
8. A. Ali, V. Baheti, A. Jabbar, J. Militky, **S. Palanisamy**, et al. "Effect of jute fibre treatment on moisture regain and mechanical performance of composite materials," *IOP Conf. Series: Materials Science and Engineering,* pp. 254, 2017.	Web of Science
9. D. Karthik, V. Baheti, V. Tunakova, J. Militky and **S. Palanisamy**. "Development of electrically conductive activated carbon fabric from kevlar fabric for effective EMI shielding applications," *Textile Bioengineering and Informatics Symposium,* 2017.	Web of Science
10. D. Karthik, V. Baheti, J. Militky and **S. Palanisamy.** "Studies on organic and inorganic micro/nano particle reinforced epoxy composites," *Textile Bioengineering and Informatics Symposium Proceedings*, pp.149, 2018.	Web of Science
11. A. Ali, H. Taimoor A. Awan, A. Aslam, A. Ali**, S. Palaniamy**, D. kremenakova, "Electrically conductive sustainable green composites," *International conference on polymers and composites (ICPC-2021)*, 2021, Faisalabad, Pakistan.	-
12. A. Ali, J. Militky, **S. Palanisamy** et al., "Copper and silver coated cotton fabrics," *23rd STRUTEX*, 2022, Liberec, Czech Republic.	-